DOT/FAA/AR-02/121

Office of Aviation Research
Washington, D.C. 20591

Guidelines for Analysis, Testing, and Nondestructive Inspection of Impact-Damaged Composite Sandwich Structures

March 2003

Final Report

U.S. Department of Transportation
Federal Aviation Administration

NOTICE

This document is disseminated under the sponsorship of the U.S. Department of Transportation in the interest of information exchange. The United States Government assumes no liability for the contents or use thereof. The United States Government does not endorse products or manufacturers. Trade or manufacturer's names appear herein solely because they are considered essential to the objective of this report. This document does not constitute FAA certification policy. Consult your local FAA aircraft certification office as to its use.

This report is available at the Federal Aviation Administration William J. Hughes Technical Center's Full-Text Technical Reports page: actlibrary.tc.faa.gov in Adobe Acrobat portable document format (PDF).

Technical Report Documentation Page

1. Report No.	2. Government Accession No.	3. Recipient's Catalog No.
DOT/FAA/AR-02/121		

4. Title and Subtitle

GUIDELINES FOR ANALYSIS, TESTING, AND NONDESTRUCTIVE INSPECTION OF IMPACT-DAMAGED COMPOSITE SANDWICH STRUCTURES

5. Report Date

March 2003

6. Performing Organization Code

7. Author(s)

P. Shyprykevich[3], J. Tomblin[1], L. Ilcewicz[4], A.J. Vizzini[2], T.E., Lacy[1], and Y. Hwang[2]

8. Performing Organization Report No.

9. Performing Organization Name and Address

[1]Wichita State University
1845 Fairmount, Wichita, KS 67260-0044

[2]University of Maryland
College Park, MD 20742

[3]FAA William J. Hughes Technical Center
Atlantic City International Airport, NJ 08405

[4]Seattle Aircraft Certification Office
Renton, WA 98055

10. Work Unit No. (TRAIS)

11. Contract or Grant No.

GA05

12. Sponsoring Agency Name and Address

U.S. Department of Transportation
Federal Aviation Administration
Office of Aviation Research
Washington, DC 20591

13. Type of Report and Period Covered

Final Report

14. Sponsoring Agency Code

AIR-120

15. Supplementary Notes

The FAA William J. Hughes Technical Center Technical Monitor was Peter Shyprykevich.

16. Abstract

Sandwich construction composites are used in a wide variety of structural applications largely because of their relative advantages over other designs in terms of improved stability, weight savings, and ease of manufacture and repair. While the design of sandwich structures is at a fairly mature stage of development, less progress has been made in understanding the effect of adverse in-service impact events on structural integrity. Foreign object impact damage in sandwich composites can be attributable to a number of fairly common discrete sources and may result in drastic reductions in composite strength, elastic moduli, and durability and damage tolerance characteristics.

In this report, past work is summarized and synthesized to provide guidance for analysis, testing, and nondestructive inspection of impact-damaged composite structures.

17. Key Words	18. Distribution Statement
Composites, Sandwich, Honeycomb, Damage tolerance, Impact, Residual strength, Finite element analysis	This document is available to the public through the National Technical Information Service (NTIS), Springfield, Virginia 22161.

19. Security Classif. (of this report)	20. Security Classif. (of this page)	21. No. of Pages	22. Price
Unclassified	Unclassified	94	

TABLE OF CONTENTS

LIST OF FIGURES

LIST OF TABLES

Tables Page

EXECUTIVE SUMMARY

This report contains a summarized version of the results obtained over several years of research into the damage tolerance of composite sandwich structures. The research was spurred by the use of sandwich structure in general aviation (small airplanes and business jets), where newly certified aircraft are entering service and by the maintenance difficulties encountered with existing commercial transport aircraft parts. The research was in three areas: testing, analysis, and nondestructive inspection (NDI).

Testing was performed under static and fatigue compressive loads of impacted 8″ x 10″ panels. The results characterized the damage resistance and tolerance of flat and curved sandwich panels. Response surfaces for damage resistance and damage tolerance were drawn from the testing data in order to extend the database to other than tested configurations. Field level NDI was performed to find internal damage for both honeycomb and foam cores. Analyses of impacted panels were used to determine damaged sandwich response, predict final failure, and correlate with tests. Analysis, whether performed by closed form solutions or finite element models, can be useful in design and certification of impact-damaged composite sandwich structures. The state of the art is such that analysis cannot stand by itself but can be useful in directing and analyzing test results and expanding test data to untested configurations by semiempirical methods. The analytical work described in this report showed that careful modeling can describe the structural response of the impacted panel under compressive load, but some adjustments were needed to predict failure. The analysis performed also showed that damage progression capability is vital to the fidelity of the analysis.

Inferences from the research helped formulate guidelines for testing, analysis, and NDI, which characterized the effects of impact damage on sandwich panels. These guidelines should prove useful for development and certification efforts. A need to extend the current effort to larger structures was identified. The full-scale tests will be able to interrogate the effects of rogue damage on nonpressurized and pressurized fuselage structures that include curvature.

1. INTRODUCTION.

It is well established that impact damage in composite sandwich structures is a serious threat to maintaining structural integrity, particularly under compression loading. Industry response to this threat has been to inflict impact damage on a structure to the extent that the damage is barely visible and demonstrate by testing that the structure can withstand ultimate static load and one lifetime of spectrum loads. Structure subjected to higher levels of impact damage, which is clearly visible, must sustain spectrum loads for inspection interval and maintain a residual strength of at least limit load.

The approach described above has several difficulties. The selection of impactor diameter and geometry, in general, can change the visibility characteristics dramatically. Impact damage created by small-diameter sharp objects will be much more visible than impacts from blunt impactors. The industry standard of using spherical impactors, which are 1-inch diameter or smaller, may not be conservative. The indentation caused by impact can also spring back and become invisible. The determination of what energy level is needed to create visible damage in a full-scale structure is hard to ascertain from small coupon tests. The visibility criteria often result in many unnecessary repair actions during maintenance, because the operator generally does not know the effect of the damage on strength but only knows that all visible damage must be repaired. The visibility criteria may also penalize designs that are damage resistant, either through the use of tougher material or design configuration. For instance, thicker facesheets and heavier core densities would tend to have lower allowable design strains for Barely Visible Impact Damage (BVID) and ultimate load levels. The latter practice can lead to heavy, but fortunately safe designs.

1.1 BACKGROUND AND PHILOSOPHICAL APPROACH.

The damage tolerance philosophy is well established for metallic airframes. An industry consensus exists on what methods (structural analysis and inspection procedures) and supporting databases are to be used to detect damage and predict crack growth and residual strength. However, the damage characteristics, inspections procedures, analysis methods, and experimental databases necessary for applying a damage tolerance philosophy to composite structures, including sandwich construction, are not well understood. The determination of the damage tolerance characteristics of sandwich panels has been limited in previous investigations to relatively few sandwich configurations and damage states [1].

The state of composite impact damage is complex and dependent on a number of variables. The two main classes of variables include the intrinsic design properties of the sandwich constructions and the extrinsic parameters that define the damage causing the impact event. Further, the BVID, allowable damage limit (ADL), and critical damage threshold (CDT) are not clearly defined in terms of a rational damage metric. Traditionally, visual inspection procedures have been used for detecting damage in composite structures (in service) and, hence, BVID came into existence. The current definitions of BVID are typically based on the residual indentation depth, which has been shown by testing to be sandwich configuration and impactor diameter dependent. Another issue coupled with this, is the choice of the nondestructive inspection (NDI) techniques used to determine the extent of the internal damage. The choice of NDI method can

affect the damage metric. Nevertheless, an NDI measure of the damage metric has proven to be a more reliable indication of the residual strength than indentation depth.

The current efforts started with a thorough literature review to summarize the various intrinsic and extrinsic variables used by different investigations to study the effects of impact on composite sandwich panels. Any trends in past studies were used in planning a research program for a thorough investigation of the damage resistance and tolerance of sandwich panels. The details of the literature review may be found in reference 1. Additional companion reports outlining the complete program and results may be found in references 2, 3, 4, 5, 6, and 7. The purpose of the research investigation was to determine the effect of a wide variety of impact damage states on the damage tolerance characteristics of composite sandwich panels over a significant range of panel configurations commonly used in aerospace applications. A summary of these efforts is given in this document, providing a basis for understanding the damage tolerance of composite sandwich structure. The associated guidelines should be useful in engineering design, analysis, and testing as related to satisfying the relevant Federal Aviation Administration (FAA) certification requirements.

The general philosophy applied during damage tolerance certification, shown schematically in figure 1-1, relates representative damage size to design load requirements. As in the case of metal aircraft, ultimate strength and damage tolerance philosophies are used to maintain a reliable and safe operation of composite structures. As shown in figure 1-1, this philosophy may be described using three distinct regions that are summarized as follows:

1. Nonvisible, or BVID, or defects that are not detectable during manufacturing inspections and service inspections must withstand ultimate load and not impair operation of the aircraft for its lifetime. In this region, it is assumed that the damage may never be discovered during the aircraft's lifetime and must support ultimate design load.

2. When the damage is larger than the ADL, it must be repaired when discovered. This damage is visible during service inspections and must withstand a once per lifetime load (limit load) after experiencing repeated service loads for the specified inspection interval. It is necessary in a damage-tolerant design that service damage falling in this region be found and characterized using practical inspection techniques. Damage approaching CDT must be found with an extremely high probability using the selected inspection scheme.

3. The last region is associated with a damage state that should be immediately obvious. Usually, this damage occurs in flight and is apparent to the operator. Under this condition, a CDT may be exceeded and the aircraft must withstand limit load capability under limited maneuvers necessary for continued safe flight. Note that the load requirement for pressure critical structure remains unchanged for the last two regions.

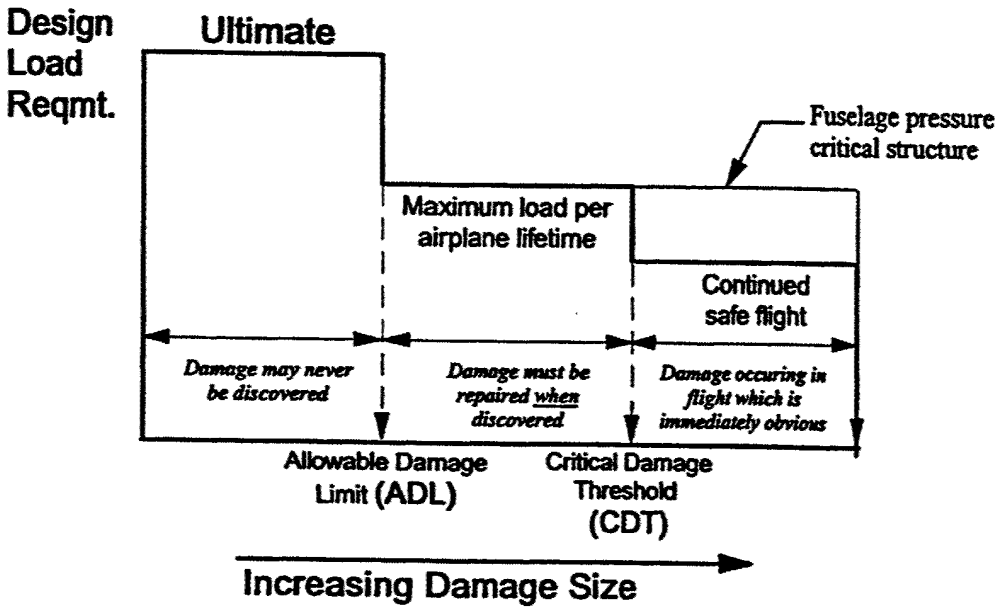

FIGURE 1-1. DAMAGE-TOLERANT DESIGN PHILOSOPHY

1.2 SCOPE.

To address the difficulties enumerated in the previous section, the FAA has invested in a sizeable research program in characterization, analysis, and testing of impact-damaged sandwich structures. The research was spurred by the use of sandwich structure in general aviation (small airplanes and business jets), where newly certified aircraft are entering service and by the maintenance difficulties encountered with existing commercial transport aircraft parts. The research was designed to address the following issues:

- What reduction in compressive residual strength can be expected as a function of impactor diameter, impactor velocity, visible damage, internal damage, and sandwich configurations?

- Can damage resistance, in terms of both visible and invisible damage, be formulated into a response surface as a function of impact and configuration parameters? In other words, can the data generated by this program be used to estimate damage resistance of sandwich panels?

- What is the capability of current field inspection techniques to measure internal damage?

- Can reliable analysis methods replace testing and reduce certification cost?

  - Is off-the-shelf finite element modeling useful in predicting compression response of panels with impact damage, including failure load?

  - Can the numerical model, developed initially by Minguet [8], predict impact damage growth?

- How can coupon test results be scaled to full-scale structure?
- What role does curvature play in damage resistance and tolerance?

This report summarizes the results of this research in three areas of interest: testing, analysis, and NDI. Section 2 describes the testing that was performed under static and fatigue compressive loads on impacted 8″ x 10″ panels. The results characterized the damage resistance and tolerance of flat and curved sandwich panels. Section 3 describes the response surfaces for damage resistance and damage tolerance that were drawn from the test data to extend the database to other than the tested configurations. Section 4 describes the field level NDI that were performed to find internal damage for both honeycomb and foam cores. Section 5 provides the analytical portion of the research and shows the correlation with tests described in section 2. Section 6 is essentially a conclusion section that starts with general guidance and draws inferences from the research to formulate guidelines on how to perform testing, analysis, and NDI to characterize the effects of impact damage on sandwich panels. The information contained in this section should prove useful for development and certification efforts. Section 7 delineates the current understanding as to what needs to be done in the future to extend the knowledge base.

2. IMPACT DAMAGE CHARACTERIZATION.

The successful implementation of damage tolerance programs for composite sandwich airframe structures requires a good understanding of the potential damage states in sandwich panels, the capability to detect and characterize these damage states, and the behavior of the damaged structure under service loads. The formation of damage in sandwich airframes have been attributed to transient transverse normal loads arising due to low-velocity impacts by foreign objects. The behavior of sandwich structures under such transient loads and the resulting damage states are governed by several variables, which have been classified as intrinsic variables and extrinsic variables [1]. The impact responses and the damage states in flat sandwich panels with thin facesheets were reported to be dependent on the diameter of the spherical steel impactor [3]. The smaller (1″) diameter impactors produced localized facesheet damage with noticeable residual indentations of the order of the facesheet thickness while the larger (3″) diameter impactor produced widespread core damage with residual indentations of the order of ply thickness (0.01″) or less.

2.1 STATIC LOADS AND RESIDUAL STRENGTH.

The damage tolerance of the impact-damaged sandwich panels during these investigations were evaluated by conducting compression-after-impact (CAI) tests. The specimens used for this investigation were relatively small (compared to full-scale) 8″ by 10″ sandwich panels. The residual strength and failure modes of the sandwich panels under in-plane compressive loads were found to be governed by the relative distribution of facesheet and core damage states. The impact damage due to smaller impactors produced a stress concentration governing compressive failure of the facesheet across the width of the sandwich panel, with the crack originating from the damage zone and propagating towards the lateral edges. The impact damage due to the larger impactor promoted a local buckling-initiated failure of the impacted facesheet. The residual strengths corresponding to the compressive failure of the sandwich panels were consistently higher than that of the buckling-initiated failure.

2.1.1 Experimental Setup.

The test fixturing and boundary conditions used in these investigations are reported in detail in references 3 and 6. The typical specimen geometry along with the locations of the strain gages and the location for the measurement of out-of-plane displacement is illustrated in figure 2-1. An additional strain gage was mounted at the center of the damage region to monitor the surface strains in the skin. A spring-loaded linear variable differential transformer (LVDT) was used to measure the out-of-plane displacement at aforementioned location. In addition, a deflectometer was used to measure the end-shortening of the specimen. The LVDT and deflectometer along with the specimen in the test fixture are illustrated in figure 2-2.

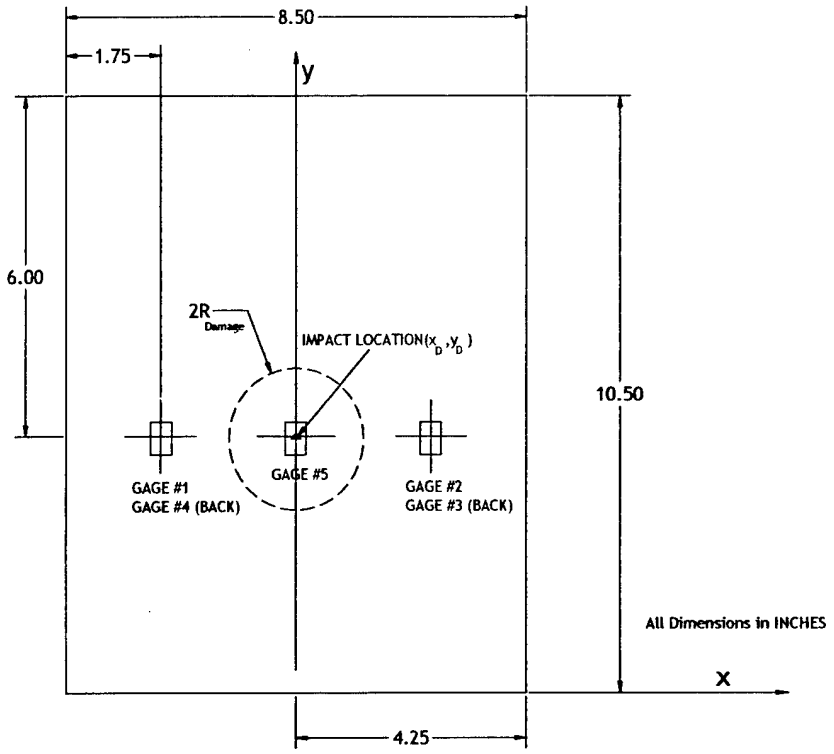

FIGURE 2-1. SPECIMEN GEOMETRY AND STRAIN GAGE LOCATIONS

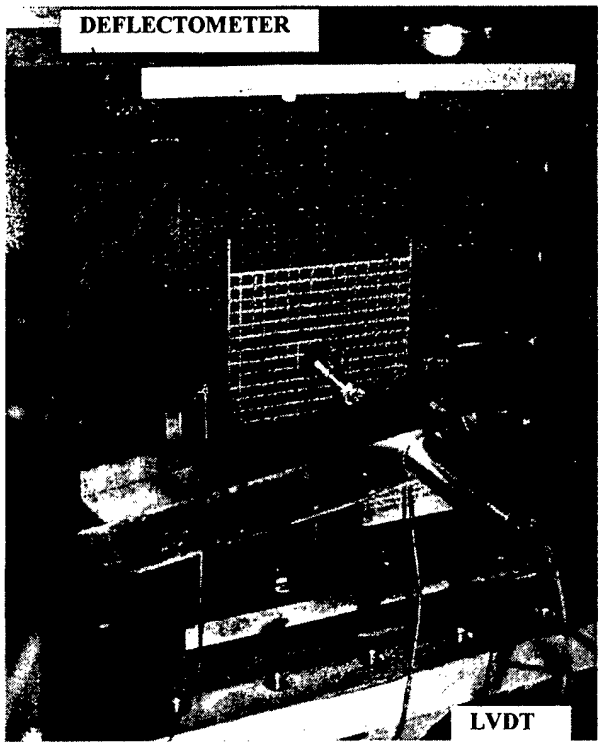

FIGURE 2-2. THE SANDWICH SPECIMEN IN THE TEST FIXTURE, LVDT, AND THE DEFLECTOMETER

The $[(90/45)/CORE]_s$ and $[(90/45)_2/CORE]_s$ sandwich panels with honeycomb and foam cores were impact damaged and tested under compressive loads using the previously discussed instrumentation. The test data obtained for each specimen along with the associated damage metrics, proposed damage growth mechanisms, and final failure modes are summarized and presented in the following sections. A detailed presentation of the data and experimental results is available in references 3 and 6.

2.1.2 CAI Testing of $[(90/45)/CORE]_s$ Specimen With Honeycomb Core.

An example of the data colleted during these investigations is provided to show the type of specimens and data collected. For example, the $[(90/45)/CORE]_s$ sandwich panel with plain-weave carbon facesheets was impacted with a 3.00″ diameter impactor at an energy level of 125 lbf-in. The planar damage area associated with the impact damage was $D_A = 4.02$ in^2 ($2R_{damage} = 2.28$ in). The maximum residual indentation depth associated with the damage was measured to be $\Delta_{RMAX} = 0.017$ in. The sandwich specimen was then statically tested to failure under in-plane compressive loads. An example of the test data is plotted in figure 2-3.

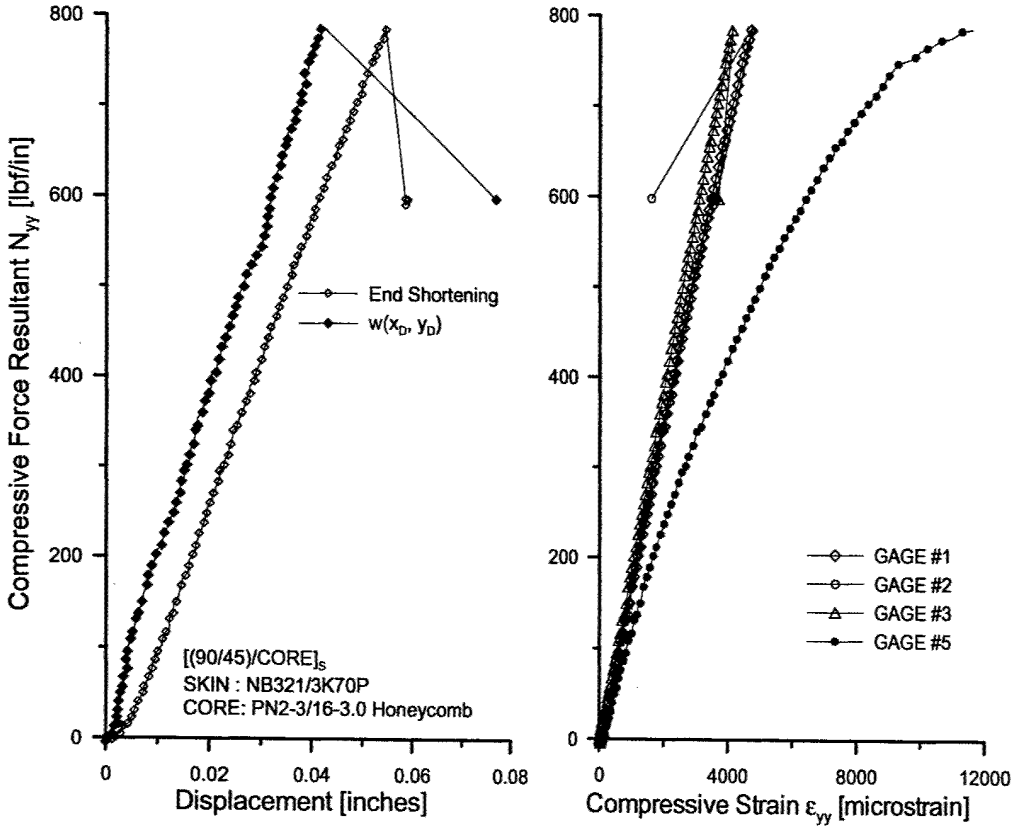

FIGURE 2-3. CAI TEST DATA FOR $[(90/45)/CORE]_s$ SANDWICH PANEL WITH PLAIN-WEAVE CARBON FACESHEETS

The displacements associated with the end-shortening and the out-of-plane displacement at the center of the damage was observed to vary linearly with the applied load. The strain gage at the center of the damage, however, was nonlinear and more compliant compared to the far-field

strain gages. This can be attributed to the additional bending component of strain associated with the skin in the damage/dimple region. The linearity of the out-of-plane displacement at the center of the damage implies that there was no increase (growth) in damage area. However, the skin within the damage region was subjected to high bending strains leading to a strain-related failure. The damage growth mechanism resulting in final failure process is illustrated in figure 2-4. The in-plane compressive loads bend the skin within the damage zone due to the lack of support from the damaged core. This bending increases until the strains in the skin exceed a critical strain value initiating skin fractures at the edge of the damage region. These cracks propagate out laterally, towards the edges of the specimen leading to complete fracture. This failure type indicates a specific mode of failure commonly observed during testing, which is typical of a stress concentration, open-hole failure, and was found typically for the two-ply and shaper impact thicker skin panels.

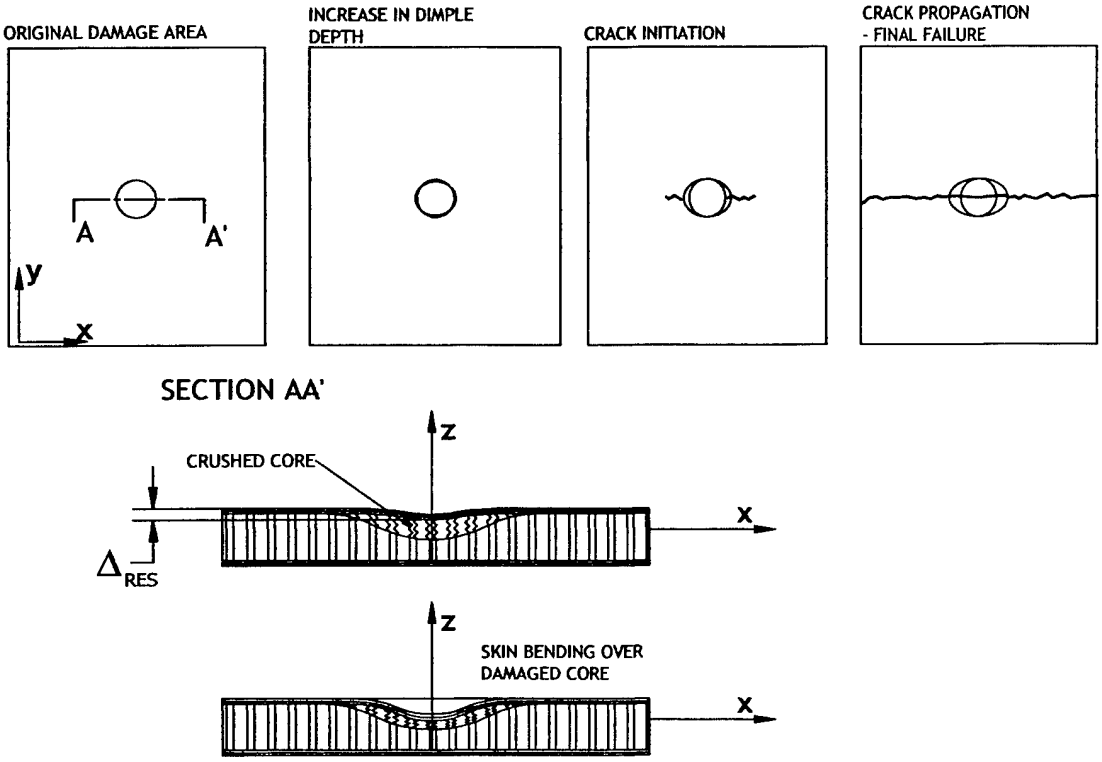

FIGURE 2-4. DAMAGE GROWTH MECHANISM AND FINAL FAILURE MODE OBSERVED IN $[(90/45)/CORE]_s$ SANDWICH PANEL WITH HONEYCOMB CORE (SHARP IMPACTOR)

2.1.3 CAI Testing of $[(90/45)_2/CORE]_s$ Specimen With Honeycomb Core.

In order to show differences in failure modes that were observed during these investigations, an example of a different buckling type failure follows. For example, a $[(90/45)_2/CORE]_s$ sandwich panel with plain-weave carbon facesheets was impacted with a 3.00″ diameter impactor at an energy level of 87.4 lbf-in. The planar damage area associated with the impact damage was $D_A = 4.19$ in^2 ($2R_{damage} = 2.31$ in). It should be noted that this is roughly the same damage size as presented in the previous section. The maximum residual indentation depth associated with

the damage was measured to be Δ_{RMAX} = 0.007 in. The sandwich specimen was then statically tested to failure under in-plane compressive loads. An example of the test data is plotted in figure 2-5.

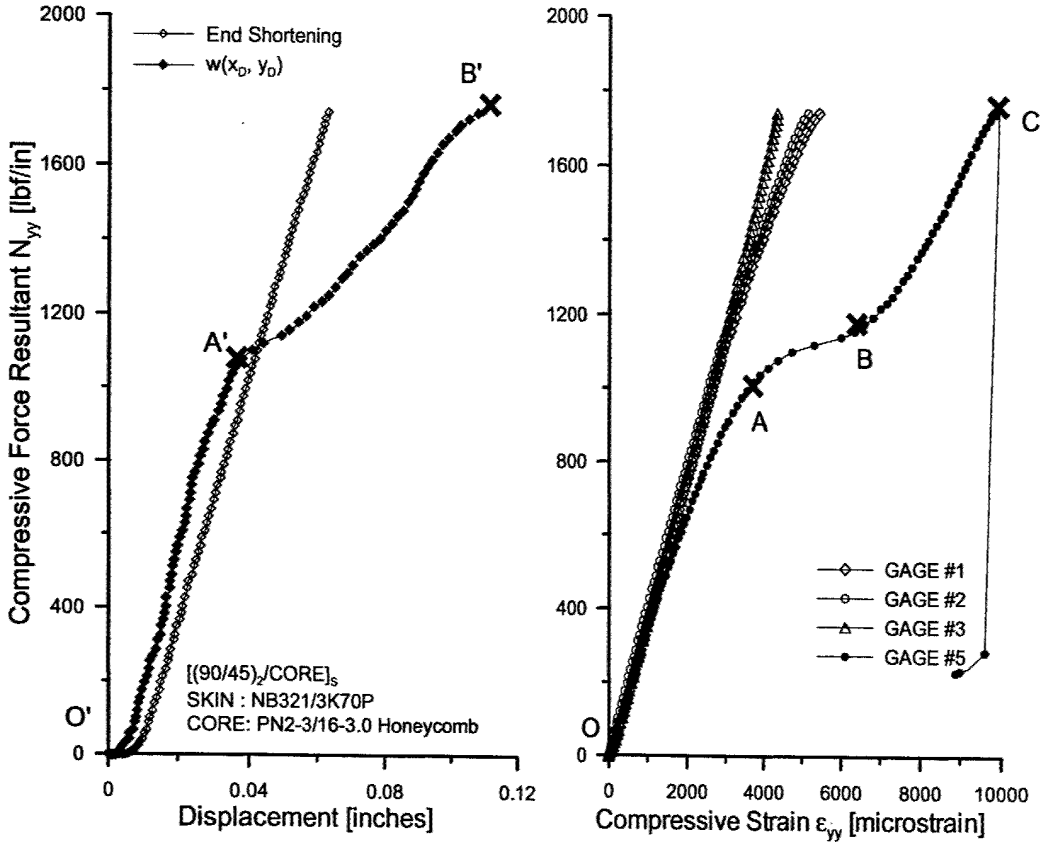

FIGURE 2-5. CAI TEST DATA FOR $[(90/45)_2/CORE]_s$ SANDWICH PANEL WITH PLAIN-WEAVE CARBON FACESHEETS

The out-of-plane displacement and the strain gage at the center of the damage region in $[(90/45)_2/CORE]_s$ sandwich panels exhibited a characteristic response, as shown in figure 2-5. A characteristic knee was observed for both curves, indicating a sudden change in compliance. The out-of-plane displacement response exhibited a nonlinear behavior past the knee point (A′ in the figure), with a slight stiffening tendency. The strain gage at the center of the damage region exhibits three distinct regions: OA, AB, and BC. The abrupt increase in compliance occurs at point A, beyond which the strain increases rapidly until point B is reached, where an appreciable increase in stiffness can be observed. The strain increases until point C, which corresponds to final failure. The observed behavior is explained using the illustrations in figure 2-6. The initial increase in strain and out-of-plane displacement (regions OA and O′A′ respectively) can be attributed to the bending of the skin over the impact pre-existing damaged core. The facesheet bends over the damaged core until the core consolidates and is able to transmit load across the thickness. When point A (or A′) is reached, there is sufficient strain energy and the moments generated in the skin are high enough to further crush the core in the thickness direction and initiate damage in the adjoining core, thereby increasing the damage area. This induces a

reduction in stiffness associated with the local bending of the facesheet and is represented by region AB in figure 2-5. The growth of the dimple in the lateral direction is arrested at point B due to the lack of sufficient energy to initiate additional core damage. The bending of the skin continues until point C is reached when there is enough energy in the skin to propagate the dimple in an unstable manner across the width of the panel, leading to final failure.

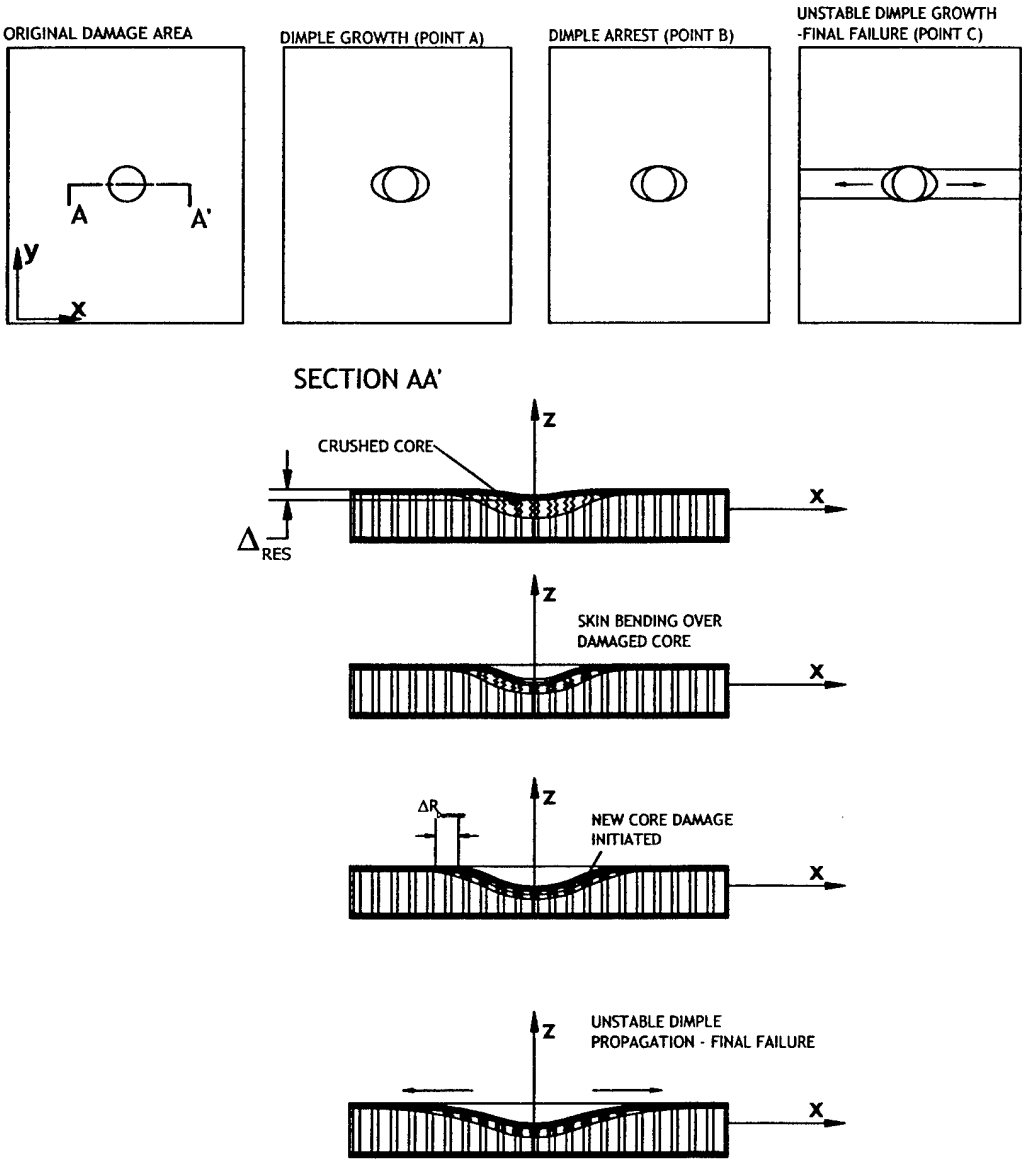

FIGURE 2-6. DAMAGE GROWTH MECHANISM AND FINAL FAILURE MODE OBSERVED IN $[(90/45)_2/CORE]_s$ SANDWICH PANEL WITH HONEYCOMB CORE

2.1.4 CAI Testing of $[(90/45)_2/CORE]_s$ Specimen With Foam Core.

To show the damage effects of different core systems, similar investigations were also conducted with foam cores. A detailed presentation of the data and experimental results is available in reference 6. Similar to the honeycomb core specimens, a $[(90/45)_2/CORE]_s$ foam core panel

with glass fabric facesheets was impacted with a 3.00″ diameter impactor at an energy level of 360 lbf-in. The maximum residual indentation depth associated with the damage was measured to be Δ_{RMAX} = 0.04 in. The sandwich specimen was then statically tested to failure under in-plane compressive loads. The test data for this specimen is plotted in figure 2-7.

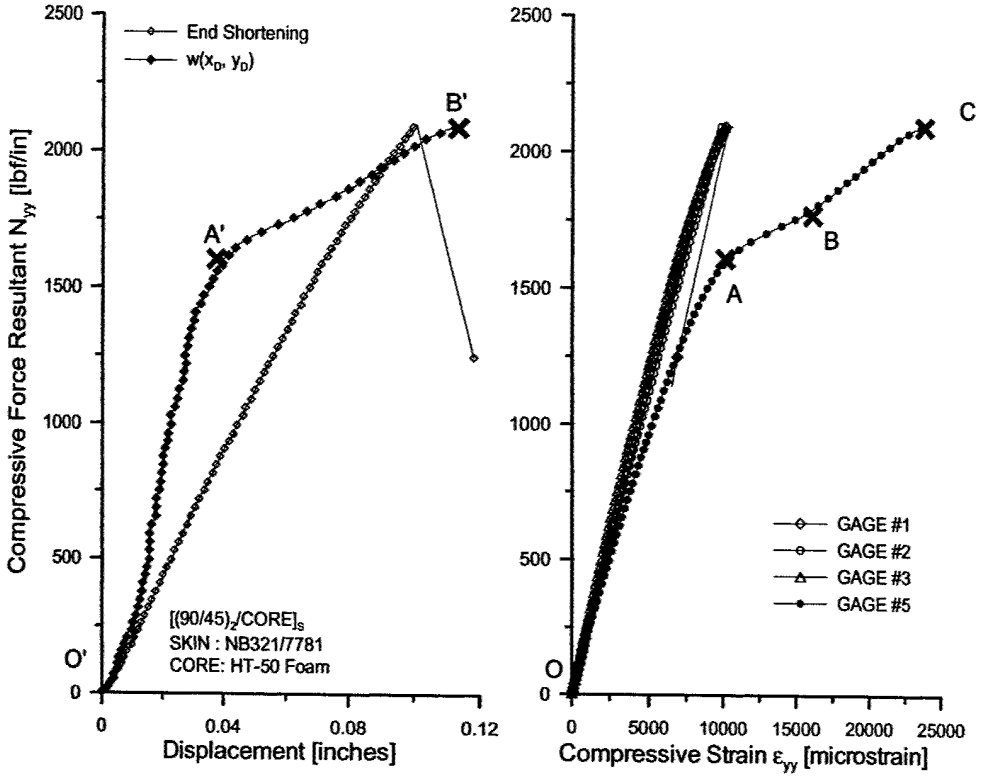

FIGURE 2-7. CAI TEST DATA FOR $[(90/45)_2/CORE]_s$ SANDWICH PANEL WITH GLASS FABRIC FACESHEETS AND FOAM CORE

The impact damage in foam core sandwich panel exhibited behavior similar to the honeycomb core panel described in the previous section. However, upon the initiation of further core crushing, there was no evidence of a dimple arrest mechanism, as seen from the strain data. This is due to the different transverse compressive behavior of the foam core when compared with the honeycomb cores [9]. The foam cores under transverse compression behave in an elastic-plastic manner, while the honeycomb cores can sustain transverse compressive loads several times that of their yield/crush load [9].

2.1.5 Planar Damage Area.

During these investigations [3 and 6], various impact parameters were studied and characterized. One of the most relevant to ongoing design and certification efforts is the relationship between planar damage area and impact energy. Instead of producing a damage state in area, most design and certification efforts rely on impact or surface visibility for damage tolerance purposes. Hence, the question that arises is, "How much energy or surface visibility we hit this panel with?" The answer to this question is dependent on the particular application and usage the

structure may experience during its service life. Figures 2-8 and 2-9 show the relationship between planar damage area and impact energy for a small (relatively sharp) (1″) impactor and a blunt (3″) impactor, respectively. As seen from these figures, the impact diameter plays a large role in the resulting planar damage area. It is also interesting to note the role that the core thickness plays with respect to planar damage area (particularly for high-energy impacts).

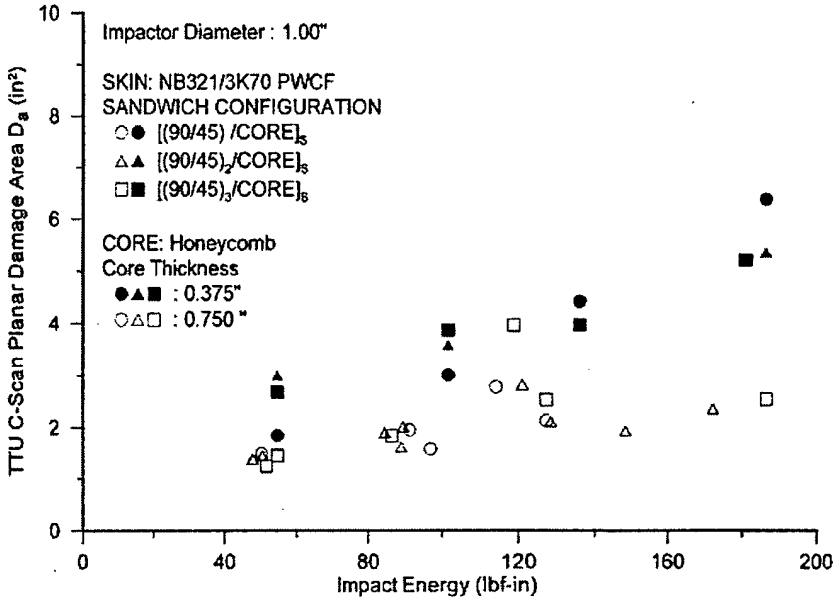

FIGURE 2-8. PLANAR DAMAGE RELATIONSHIP AS A FUNCTION OF IMPACT ENERGY FOR THE RELATIVELY SHARP (1″) IMPACTOR

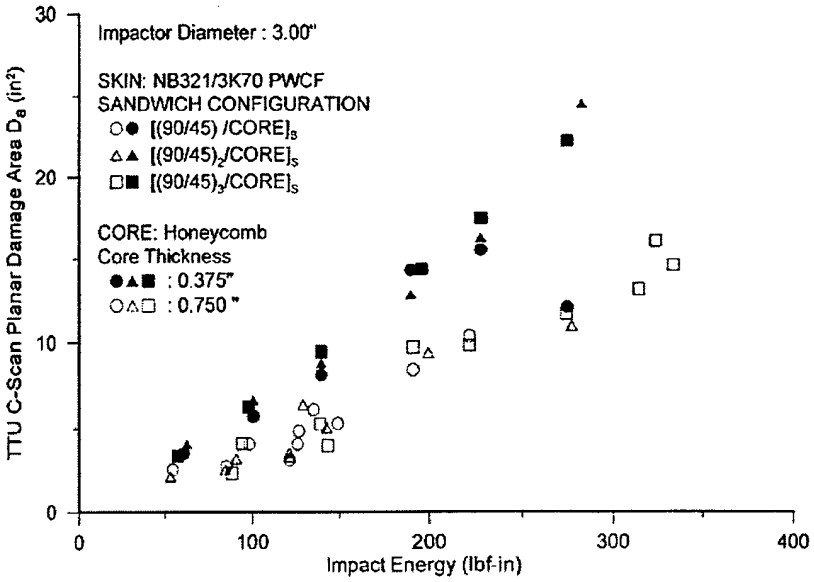

FIGURE 2-9. PLANAR DAMAGE RELATIONSHIP AS A FUNCTION OF IMPACT ENERGY FOR THE BLUNT (3″) IMPACTOR

2.1.6 Residual Strength.

The impact damage in sandwich panels due to blunt impactors behave in a characteristic manner(s) leading to contrasting final failure modes under in-plane compressive loads. The impact damage, which manifests in the form of a dimple, will be active well before the final failure occurs. The amount of this activity will be dependent on the flexural properties of the facesheet, transverse compressive properties of the core, and the damage metrics. A thin facesheet with negligible flexural stiffness will promote a strain-based failure mechanism, due to the inability of the skin to drive the dimple against the core. However, given enough flexural stiffness, the facesheet could drive this dimple through a characteristic sequence of events leading to a stability-based failure mechanism.

The normalized (to undamaged strength) residual strengths of sandwich panels impacted with 1″ and 3″ diameter impactors are plotted as a function of planar damage area in figure 2-10(a). It can be observed that the data is scattered around a hypothetical degradation curve irrespective of the impactor diameter. However, the data points corresponding to the smaller diameter impactor are spread over the initial portion of the curve, while those of the larger impactor fall over the asymptotic region of the curve. The impact damage states in practice will only undergo a posteriori analysis based on the damage metrics, without any knowledge of the associated impact energies. The maximum residual indentation has been typically used as a measure of the severity of impact damage. The threshold of detectability based on the residual indentation is known as Barely Visible Impact Damage. There is no consensus on a standard value for the BVID, even though it has been assumed that the strength degradation is proportional to the residual indentation depth. It has been shown in the previous study [3] that the maximum residual indentation depth does not necessarily correlate well with the CAI strength. It can be seen from figure 2-10(b) that large planar damage areas can exist while the maximum residual indentation is on the order of a few ply thicknesses (0.008″ in this case). Thus, it was concluded that residual indentation depth is not a reliable indicator of impact damage; rather, the planar damage size better reflects the residual strength degradation in sandwich panels. To quantify the planar damage, damage state, or the structure's residual strength capability, it becomes necessary to identify damage detection techniques and their effectiveness in light of this observation.

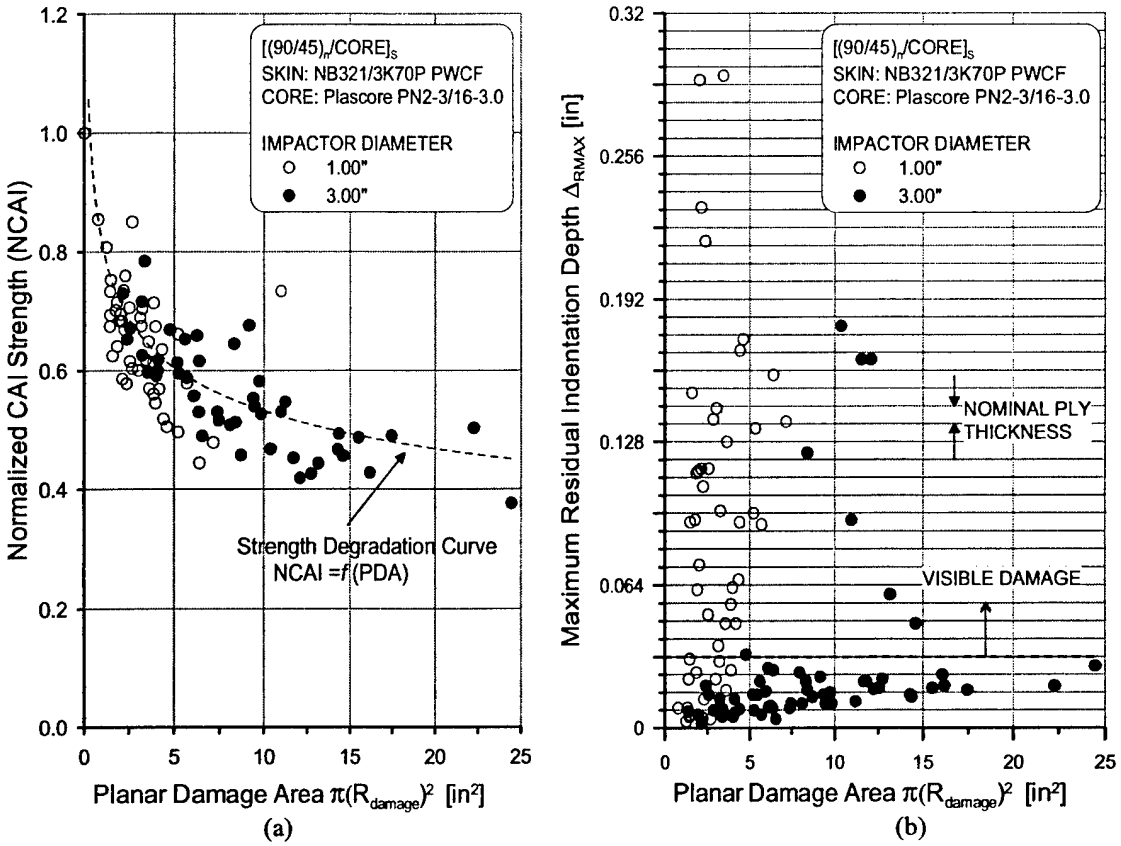

FIGURE 2-10. (a) NORMALIZED RESIDUAL STRENGTH FOR $[(90/45)n/CORE]_s$ (n=1,2,3)* SANDWICH PANELS WITH HONEYCOMB CORE (3/8″ AND 3/4″ THICK) AND (b) VARIATION OF MAXIMUM RESIDUAL INDENTATION DEPTH WITH PLANAR DAMAGE AREA FOR THE SANDWICH PANELS

2.2 IMPACT DAMAGE IN SANDWICH PANELS.

The damage states in sandwich panels can be broadly classified as material damage states and geometric damage states. The material damage states include facesheet damage, core damage, and facesheet-core interface disbonds. The facesheet damage states encompass delaminations, matrix cracks, and facesheet/ply fractures. The core damage states may comprise of core crushing (foam cores), cell wall buckling (honeycomb cores), and core fractures. The geometric damage state in sandwich panels manifests as a residual indentation distribution around the point of impact. The various damage states may occur simultaneously with the relative proportions being dictated by the intrinsic and extrinsic variables. In this section, the damage states observed during the experimental program are enumerated.

* The sandwich layup configurations listed throughout this document shall imply that the layup is symmetric about the core, i.e., $[(90/45)_n/CORE]_s$ means $[(90/45)_n/CORE/(45/90)_n]$.

2.2.1 Facesheet Damage.

The facesheet damage states may be comprised of facesheet delaminations, matrix cracking, and ply/facesheet fractures [6 and 9]. The initiation of facesheet damage was observed to be dependent on the impactor size (diameter). A limited number of sandwich panels ($[(90/45)_2/CORE]_s$) with fiberglass facesheets and honeycomb cores (Plascore PN2-3/16-3.0; 0.75″ thick) were impacted to study the facesheet damage states in sandwich panels. The translucency of the fiberglass facesheets was exploited to observe the facesheet damage states, since the underlying core damage masks the facesheet damage during the through-transmission ultrasonic C-scan (TTU C-scan) measurements [9 and 10].

The facesheet damage was observed to initiate in the form of delaminations between the plies adjacent to the facesheet-core interface, and these delaminations occurred above the honeycomb cell walls [9]. A network of delaminations was observed at higher-impact energy levels. The area over which delamination networks occurred was found to increase with impact energy up to the point when facesheet fracture was initiated. The typical delamination network in sandwich panels impacted with the 3.00″ diameter impactor are illustrated in figure 2-11. It was observed that the damage area measured by the TTU C-scan method was consistently higher than the area corresponding to the facesheet delaminations. This implies that, in practice, the facesheet damage may go undetected in the absence of a conspicuous facesheet fracture. Further, the presence of a layer of paint or a nontranslucent facesheet will make it difficult to detect these facesheet damage states.

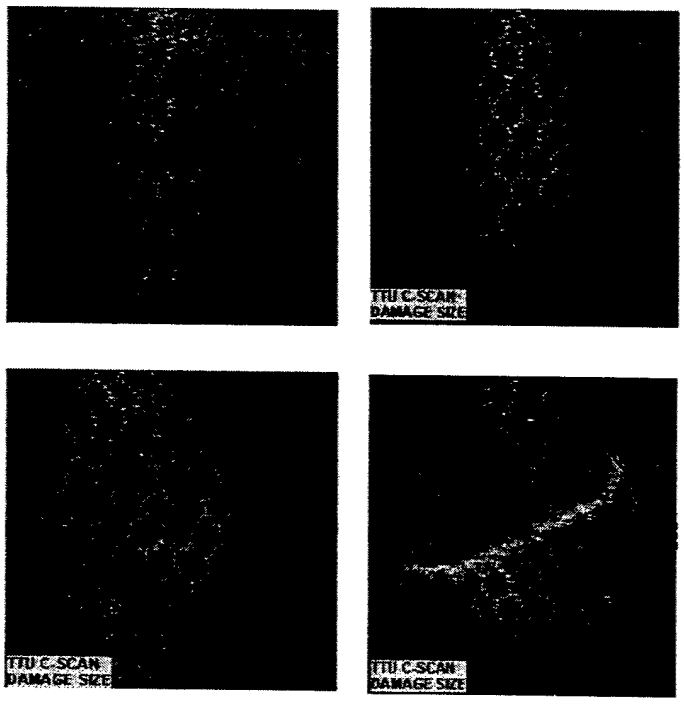

FIGURE 2-11. TYPICAL NETWORK OF DELAMINATIONS OBSERVED IN $[(90/45)_2/CORE]_s$ SANDWICH PANELS WITH FIBERGLASS FACESHEETS AND HONEYCOMB CORES, IMPACTED WITH A 3.00″ DIAMETER IMPACTOR

2.2.2 Core Damage.

The core damage in honeycomb core sandwich panels was observed to be predominantly cell wall buckling, core crushing, and cell wall fracture. The incipient failure mode in all cases was observed to be cell wall buckling, which propagated across the planar dimensions of the panel. The damage metrics associated with the core damage in sandwich panels (honeycomb core) is illustrated in figure 2-12. The TTU C-scan method measures the planar damage size, $2R_{damage}$, of the core reasonably well. The damaged core increases the impedance of the honeycomb core to the ultrasonic waves and, thus, can be detected. The through-thickness distribution of the core damage may be characterized by the maximum crush depth of the core Δ_{CRUSH}. This damage metric is of particular importance in analytical models for predicting residual strength of impact-damaged sandwich panels. The damaged core within the crushed region will offer no reaction to the facesheet under subsequent in-plane loads, until the indentation depth increases by Δ_{CRUSH}. The ratio of planar damage size ($2R_{damage}$) to the maximum crush depth (Δ_{CRUSH}) will, in general, depend on the impactor size, facesheet stiffness and the transverse compressive behavior of the core. Additional destructive sectioning of impact-damaged sandwich panels will be necessary to characterize the effects of facesheet stiffness and core properties on the core crush depths associated with planar damage size.

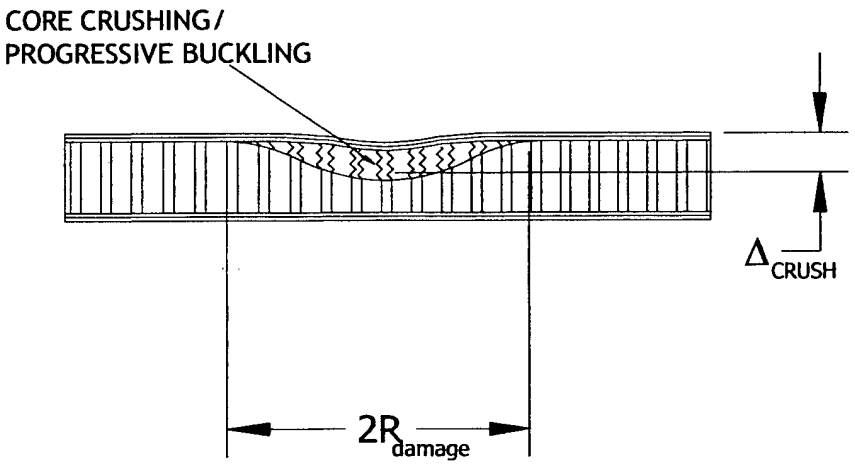

FIGURE 2-12. ILLUSTRATION OF CORE DAMAGE AND ASSOCIATED DAMAGE METRICS FOR HONEYCOMB CORE SANDWICH PANELS

2.2.3 Residual Indentation.

The material damage states in sandwich panels were confined to the facesheet and the core only. However, due to the structural interaction between the (damaged) components of the sandwich panels, a geometric imperfection exists in impact-damaged sandwich panels. The geometric imperfection manifests as a residual indentation distribution as illustrated in figure 2-13. The residual indentation distribution is characterized by the maximum residual indentation, Δ_{RMAX}, occurring at the center of the indentation region (point of impact) and the planar size, $2R_{ind}$, of the region of nonzero residual indentation. The residual indentation distribution exists because of the residual tensile reaction force offered by the damaged core [9]. During the loading phase, the core reaction will tend to resist the collapsing of the facesheet into the core. Upon unloading,

the facesheet tends to spring back to its original undeformed state. However, the damaged core suffers a permanent set in compression and, thus, will generate a tensile reaction force opposing the spring-back action of the facesheet. A residual tensile core traction field [9] will thus exist at the facesheet-core interface, equilibrating the bending moments generated in the facesheet due to residual indentation distribution. The Δ_{RMAX}, for a given planar damage size of the core $2R_{damage}$, will depend on the facesheet stiffness and the degraded tensile properties of the damaged core. The preceding argument is consistent with the experimental observations reported in reference 3, where the thicker-skinned sandwich panels suffered smaller residual indentations in spite of large planar damage areas. Also, a core that fractures under the impact loads will provide no tensile resistance to the facesheet spring back, further reducing the residual indentation and making it difficult to detect damage visually. The damage metrics associated with the sandwich components, quantification methods, and associated degraded properties are summarized in table 2-1.

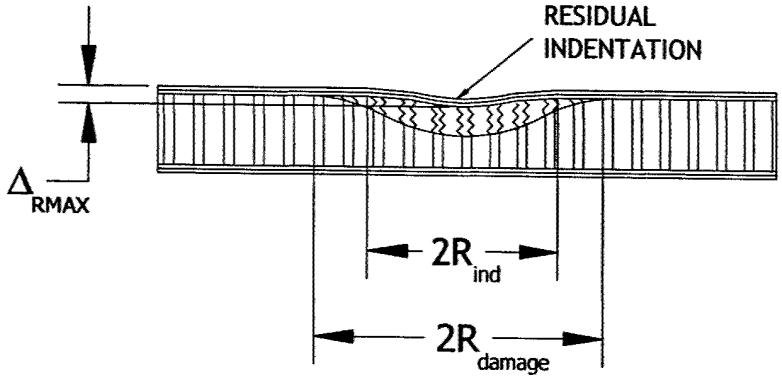

FIGURE 2-13. RESIDUAL INDENTATION IN IMPACTED SANDWICH PANELS

TABLE 2-1. SUMMARY OF DAMAGE METRICS AND ASSOCIATED DEGRADED PROPERTIES

Sandwich Component	Damage Metric(s)	Measurement Method	Degraded Properties	Comments
Facesheet	Planar facesheet damage size $2R_{skin}$	Visual, Destructive sectioning	Facesheet stiffness (flexural)	Region not necessarily circular
Core	Planar core damage size $2R_{damage}$	NDI	Transverse properties of core	Region not necessarily circular
	Maximum Core Crush depth Δ_{CRUSH}	Destructive sectioning		
Facesheet	Maximum residual indentation Δ_{RMAX}	Coordinate measurement machine	N/A	Region not necessarily circular
	Planar size of residual indentation region $2R_{ind}$			
Interface	Residual traction field on facesheet due to damaged core	Analytical model	N/A	N/A

2.3 EFFECTS OF PANEL CURVATURE.

The damage resistance and tolerance investigations for sandwich panels investigated previously have been mostly limited to flat panels. However, the real airframe structures are not necessarily flat, and certain curvatures are associated with their geometry as dictated by the aerodynamic design. Thus, it would be important to understand the effects of panel curvature on the impact response and associated impact damage metrics in sandwich panels. In this study, a limited experimental investigation was conducted to observe the effects of curvature on the damage resistance of cylindrical sandwich panels. The specimen geometry, specimen fabrication, test fixturing, and summary of test results are reported in detail in reference 6. A typical specimen showing the related geometric parameters is shown in figure 2-14.

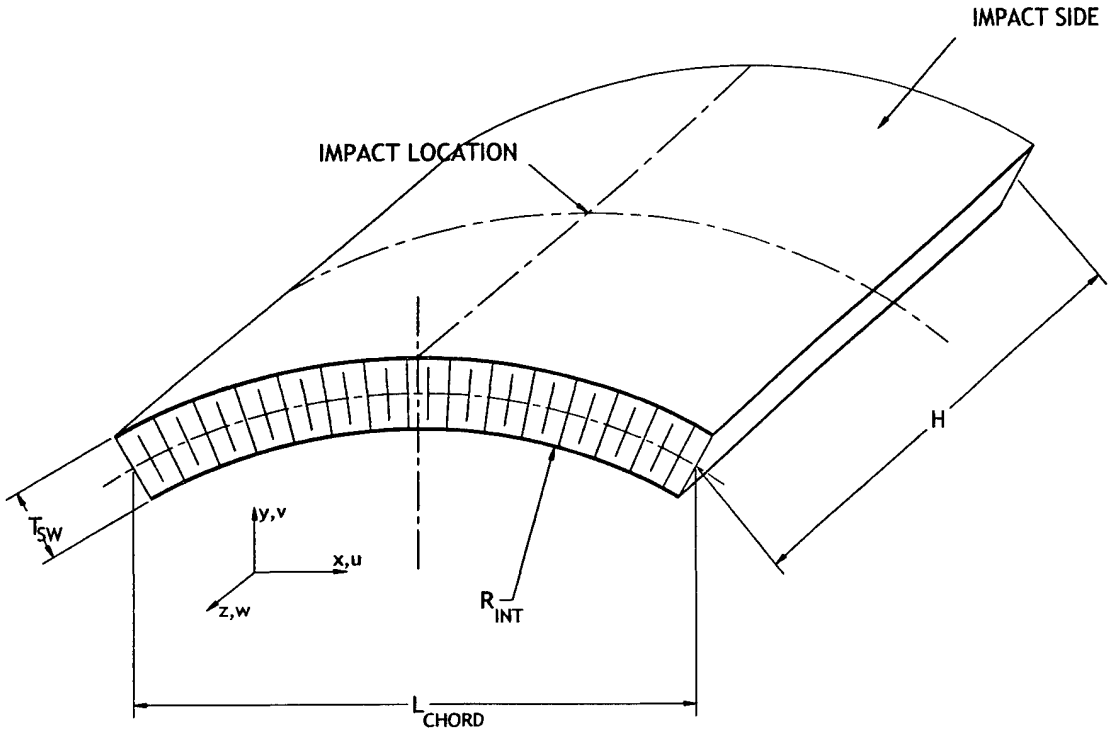

FIGURE 2-14. GEOMETRY OF CYLINDRICAL SANDWICH PANELS AND ASSOCIATED NOMENCLATURE

Three internal radii of curvature of R_{INT1} = 6.00″, R_{INT2} = 24.00″, and R_{INT3} = 48.00″ were used for the specimens in this investigation. The above radii are representative of different locations on a general aviation airframe. The internal radius was controlled as it formed the tool side of the sandwich specimen during the fabrication process. Thus, the external radius (R_{INT} + T_{SW}) was not constant across different sandwich configurations.

The cylindrical sandwich specimens were impacted on the convex side at their respective geometric centers. The specimens were supported along their longitudinal edges using three different boundary supports with varying degrees of end fixity. The boundary conditions investigated in this study are illustrated in figure 2-15.

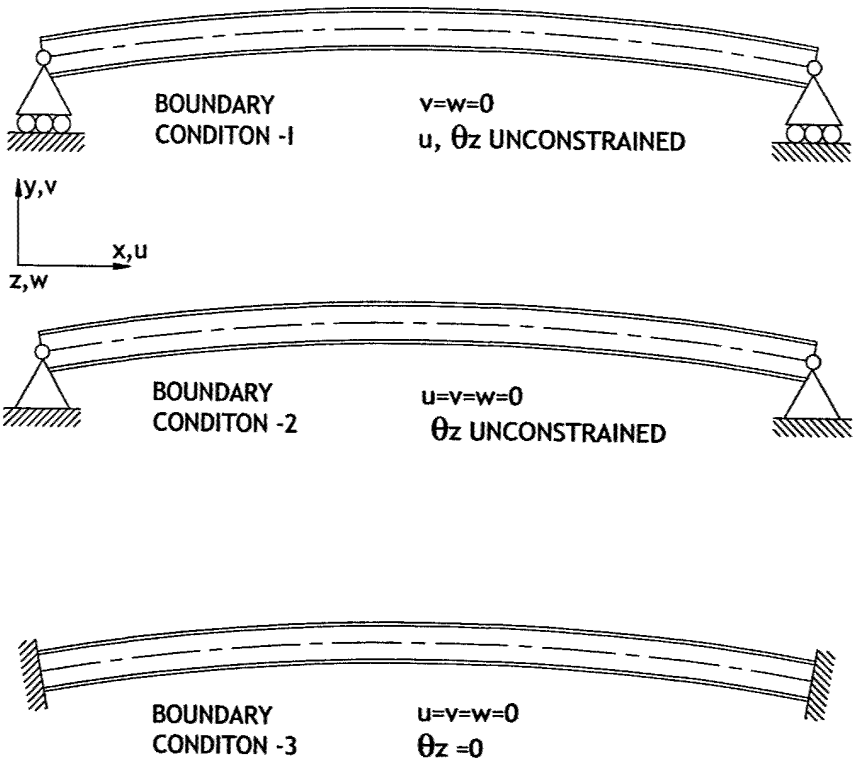

FIGURE 2-15. BOUNDARY SUPPORT CONDITIONS USED DURING IMPACT TESTING OF CYLINDRICAL SANDWICH PANELS

The three boundary conditions were used to simulate the adjoining structure in an actual airframe. The sandwich specimens are free to translate and rotate at the boundaries under boundary condition-1. Boundary condition-2 allows free rotation at the ends but constrains the translations, while boundary condition-3 simulates a rigid adjoining structure. The three boundary conditions will generate different levels of flexural stiffnesses in the curved panels. The edges along the width are, however, unconstrained in all the three cases. In this study, boundary condition-1 was used for all sandwich configurations, while boundary conditions-2 and -3 will be used in a limited number of tests to observe the boundary constraint effects.

2.3.1 Impact Event Characterization.

The impact responses of curved sandwich panels were influenced by their curvature, boundary condition type, impactor size, and core density. The typical impact responses of $[(90/45)_2/\text{CORE}]_s$ sandwich panels with nominal internal radii of 6″, 24″, and 48″ at comparable energy levels are shown in figure 2-16. The specimens were tested under boundary condition-1 with an impactor diameter of 3.00″. At an energy level of 40 lbf-in, the peak impact force increases with decreasing R_{INT}, which can be attributed to the higher flexural stiffness associated with the specimen with smaller R_{INT}.

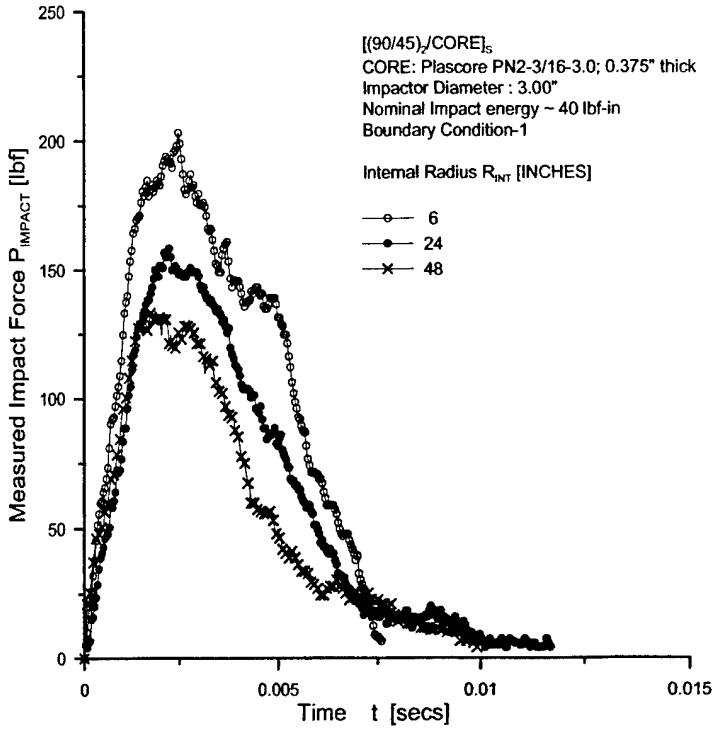

FIGURE 2-16. IMPACT RESPONSES OF $[(90/45)_2/CORE]_s$ SANDWICH PANELS WITH DIFFERENT INTERNAL RADIUS R_{INT} AT NOMINAL IMPACT ENERGY OF 40 lbf-in

The effects of boundary constraint on the peak impact force recorded during the impact tests for $[(90/45)/CORE]_s$ and $[(90/45)_2/CORE]_s$ sandwich panels are shown as an example of the results in figure 2-17. The stiffening effect of constraining the translation of the supports (boundary condition-2) is evident from this figure. However, no significant differences were observed between boundary conditions-2 and -3. This implies that constraining the rotation and the translation does not increase the bending stiffness of the curved panels' significantly.

The aforementioned results have been presented for the 3.00″ diameter impactor only. However, tests were also conducted with the 1.00″ diameter impactor. The curved sandwich panels suffered skin fractures at relatively low energy levels when impacted with the 1.00″ diameter impactor. The impactor size and the curvature of the sandwich panels limit the region over which the contact loads were distributed. The smaller contact regions lead to an early skin fracture initiation. The planar damage size was saturated with the initiation of skin fracture and no trends could be observed for the range of impact energies investigated with the 1.00″ diameter impactor.

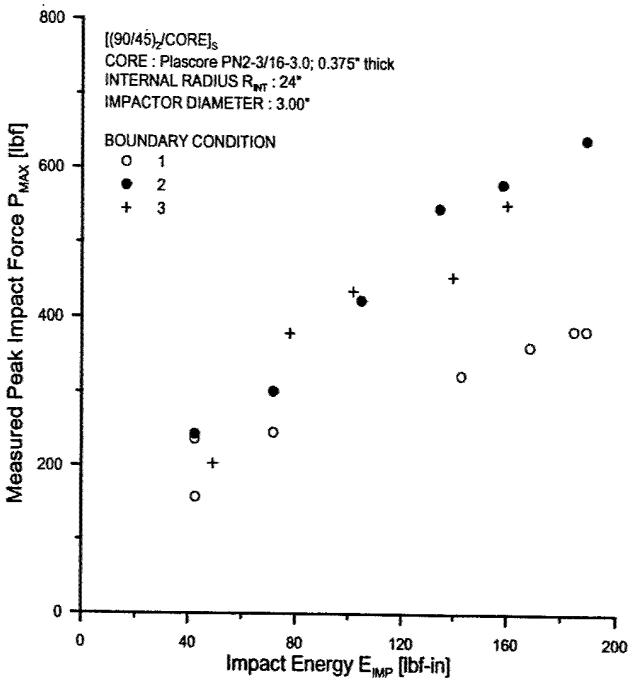

FIGURE 2-17. PEAK IMPACT FORCE AT VARIOUS ENERGY LEVELS FOR $[(90/45)_2/CORE]_s$ SPECIMENS WITH DIFFERENT BOUNDARY CONDITIONS

2.3.2 Damage Characterization.

The impacted sandwich panels were inspected for any impact damage using TTU C-scan, and the maximum residual indentation was measured using the setup described in reference 3. The TTU C-scan was used to quantify the planar damage area, which corresponds to the planar extent of core damage [3]. The effects of panel curvature on the planar damage area created in $[(90/45)/CORE]_s$ and $[(90/45)_2/CORE]_s$ sandwich panels are summarized in figures 2-18 and 2-19, respectively. The planar damage area was observed to increase the decreasing R_{INT}. This can again be attributed to the reduced core strength because of the alignment of the cell walls along the radial direction [6]. The end of the cell walls at their interface with the impacted skin will experience a component of shear in addition to the normal forces. This shear component was instrumental in reducing the transverse compressive strength of the core. Thus, in a specimen with smaller R_{INT}, the core adjacent to the point of impact will experience a higher shear component leading to a low failure strength of the core, and for the case of a blunt impact, the increase in curvature will create a larger damage area as compared to that of a flat panel.

In contrast to the planar damage area, the maximum residual indentation depths decreased with increasing internal radius R_{INT} under the case of blunt impacts. Unlike flat panels [3], the curved panels did not suffer appreciable permanent residual indentations. It can be observed from the experiments [6], that the maximum residual indentations rarely exceed the nominal ply thickness (0.008″) of the facesheet material. In addition, the residual indentations for $R_{INT} = 48″$ are consistently higher compared to $R_{INT} = 6″$ and 24″. This is in contrast to the impact damage due to the 1.00″ impactor, which were predominantly facesheet fractures associated with large indentation depths.

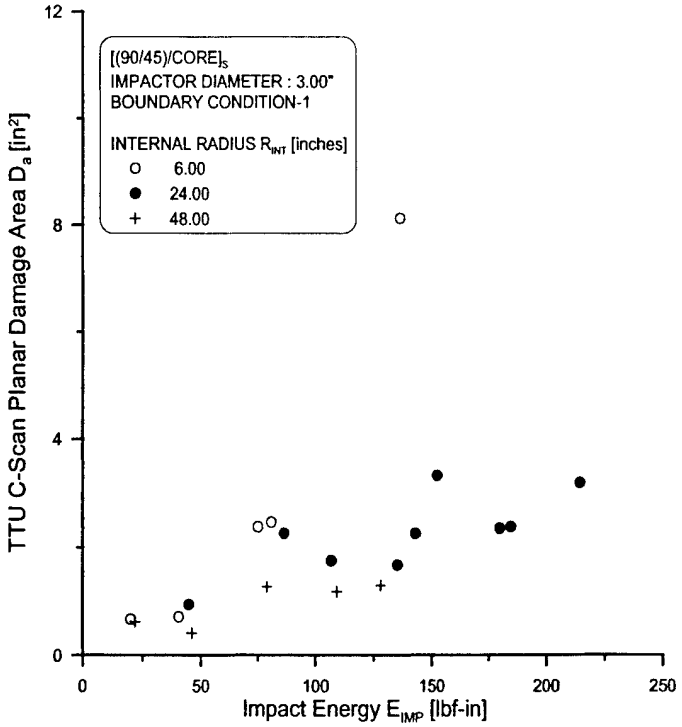

FIGURE 2-18. PLANAR DAMAGE AREA FOR $[(90/45)/CORE]_s$ SANDWICH PANELS WITH DIFFERENT INTERNAL RADII R_{INT}

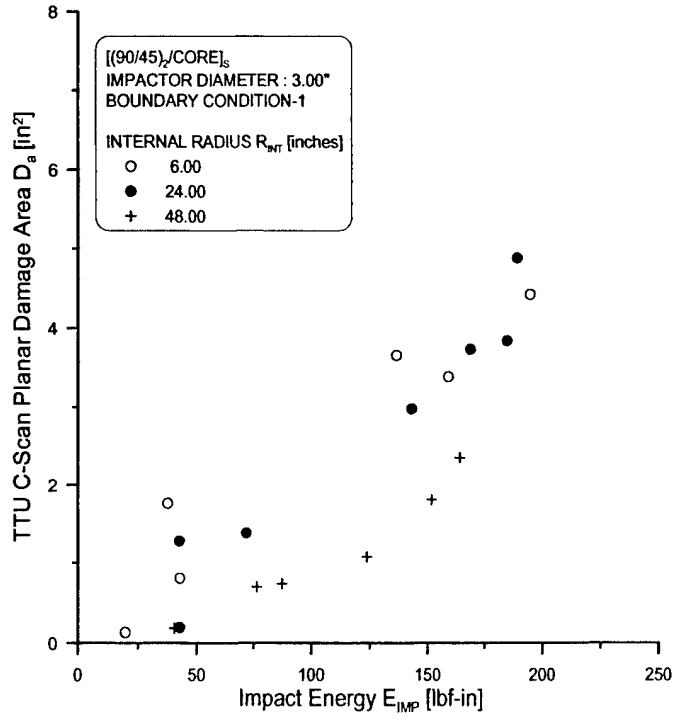

FIGURE 2-19. PLANAR DAMAGE AREA FOR $[(90/45)_2/CORE]_s$ SANDWICH PANELS WITH DIFFERENT INTERNAL RADII R_{INT}

The low residual indentations in curved sandwich panels can be attributed to the high restoring force associated with the curved facesheets. The facesheets collapse on the core during the loading phase, creating damage in the core. During unloading, the facesheet tends to pull itself back to its undeformed position [9], while the core tends to pull it down, creating the residual indentation. In curved panels, the moments generated in the skin are higher compared to that of the flat panels and, thus, relatively low indentations will be observed. From a damage tolerance point of view, the use of a visual inspection method to detect damage will be more difficult for sandwich structures with curvatures, when impacted with larger diameter (blunt) impactors. However, the impact damage states due to smaller impactors will be more conspicuous because of the presence of skin fractures.

The residual strength of the curved specimens and damage growth characteristics were not characterized in these investigations. Future work should incorporate these curvature aspects into residual strength full-scale components and/or subcomponents experiments.

2.4 REPEATED LOADING EFFECT.

The behavior of impact-damaged sandwich panels under the action of repeated loads was also investigated experimentally. The impact damage states due to the 3.00″ diameter impactor was of particular interest because of the high degradation of residual strengths associated with such damage states and also the difficulties in detecting them using nondestructive inspection. The fatigue lives associated with different levels of impact damage in both honeycomb core and foam core sandwich panels were studied. The details of the various aspects of the fatigue-testing program are reported in detail in reference 6.

The impact damage states selected for repeated loads study correspond to two distinct regions of the residual strength degradation curve illustrated in figure 2-20. The data corresponds to sandwich specimens impacted with a 3.00″ diameter impactor at different energy levels. The lower energy level (E_1) corresponds to the knee region of the curve, where the normalized residual strength (NCAI) ranges between 0.8 to 0.6 (typical), and the higher energy level (E_2) corresponds to the asymptote of the curve, where the NCAI is about 0.5 or lower (typical). The damage states corresponding to these energy ranges was purely subsurface (core) damage with no visible skin damage. The typical damage areas corresponding to these energy levels are shown in figure 2-20.

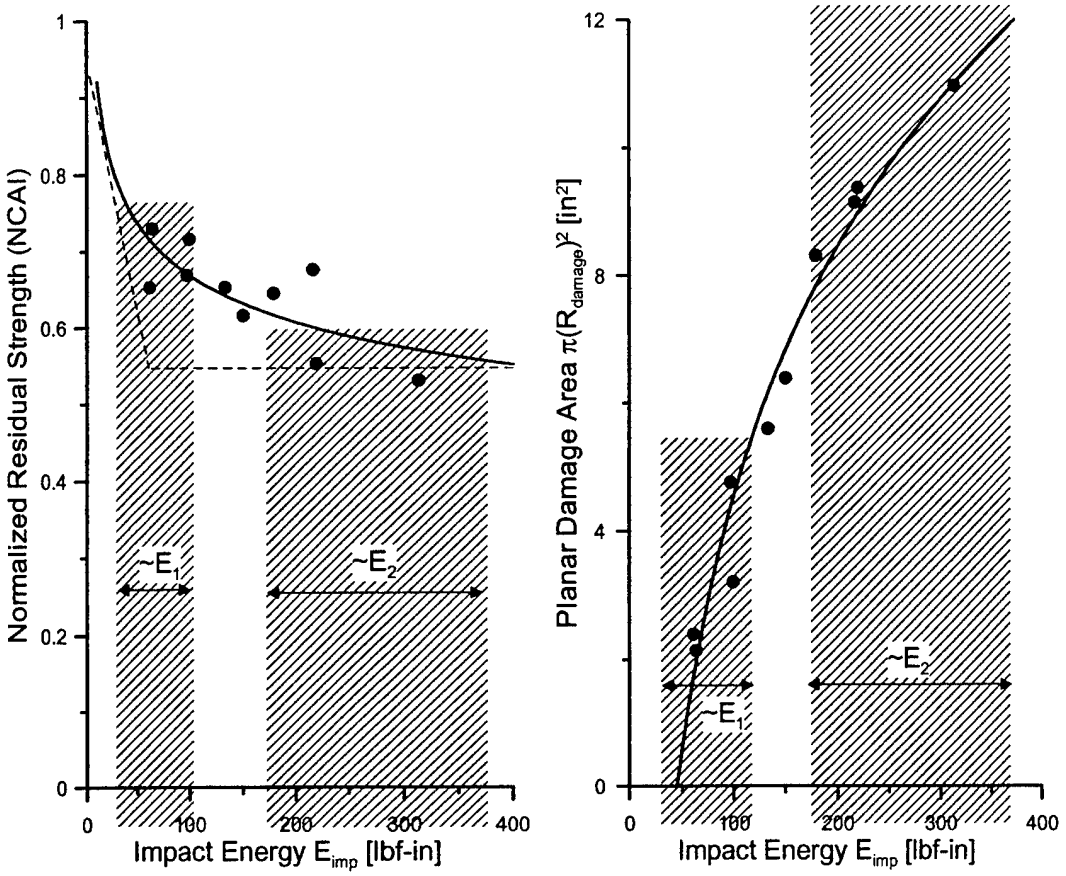

FIGURE 2-20. TYPICAL RANGES OF IMPACT ENERGY LEVELS FOR FATIGUE PROGRAM

The fatigue-testing program was divided into three phases.

- The first phase consisted of the generation of the static residual strength data for sandwich panels impacted with different impact energy levels. The characteristic residual strength degradation curve (curve fit) was then analyzed to select two candidate impact energy levels (E_1 and E_2) for use in the fatigue program.

- In the second phase, the experimental data from the residual strength test of the specimens impacted with the candidate energy levels was analyzed to select the stress/load* levels (N_{yy}) for the generating the fatigue loads.

- The third phase consisted of the fatigue testing of the impact-damaged sandwich specimens, monitoring of damage growth, and residual strength testing of specimens that successfully completed the predefined infinite life N_∞ and to assess any further degradation in residual strength. Details of the program are presented in reference 6.

*The residual strengths were expressed in terms of the stress resultants N_{yy} (lbf/in) rather than the stress σ_{yy}. Thus, throughout this report, the word load rather than stress will be associated with the nomenclature for defining the fatigue tests, e.g., stress ratio will be referred to as the load ratio.

Since the fatigue life of the impact-damaged sandwich specimen was not known a priori, the load levels selected were only initial estimates. The loads were increased or decreased appropriately to introduce failures or runouts (i.e., survive N_∞) to obtain meaningful data.

2.4.1 Fatigue Life.

The sandwich specimens were subjected to fatigue loading using the load levels and load ratios defined in reference 6. The number of cycles to failure, N_f, at each load level and load ratio combination was recorded. The specimens surviving N_∞ (=150,000) cycles were subsequently tested to failure under static loading to assess any further degradation in residual strength. The plots of the fatigue life at different minimum load levels for the sandwich configurations are shown in figures 2-21 to 2-24. The figures indicate the static strength of the virgin specimen and the static residual strength of a similar specimen prior to fatigue loading. The following observations were made regarding the fatigue life of sandwich specimens at different load levels.

- A fatigue life curve (S-N curve) could not be generated due to the limited data set. The model fitting procedure presented by Sendeckyj [11] requires a minimum of (m+2) uncensored (i.e., not a runout) data points at (m+1) stress levels, where m is the number of parameters for the fatigue model. Thus, if a two-parameter model was used at every stress level, at least four uncensored data points would be required.

- The fatigue life at higher load levels exhibited dependence on the load ratio. The fatigue life decreased when the load ratio was increased. It is speculated that at higher load ratios, the damaged core may experience a transverse tensile stress field, which could lead to core fracture.

- The change in compliance associated with the end-shortening was insignificant for load levels at which the specimens lasted 150,000 cycles. Since most specimens that did fail before N_∞ had $N_f < 75{,}000$ cycles, the compliance test interval (25,000) was too large to obtain enough data points to draw meaningful conclusions regarding compliance changes. Selected tests may need to be repeated to monitor the compliance changes at smaller intervals.

- The TTU C-scan inspection of honeycomb core sandwich panels did not indicate a significant increase in damage size ($2R_{damage}$). Additional destructive tests at shorter intervals may be necessary to observe the growth of core damage across the thickness of the specimen.

- The growth of skin damage (delaminations), discussed previously, could not be observed for carbon facesheets (honeycomb core panels). The decrease in fatigue life may be a combined effect of growths in skin and core damage states. The skin damage growth, if any, may be observed by using sandwich panels with fiberglass facesheets.

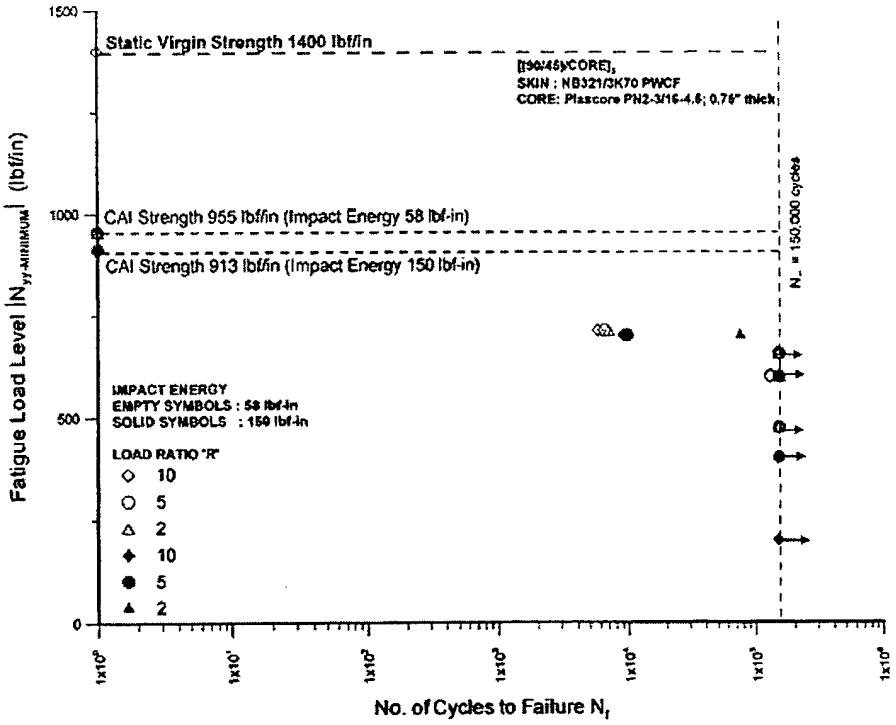

FIGURE 2-21. FATIGUE LIFE DATA FOR $[(90/45)/CORE]_s$ SANDWICH PANELS WITH HONEYCOMB CORE

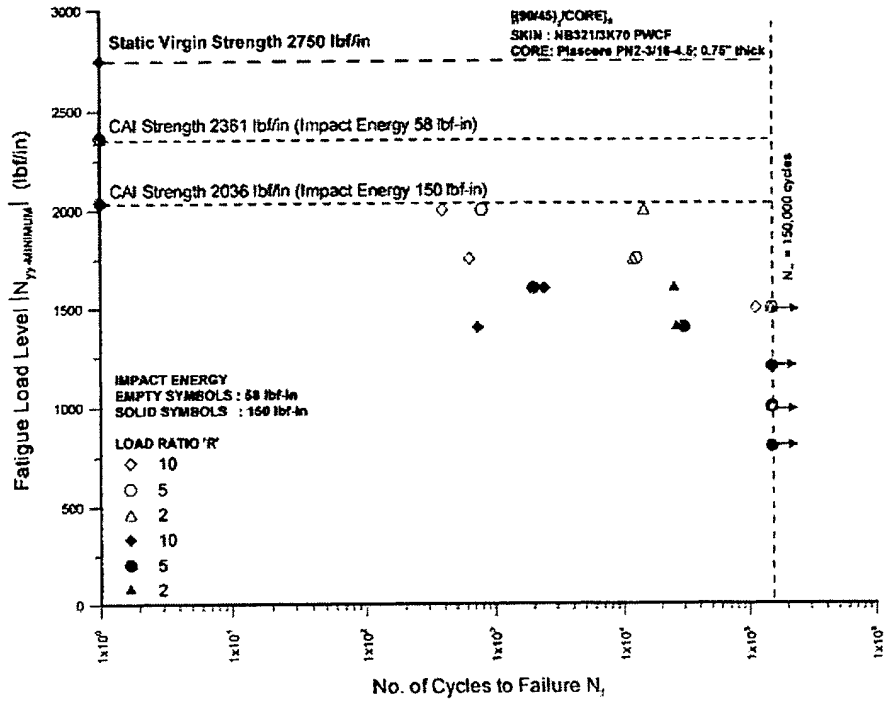

FIGURE 2-22. FATIGUE LIFE DATA FOR $[(90/45)_2/CORE]_s$ SANDWICH PANELS WITH HONEYCOMB CORE

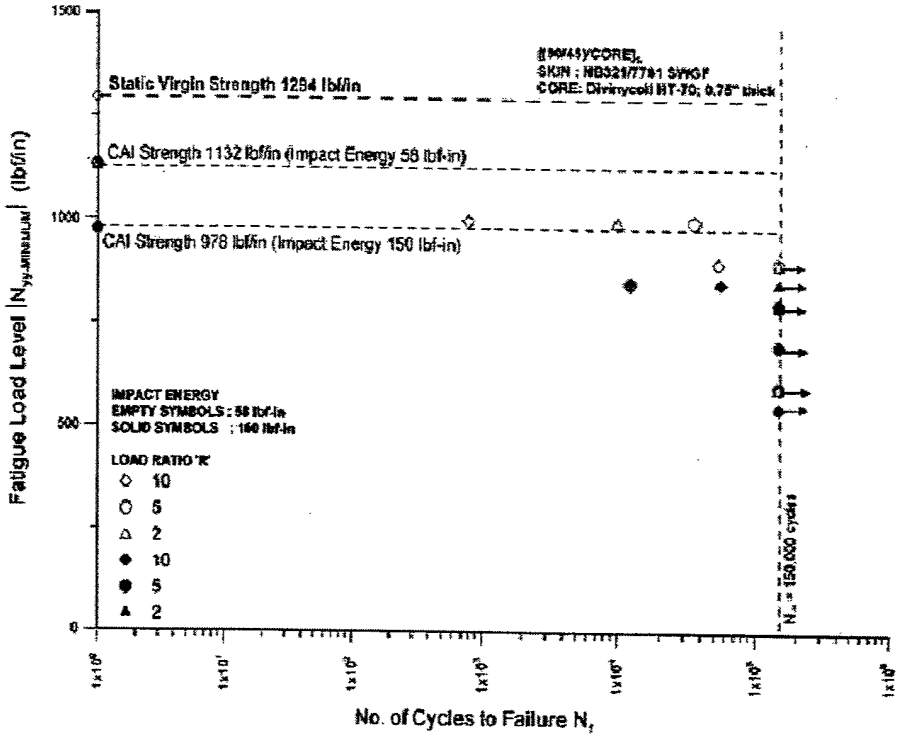

FIGURE 2-23. FATIGUE LIFE DATA FOR $[(90/45)/CORE]_s$ SANDWICH PANELS WITH FOAM CORE

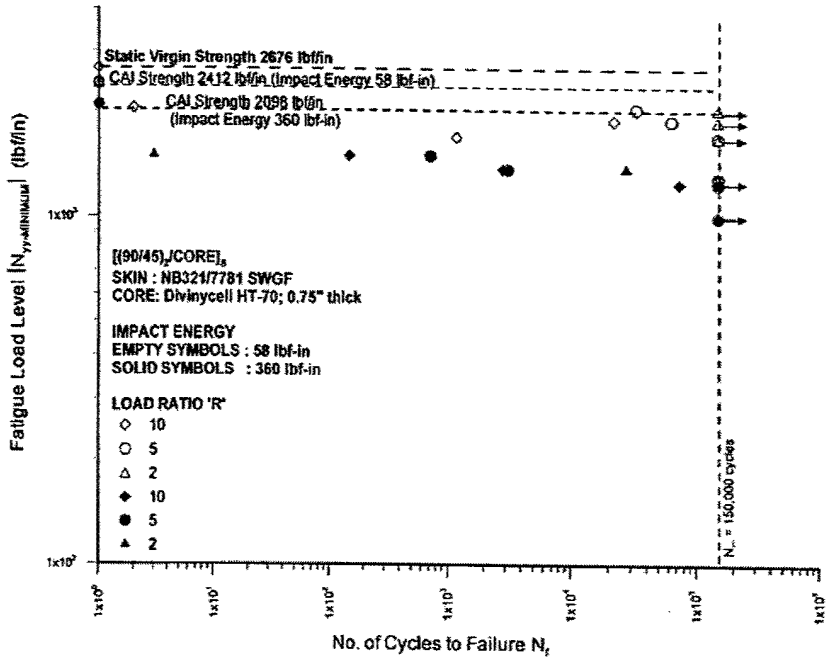

FIGURE 2-24. FATIGUE LIFE DATA FOR $[(90/45)_2/CORE]_s$ SANDWICH PANELS WITH FOAM CORE

2.4.2 Residual Strength Degradation.

The degradation of residual strength of sandwich specimens due to fatigue loading was determined by conducting static residual strength tests on the specimens surviving N_∞ cycles (runout). The residual strength degradation was defined in terms of a normalized runout residual strength defined below.

$$\text{Normalized Runout Residual Strength} = \frac{N_{yy\text{-}\infty}}{N_{yyRS\text{-}E_i}}$$

where, $N_{yy\text{-}\infty}$ is the minimum load level at which the specimen survived N_∞ , and $N_{yyRS\text{-}E_i}$ is the static residual strength of the sandwich specimen impacted with impact energy level E_i (i=1,2). The normalized runout residual strengths were further plotted versus a normalized minimum load level defined as follows.

$$\text{Normalized Minimum Load Level} = \frac{N_{yy\text{-MINIMUM}}}{N_{yyRS\text{-}E_i}}$$

The plots of normalized runout residual strength versus normalized minimum load levels for the sandwich configurations investigated are shown in figures 2-25 to 2-28. The data points lying on the x axis indicate that the specimens did not survive N_∞ at that particular load level. Based on the experimental data, the following observations were made.

a. $[(90/45)/CORE]_s$ panels with honeycomb core (see figure 2-25)

1. For impact energy level E_1, no significant degradation was observed for the minimum load between 50% and 70% (approx.) of the static residual strength (the specimen corresponding to a minimum load level of ~62% of static residual strength failed under fatigue loading). Some of the specimens exhibited an anomalous increase in residual strength (e.g., see figure 2-26), which can be attributed to generating residual strength data using a single specimen at each energy level. A scatter in data is implied based on the above observation.

2. For impact energy level E_2, no significant degradation was observed for minimum load levels between 20% and 70% (approx.) of the static residual strength for load ratios of 5 and 2. However, for the load ratio of 10, the degradation in residual strength increased from 0% to 20% when the minimum load in fatigue was increased from 20% to 70% of the static residual strength.

b. $[(90/45)_2/CORE]_s$ panels with honeycomb core (see figure 2-26)

1. For impact energy level E_1, average degradation in residual strength of 10% was observed for load levels less than 50% (R=10), 65% (R=5), and 70% (R=2) of the static residual strength.

2. For impact energy level E_2, average degradation in residual strength up to 15% was observed for load levels less than 60% (all load ratios) of the static residual strength.

c. $[(90/45)/CORE]_s$ panels with foam core (see figure 2-27)

1. For impact energy level E_1, no significant degradation in residual strength for minimum load levels lower than 80% (approx.) of the static residual strength.

2. For impact energy level E_2, the residual strength degradation was observed to be negligible at all stress levels less than 80% (approx.) of the static residual strength, for load ratios of 10 and 2. A degradation of about 18% was observed for a minimum fatigue load level corresponding to 70% of the static residual strength when the load ratio was 5.

d. $[(90/45)_2/CORE]_S$ panels with foam core (see figure 2-28)

1. For impact energy level E_1, an average degradation of 5% was observed for minimum load levels lower than 90% (approx.) of the static residual strength and a load ratio of 2. When the load level was about 55% of the static residual strength, an average degradation of 10% was observed at all three load ratios.

2. For impact energy level E_2, an average degradation of 30% was observed for minimum load levels lower than 60% (approx.) of the static residual strength at all load ratios.

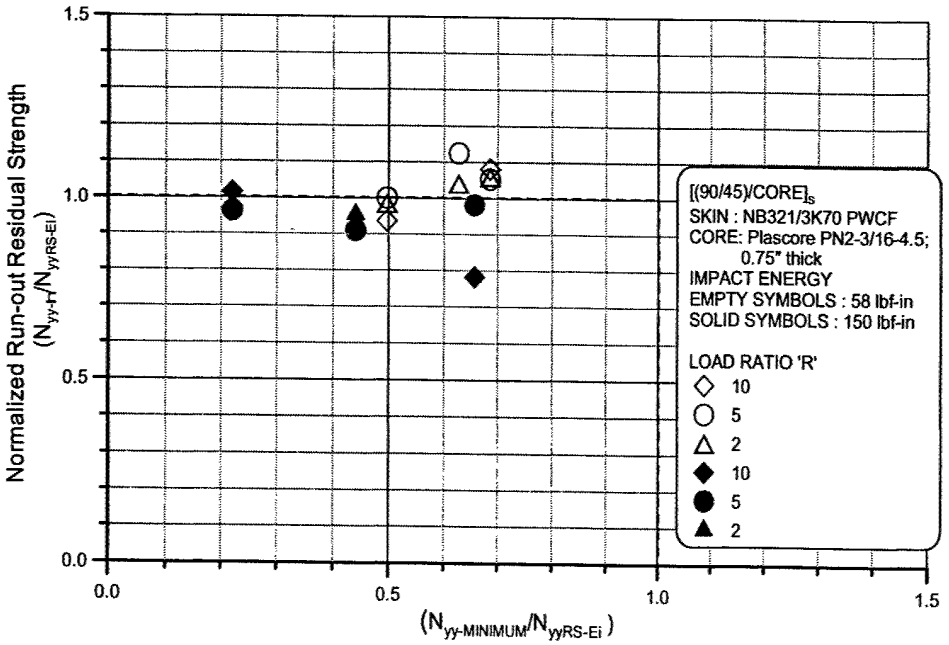

FIGURE 2-25. RESIDUAL STRENGTH DEGRADATION FOR $[(90/45)/CORE]_s$ SANDWICH PANELS WITH HONEYCOMB CORE

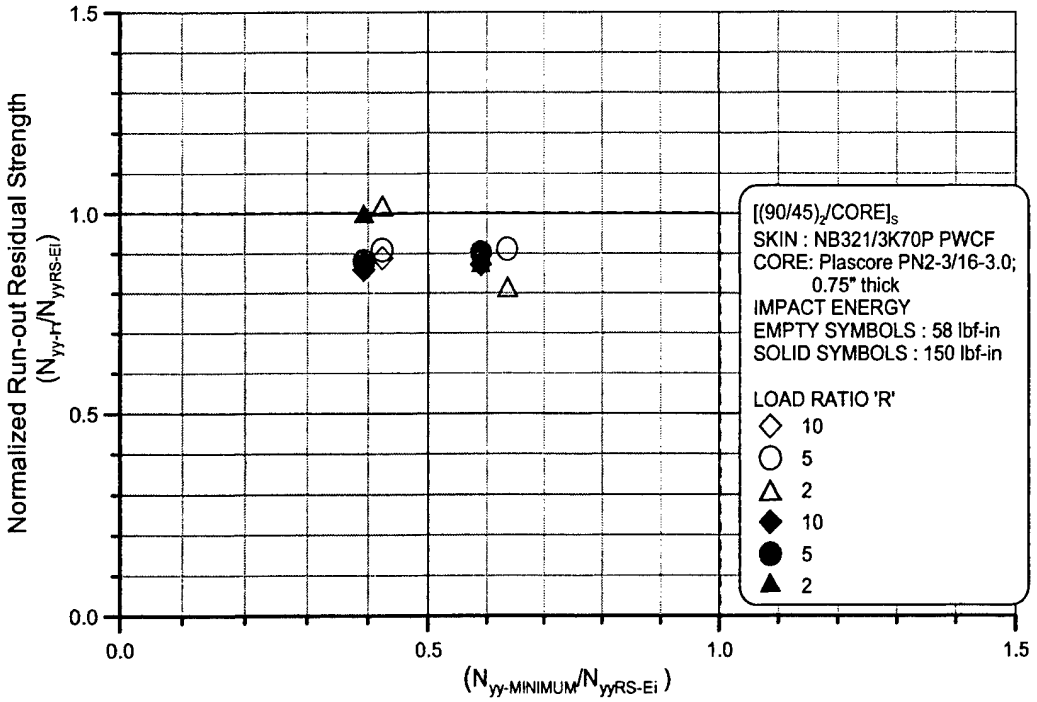

FIGURE 2-26. RESIDUAL STRENGTH DEGRADATION FOR [(90/45)$_2$/CORE]$_S$ SANDWICH PANELS WITH HONEYCOMB CORE

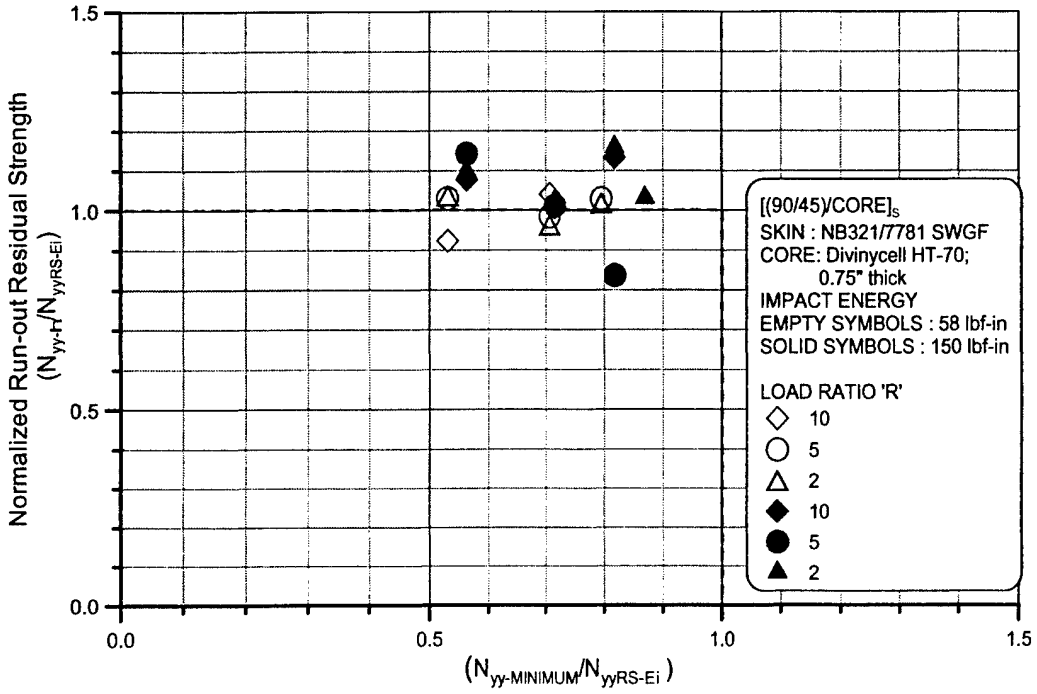

FIGURE 2-27. RESIDUAL STRENGTH DEGRADATION FOR [(90/45)/CORE]$_S$ SANDWICH PANELS WITH FOAM CORE

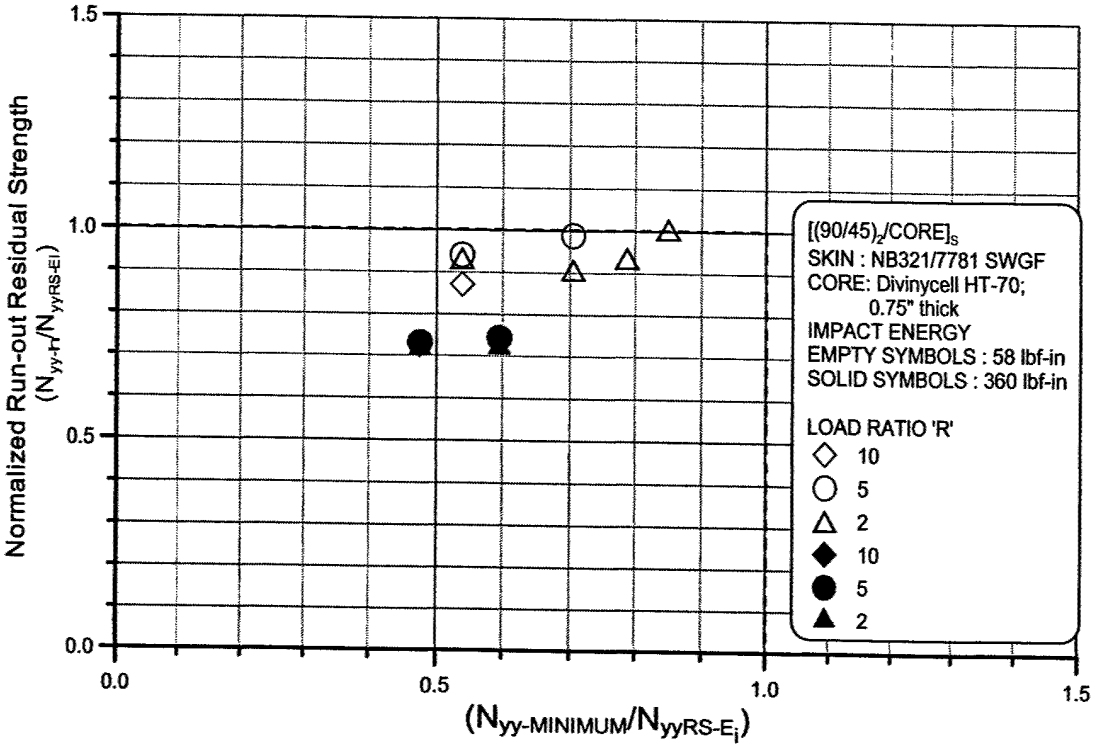

FIGURE 2-28. RESIDUAL STRENGTH DEGRADATION FOR $[(90/45)_2/CORE]_s$ SANDWICH PANELS WITH FOAM CORE

2.4.3 Summary.

The fatigue life and residual strength degradation of honeycomb and foam core sandwich panels were experimentally investigated. The sandwich panels were damaged by impacting them with a 3.00″ diameter impactor at two different energy levels. The fatigue life of the sandwich specimens were found to be dependent on the load ratio of the fatigue load. The fatigue life decreased as the load ratio was increased at certain minimum fatigue load levels. Further degradation of the residual strength, ranging between 5% and 30%, was typical of sandwich specimens that survived the prespecified infinite life of 150,000 cycles. Additional tests may be necessary to statistically strengthen the observed trends.

3. RESPONSE SURFACES.

Response surfaces for damage resistance and damage tolerance of sandwich structure were formulated using the test data generated by this program. The methodology that was used was the Box-Behnken method [12] that was fully described in reference 4. The purpose of this research was to allow a designer or a stress engineer to estimate the damage caused by an impact and the effect of damage on the residual compression strength on honeycomb sandwich structure. This type of information is needed in the design and certification process and should be useful in narrowing and reducing testing. The variables from which the response surfaces were constructed reflected sandwich configuration parameters (facesheet ply thickness, core density, and core height) and impactor parameters (impactor diameter, impact energy, and velocity). The damage parameters were surface and internal damages.

3.1 DAMAGE RESISTANCE.

The objective was to obtain empirical values of damage in terms of dent depth and internal damage diameter as a function of the main damage resistance drivers. Thus, the response surfaces, derived as algebraic equations in terms of these parameters, can then be used as input into analysis to predict damage growth and/or residual strength.

In this study, symmetric flat composite sandwich panels comprised of plain-weave carbon fabric preimpregnated in epoxy resin (NEWPORT NB321/3K70P) facesheets and Plascore Nomex honeycomb (PN2-3/16-3.0/4.5/6.0) cores (test section dimensions, 8.0 by 8.0 in.) with clamped edges were subjected to drop-weight normal impact with a spherical steel impactor. Three different facesheet configurations (X_1 = 2 plies $[90/45]_1$, 4 plies $[90/45]_2$, and 6 plies $[90/45]_3$), core densities (X_2 = 3.0, 4.5, and 6.0 lb/ft^3), and core thicknesses (X_3 = 3/8, 3/4, and 9/8 in.) were considered in this examination. The ranges of laminate and core variables are typical of those found in common sandwich panel applications. In addition, three different impact energies (X_4 = 90.0, 120 and 150 lbf-in), impactor diameters (X_5 = 1.0, 2.0, and 3.0 in.), and impact velocities (X_6 = 65.2, 96.3, and 127 in/sec) were considered in this study. The impact parameters correspond to typical low-velocity impacts associated with relatively blunt objects. Note that each sandwich configuration and impact variable, X_i (i = 1, 2,.., 6), assumes low, symmetric midrange or center point, and high values; these may be collectively referred to as the natural values of the independent variables used in this study. Table 3-1 summarizes the range of sandwich configuration and impact parameters considered in this effort. In addition, the facesheet thickness may be characterized in terms of the number of plies (two, four, and six) associated with each facesheet configuration. The test matrix developed for this investigation is based on the Box-Behnken fractional factorial design of experiments technique, which uses the minimum number of tests required for generating a second-order, statistically reliable, polynomial expression characterizing the response function of interest (e.g., damage size) [12].

TTU C-scan and facesheet indentation measurements were used as damage metrics to characterize the degree of impact damage induced in the sandwich panels. TTU C-scan measurements provide a two-dimensional image of the projected area of the impact-damaged region. The damaged region may be characterized either in terms of the area of the C-scan image or in terms of the diameter of the damaged region, D, measured normal to the direction of

the applied CAI load. For this study, damage diameter, D, was selected because it well represented the crushing circumference of the core.

TABLE 3-1. SANDWICH CONFIGURATION AND IMPACT PARAMETERS

		Natural Values		
Material Variables	Number of Facesheet Plies, X_1	2 [90/45]	4 $[90/45]_2$	6 $[90/45]_3$
	Core Density, X_2 (lb/ft^3)	3.0	4.5	6.0
	Core Thickness, X_3 (in)	0.37	0.75	1.12
Impact Variables	Impact Energy, X_4 (lbf-in)	90.0	120	150
	Impactor Diameter, X_5 (in)	1.0	2.0	3.0
	Impact Velocity, X_6 (in/sec)	65.2	96.3	127

A 3^k fractional factorial design of experiments (DOE) approach [12] has been employed to examine the nonlinear interaction effects between relevant sandwich panel design parameters and their influence on the planar dimension, D, of the damage region and surface dent associated with a given impact event. In order to isolate parameters of interest, three different response surfaces were created.

- The first response surface isolated the coupled effects of skin and core parameters (i.e., number of facesheet plies, X_1; core density, X_2; and core thickness, X_3) on the damage resistance characteristics of sandwich composite panels; the impact energy ($X_4 = 120$ in-lb), impactor diameter ($X_5 = 3.0$ in), and impact velocity ($X_6 = 96.3$ in/sec) were held fixed in this examination.

- The second response surface isolated effects of the number of facesheet plies (X_1), impact energy (X_4), and impactor diameter (X_5) on the damage resistance characteristics of sandwich composite panels. Here, the core density ($X_2 = 3.0$ lb/ft^3), core thickness ($X_3 =$ 3/4 in), and impact velocity ($X_6 = 96.3$ in/sec) were held fixed.

- The third response surface isolated effects of the number of facesheet plies (X_1), impact energy (X_4), and impact velocity (X_6) on the damage resistance characteristics of sandwich composite panels were examined. Here, different impact velocities were obtained by varying the impactor mass and drop height during impact testing leading to a specified value of impact energy.

This effort aimed to help clarify the influence of dynamic effects on the damage resistance properties of the given sandwich composites over a range of relatively low velocity impacts. Here, the core density ($X_2 = 3.0$ lb/ft^3), core thickness ($X_3 = 3/4$ in.), and impactor diameter ($X_5 = 3.0$ in.) were held fixed.

The first quadratic response surface characterizing the diameter of the damage diameter based upon TTU C-scan measurements and dent depth in terms of the composite sandwich panel facesheet thickness (X_1), core density (X_2), and core thickness (X_3) is expressed as

$$\begin{aligned}\hat{D} = &-2.682 + 0.8029 \cdot X_1 + 1.219 \cdot X_2 + 2.576 \cdot X_3 \\ &...- 0.06685 \cdot X_1^2 - 0.08252 \cdot X_2^2 - 0.8990 \cdot X_3^2 \qquad \text{(in.)} \\ &...- 0.03492 \cdot X_1 \cdot X_2 - 0.1200 \cdot X_1 \cdot X_3 - 0.3480 \cdot X_2 \cdot X_3\end{aligned}$$

and

$$\begin{aligned}\hat{d} = &[-36.63 + 1.500 \cdot X_1 + 15.67 \cdot X_2 + 41.33 \cdot X_3 \\ &...- 0.09375 \cdot X_1^2 - 1.278 \cdot X_2^2 - 6.222 \cdot X_3^2 \qquad \text{(in.)} \\ &...- 0.08333 \cdot X_1 \cdot X_2 - 4.333 \cdot X_1 \cdot X_3 - 3.111 \cdot X_2 \cdot X_3] \cdot 10^{-3}\end{aligned}$$

Response surface estimates of the size of the planar damage region show that increasing the thickness of the core material results in the greatest improvement in the damage resistance properties (i.e., the size of the planar region typically associated with core crushing is reduced). Independently increasing the number of facesheet plies and/or core density generally resulted in an increase in the size of the estimated internal damage, although simultaneously varying these parameters could result in either an improvement or degradation in the impact damage resistance properties. It seems reasonable that changes in material system parameters likely result in either enhanced or degraded penetration resistance and bending stiffness properties that govern the damage development. Response surface estimates for the maximum residual facesheet indentation show that increasing the number of facesheet plies results in the greatest decrease in the predicted surface damage. The regression results indicate that those combinations of sandwich configuration parameters leading to the maximum internal damage do not correspond to those that result in the greatest facesheet indentation. The equation for the dent depth did not correlate very well because the measured dent depths for the 3.0-in.-diameter impactor were very small. This equation should be used with caution.

The second response surface for the damage diameter and dent depth is as follows:

$$\begin{aligned}\hat{D} = &4.426 - 0.9876 \cdot X_1 - 1.771 \cdot 10^{-3} \cdot X_4 - 1.662 \cdot X_5 \\ &...+ 0.02103 \cdot X_1^2 - 1.618 \cdot 10^{-4} \cdot X_4^2 + 0.1084 \cdot X_5^2 \qquad \text{(in.)} \\ &...+ 7.333 \cdot 10^{-3} \cdot X_1 \cdot X_4 + 0.06400 \cdot X_1 \cdot X_5 + 0.01103 \cdot X_4 \cdot X_5\end{aligned}$$

and

$$\begin{aligned}\hat{d} = &[386.3 - 168.7 \cdot X_1 + 5.769 \cdot X_4 - 275.8 \cdot X_5 \\ &...+ 9.833 \cdot X_1^2 - 0.01185 \cdot X_4^2 + 37.33 \cdot X_5^2 \qquad \text{(in.)} \\ &...- 0.1583 \cdot X_1 \cdot X_4 + 38.75 \cdot X_1 \cdot X_5 - 0.8167 \cdot X_4 \cdot X_5] \cdot 10^{-3}\end{aligned}$$

In this investigation, the coupled influence of the number of facesheet plies, impact energy, and impactor diameter on the impact damage induced was evaluated using empirically based response surfaces for sandwich composites comprised of carbon/epoxy woven fabric facesheets and Nomex honeycomb cores. The core density, core thickness, and impact velocity were held fixed in this examination. Response surface estimates of the size of the planar damage region show that increasing the impactor diameter results in a decrease in the damage resistance properties (i.e., the size of the planar region typically associated with core crushing is increased). Given that an increase in the planar damage area is often accompanied by a corresponding decrease in residual strength, consideration of various-sized impactors is an important part of developing a damage tolerance plan for sandwich composites. An increase in the number of facesheet plies tended to an increase in the estimated planar damage dimension for a given set of impact parameters. An increase in the impact energy resulted in an increase in the size of the planar damage region for those combinations of facesheet configuration and impactor diameters, where facesheet penetration was likely not a concern. This is illustrated in figure 3-1. Similar plots for other variables are contained in reference 4. Response surface results show that the residual facesheet indentation is a decreasing function of the number of facesheet plies and impactor diameter for a given impact energy level.

The final second-order response surfaces were generated that characterize the impact damage as a function of the number of facesheet plies, impact energy, and impact velocity. An estimate of the diameter of the planar damage region associated with TTU C-scan measurements from the regression analysis is expressed in terms of natural values of the independent variables

$$\begin{aligned}\hat{D} &= 7.516 + 0.1242 \cdot X_1 + 9.073 \cdot 10^{-3} \cdot X_4 - 0.1461 \cdot X_6 \\ &\ldots + 4.292 \cdot 10^{-3} \cdot X_1^2 + 1.796 \cdot 10^{-5} \cdot X_4^2 + 7.306 \cdot 10^{-4} \cdot X_6^2 \qquad \text{(in.)} \\ &\ldots - 8.000 \cdot 10^{-4} \cdot X_1 \cdot X_4 + 1.206 \cdot 10^{-4} \cdot X_1 \cdot X_6 + 2.465 \cdot 10^{-5} \cdot X_4 \cdot X_6\end{aligned}$$

Analogously, an estimate of the maximum residual facesheet indentation from the regression analysis is expressed in terms of natural values of the independent variables

$$\begin{aligned}\hat{d} &= 8.257 \cdot 10^{-3} - 7.372 \cdot 10^{-3} \cdot X_1 + 6.093 \cdot 10^{-3} \cdot X_4 - 4.751 \cdot 10^{-4} \cdot X_6 \\ &\ldots + 9.167 \cdot 10^{-4} \cdot X_1^2 - 6.481 \cdot 10^{-7} \cdot X_4^2 + 4.825 \cdot 10^{-6} \cdot X_6^2 \qquad \text{(in.)} \\ &\ldots - 4.167 \cdot 10^{-6} \cdot X_1 \cdot X_4 - 8.039 \cdot 10^{-6} \cdot X_1 \cdot X_6 - 4.019 \cdot 10^{-6} \cdot X_4 \cdot X_6\end{aligned}$$

These response surface estimates of the size of the planar damage region typically associated with core crushing suggest that the damage development is somewhat sensitive to the velocity of the impactor. Midrange values of impact velocity resulted in damage estimates that were a relative minimum. Similar to earlier results, an increase in the number of facesheet plies and/or impact energy tended to result in an increase in the estimated planar damage dimension for a given set of impact parameters. Response surface results show that the residual facesheet indentation due to impact is also impact velocity dependent. However, as the response surface was constructed on the basis of 3.0-in.-diameter impactor (shallow indents), the validity of this response surface is questionable.

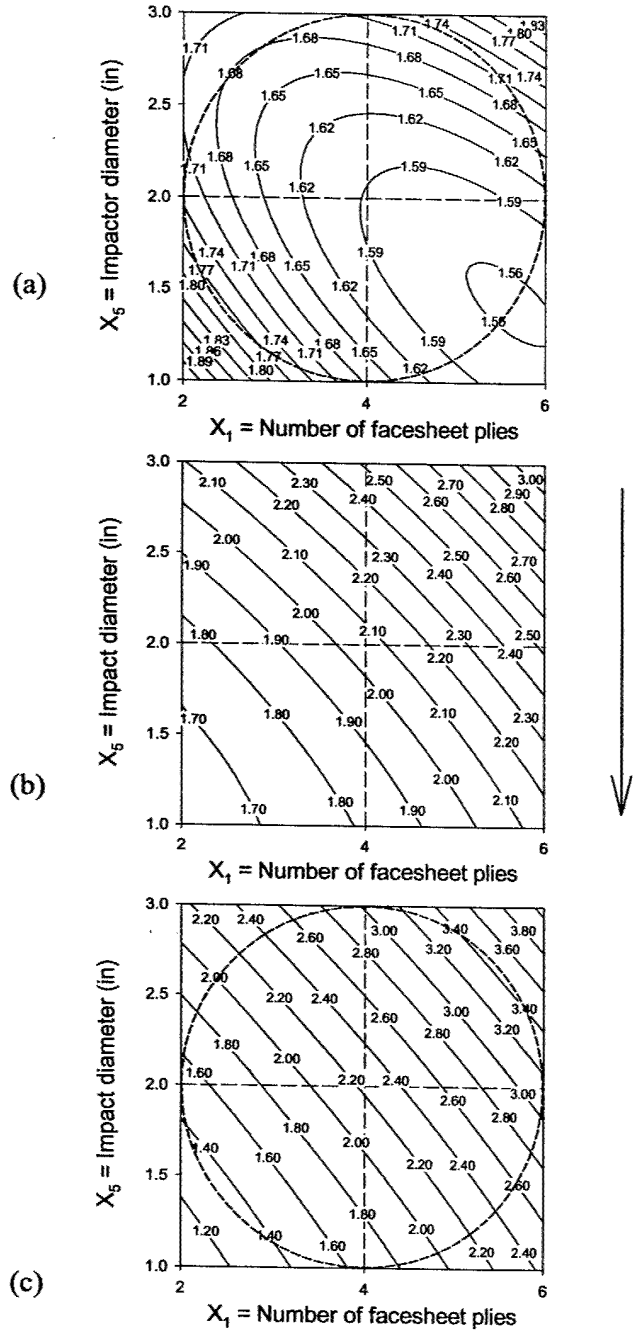

FIGURE 3-1. PREDICTED DAMAGE DIAMETER (in.): (a) $X_4 = 90.0$ in-lb, (b) $X_4 = 120$ in-lb, AND (c) $X_4 = 150$ in-lb

Changes in sandwich configurations can result in either enhanced or degraded penetration resistance and bending stiffness properties that govern the damage formation. Estimates, made using response surface for the maximum residual facesheet indentation show that increasing the number of facesheet plies results in the greatest decrease in the predicted surface damage. While

such estimates did not necessarily correlate well with experimental data for test configurations, with relatively shallow indentations, these estimates may prove useful in determining combinations of material and impact parameters that produce the greatest degree of visible facesheet damage.

In addition, the experimental results and regression analysis suggest that impact damage development in sandwich composites is highly sensitive to the diameter of the impactor, impact energy, and impact velocity. Based upon the response surface estimates, an increase in the diameter of the impactor will result in a significant increase in the planar dimension of the internal damage and a decrease in the residual facesheet indentation, particularly for those sandwich panels with thicker facesheets. This suggests that blunt-object impacts may result in appreciable damage that is not amenable to visual inspection. An increase in the impact energy generally resulted in an increase in the predicted planar damage dimension, with the exception of those combinations of impactor diameter and facesheet configuration where facesheet penetration was a concern. Moreover, response surface results indicate that the damage formation is somewhat sensitive to the velocity of the impactor.

Sandwich panel stiffness properties, energy absorption capability, and support boundary conditions all play a key role in the dynamic impact response leading to damage development. For these reasons, the response surfaces generated here can only provide an initial assessment of the damage sizes that can be expected. Because the response surfaces were generated using relatively small panels, the characterized damage states will tend to be conservative, and the predicted damage will be greater than in a full-scale component. The user of this empirical estimating tool is also cautioned against extrapolation for parameters beyond what was tested and for sandwich configuration that are much different in terms of materials of construction.

3.2 DAMAGE TOLERANCE.

The composite sandwich and impact parameters were the same as for the damage resistance response surfaces (see table 3-1). In this case, the response surfaces for the residual compression strength, as measured in a CAI test, were developed and described in detail in reference 7.

Similarly to reference 4, a 3^k fractional factorial DOE approach [12] has been employed to examine the nonlinear interaction effects between relevant sandwich panel design parameters and their influence on the CAI residual strength, N_{yy}, associated with a given impact event. To isolate the coupled effects of material system and layup parameters (i.e., number of facesheet plies, X_1; core density, X_2; and core thickness, X_3) on the damage tolerance characteristics of sandwich composite panels, the impact energy ($X_4 = 120.0$ in-lbs), impactor diameter ($X_5 = 3.0$ in.), and impact velocity ($X_6 = 96.30$ in/s) were held fixed in this examination. The regression coefficients of the response surface, characterized in terms of natural values of independent variables, are given as

$$\begin{aligned}\hat{N}_{yy} &= -2159 + 97.56 \cdot X_1 + 894.7 \cdot X_2 + 1554 \cdot X_3 \\ &\ldots + 1.441 \cdot X_1^2 - 84.56 \cdot X_2^2 - 1887 \cdot X_3^2 \qquad \text{(lbs/in)} \\ &\ldots - 18.36 \cdot X_1 \cdot X_2 + 589.4 \cdot X_1 \cdot X_3 + 11.35 \cdot X_2 \cdot X_3\end{aligned}$$

The response surfaces equation may be used to assess which combinations of sandwich configurations lead to the minimum (or maximum) degradation in CAI residual strength for the specified impact. These may be used in conjunction with the response surface predictions of the planar damage area and residual facesheet indentation developed [4] to help assess the loss of CAI strength associated with damage of various sizes and types. The potential exists to identify sandwich panel configurations that have relatively high levels of CAI residual strength over a range of impact events. This is important since large-scale internal damage (e.g., core crushing) may not necessarily be accompanied by visibly detectable damage. Of course, the compressive failure mechanisms (facesheet fracture, facesheet dimple propagation, etc.) and residual strength are likely influenced by whether or not partial facesheet penetration occurs; the nature and severity of the local damage also may be drastically different for the two cases. This is of particular concern for those impacts involving smaller diameter impactors, increased impact energy, and/or thinner facesheets. Quadratic response surfaces may have difficulty predicting the CAI strength for test panel configurations exhibiting a bifurcation between failure modes over the range of input parameters considered.

Figure 3-2 summarizes the influence of the number of facesheet plies (X_1), core density (X_2), and core thickness (X_3) on the estimate of CAI residual strength. In each of the response surface plots contained in this report, the bounds of the sphere of coded radius, $r = \sqrt{2}$, is denoted by an inscribed dashed circle. Strictly speaking, discussion of regression data falling outside the bounds of this sphere would correspond to an extrapolation of the response surface results. Figures 3-2(a), 3-2(b), and 3-2(c) show the CAI residual strength as a function of core density and core thickness for the two-, four-, and six-ply facesheet configurations, respectively. A comparison of the three figures reveals that the predicted strength increases substantially as the number of facesheet plies is increased. It is clear from figure 3-2(a) that for sandwich panels with the minimum number of facesheet plies ($X_1 = 2$ plies), the CAI strength generally increases with increasing core density, X_2. The CAI strength is a relative maximum in the vicinity of the maximum core density ($X_2 = 3.0$ lb/ft^3) and midrange core thickness ($X_3 = 3/4$ in.). The minimum strength occurs in the vicinity of $X_2 = 3.0$ lb/ft^3 and $X_3 = 3/4$ in. The relatively reduced penetration resistance associated with the two-ply facesheet configuration likely results in more localized damage development for a given impact event, particularly as the core density is decreased. Note that as the number of facesheet plies is increased to its midrange value ($X_1 = 4$ plies), the magnitude of the peak CAI strength and its location in the space of independent variables change (figure 3-2(b)). The estimated CAI strength tends to increase rapidly with increasing core thickness and is less sensitive to the density of the core.

For the relatively blunt object impacts considered here, enhanced penetration resistance associated with an increase in the number of facesheet plies often results in CAI failure processes characterized by facesheet dimple propagation across the width of the test specimen [3]. The applied load level (e.g., strength) at which this process initiates apparently is influenced by core thickness (e.g., increasing the core thickness may provide enhanced bending rigidity that serves to delay the onset of facesheet dimple propagation). The peak predicted CAI strength occurs in the vicinity of $X_2 = 6.0$ lb/ft^3 and $X_3 = 9/8$ in.; the strength is a relative minimum for $X_2 = 3.0$ lb/ft^3 and $X_3 = 3/8$ in., corresponding to the extreme ranges of the tested values.

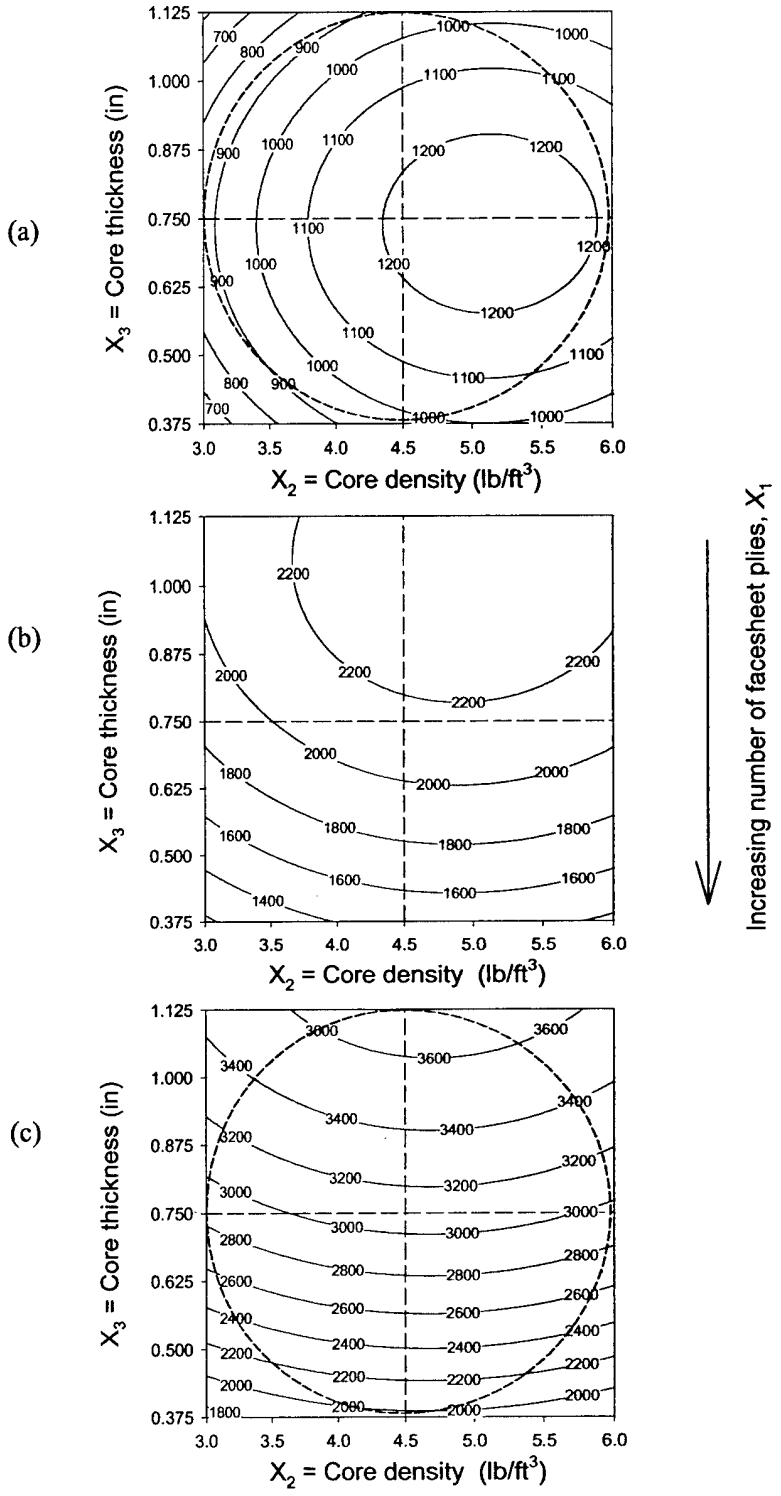

FIGURE 3-2. PREDICTED RESIDUAL STRENGTH (lbs/in): (a) X_1 = 2 PLIES $[90/45]_1$, (b) X_1 = 4 PLIES $[90/45]_2$, AND (c) X_1 = 6 PLIES $[90/45]_3$

Figure 3-2(c) shows that for sandwich panels with six-ply facesheet configurations ($X_1 = 6$ plies), the estimated CAI strength increases significantly with increasing core thickness and is fairly insensitive to core density. There is likely a competition between enhanced penetration resistance and improved bending stiffness associated with changes in independent variables that govern the damage development and residual strength.

Figure 3-3 contains a comparison of the response surface predictions of the TTU C-scan diameter from reference 4 to the response surface predictions of CAI residual strength developed in this examination. For illustration purposes, the CAI residual strength of each damaged panel was normalized by the CAI residual strength of an undamaged (virgin) panel of identical facesheet configuration prior to determination of the regression coefficients. A comparison of figures 3-3(a), 3-3(b), and 3-3(c) to figures 3-3(d), 3-3(e), and 3-3(f), respectively, suggests that with the exception of the two-ply facesheet configuration (figures 3-3(a) and 3-3(d)), the predicted normalized CAI residual strength is generally inversely proportional to the size of the planar damage area, D, for the given impact. This is consistent with the observations of Tomblin, et al. [6].

Lacy, et al. [4] noted that the reduced penetration resistance associated with the two-ply facesheet configurations likely results in a decrease in the planar size of the internal damage for a given impact event. There may be, however, appreciably more localized facesheet damage (ply fracture, fiber breaks, matrix cracks, etc.) that reduces the facesheet load transfer across the impact site. The loss of load carrying capability of the facesheet coupled with the reduced bending stiffness associated with the two-ply facesheet configuration may result in a bifurcation between compressive failure modes (i.e., facesheet fracture may occur rather than progressive facesheet dimple propagation). Hence, there may be no clear correlation between the measured TTU C-scan diameter and residual strength for impacts involving partial facesheet penetration.

Clearly, the use of continuous function response surfaces to predict residual strength should be used with extreme caution over ranges of independent variables where a potential bifurcation between failure modes may result in an apparent step discontinuity in the actual residual strength, particularly for those impacts involving smaller diameter impactors, increasing impact energy, and/or thinner facesheets. This may explain why the disparity between the measured and predicted CAI residual strengths was the greatest for sandwich composites with two-ply facesheet configurations. Similar to the results shown in figure 3-2, the estimated residual strength for the four- and six-ply facesheet configurations may increase significantly with increasing core thickness. A comparison of figures 3-3(d), 3-3(e), and 3-3(f) suggests that the given impact can result in residual strength values that range between roughly 50% and 90% of the virgin panel strength for a given facesheet configuration. Similar response surfaces may allow manufacturers to estimate the peak degradation in CAI residual strength for a given class of impact (i.e., establish conservative knockdown factors to the virgin panel strength).

In a second study, the isolated effects of the number of facesheet plies (X_1), impact energy (X_4), and impactor diameter (X_5) on the damage tolerance characteristics of sandwich composite panels are investigated using the Box-Behnken experimental design. Lacy, et al. [4] conducted a similar study investigating the influence of these parameters on the damage resistance characteristics of sandwich composites for the same set of test specimens considered here. The

core density ($X_2 = 3.0$ lb/ft^3), core thickness ($X_3 = 3/4$ in.), and impact velocity ($X_6 = 96.3$ in/s) were held fixed.

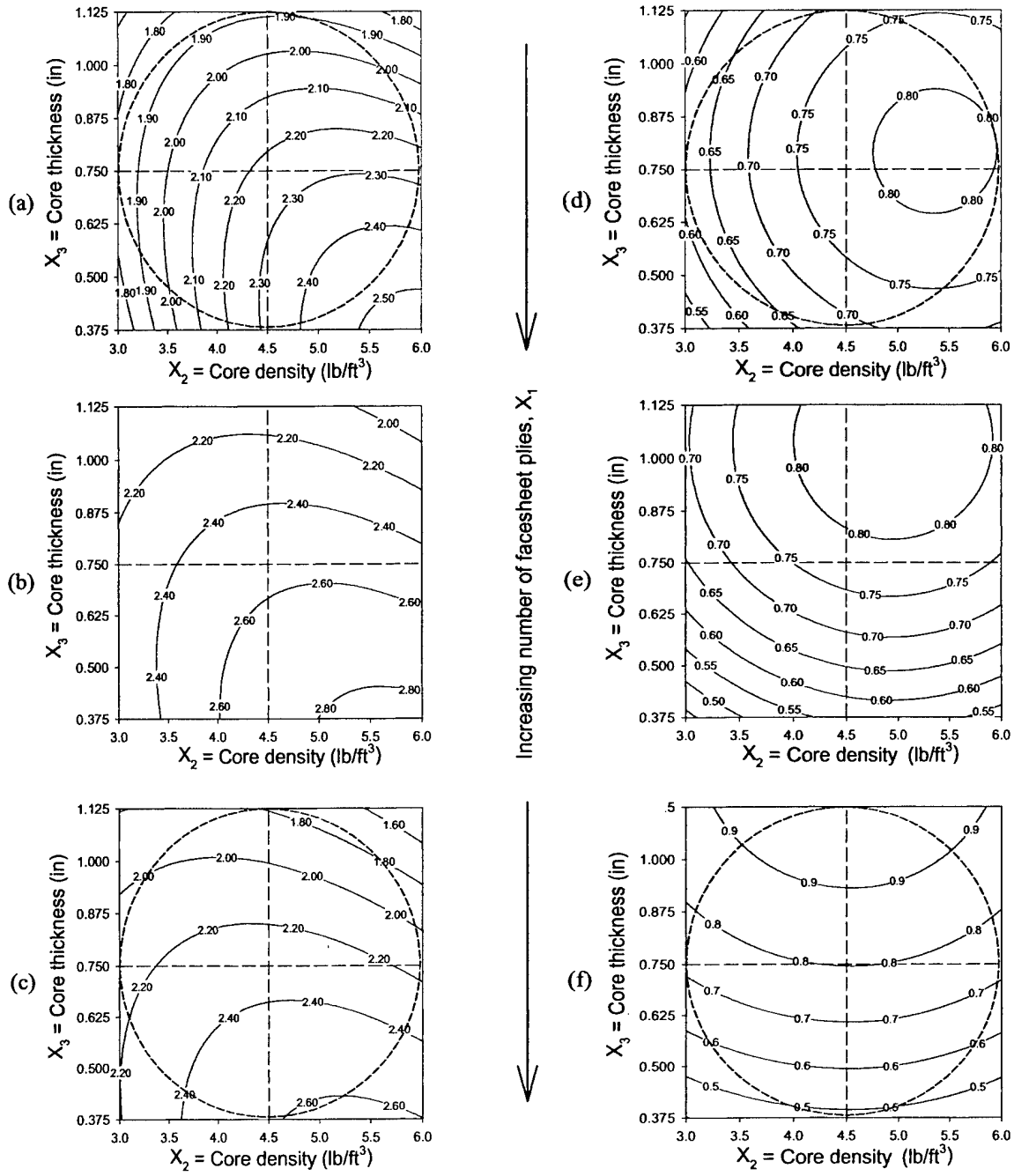

FIGURE 3-3. PREDICTED DAMAGE DIAMETER (in.) FOR X_1 = (a) 2, (b) 4, AND (c) 6 PLIES [13]. PREDICTED NORMALIZED RESIDUAL STRENGTH FOR X_1 = (d) 2, (e) 4, AND (f) 6 PLIES.

An estimate of the CAI residual strength from the regression analysis expressed in terms of natural values of the independent variables is

$$\hat{N}_{yy} = -2537 + 1238 \cdot X_1 + 4.176 \cdot X_4 + 1286 \cdot X_5$$
$$\ldots - 33.50 \cdot X_1^2 + 0.033 \cdot X_4^2 - 177.1 \cdot X_5^2 \qquad \text{(lbs/in)}$$
$$\ldots - 3.684 \cdot X_1 \cdot X_4 - 80.78 \cdot X_1 \cdot X_5 - 2.416 \cdot X_4 \cdot X_5$$

Similar to the previous results, response surface estimates of the CAI residual strength suggest that increasing the number of facesheet plies results in the greatest improvement in the damage tolerance properties. For the cases where facesheet penetration was likely not a concern (e.g., four- and six-ply facesheets), an increase in the impact energy generally resulted in a decrease in the CAI residual strength; at higher impact energy levels, the estimated strength decreased somewhat with increasing impactor diameter. Impact diameter is not a viable parameter to draw response surfaces for the degradation in residual strength because different failure modes are present within the space of experimental parameters.

In the final study in this examination, the isolated effects of the number of facesheet plies (X_1), impact energy (X_4), and impact velocity (X_6) on the damage tolerance characteristics of sandwich composite panels are investigated using the Box-Behnken experimental design. Different impact velocities leading to a specified value of impact energy were obtained by varying the impactor mass and drop height during the impact testing. This effort aims to help clarify the influence of dynamic effects on the damage tolerance properties of the given sandwich composites over a range of relatively low velocity impacts. The core density (X_2 = 3.0 lb/ft^3), core thickness (X_3 = 3/4 in), and impactor diameter (X_5 = 3.0 in) were held fixed.

Following the procedure outlined earlier, statistically reliable, second-order response surfaces were generated that characterize the CAI residual strength as a continuous function of the number of facesheet plies, impact energy, and impact velocity. An estimate of the CAI residual strength from the regression analysis in terms of natural values of the independent variables is, i.e.

$$\hat{N}_{yy} = -1740 + 853.0 \cdot X_1 - 39.86 \cdot X_4 + 77.83 \cdot X_6$$
$$\ldots - 24.42 \cdot X_1^2 + 0.1710 \cdot X_4^2 - 0.4127 \cdot X_6^2 \qquad \text{(lbs/in)}$$
$$\ldots - 1.984 \cdot X_1 \cdot X_4 - 0.3231 \cdot X_1 \cdot X_6 + 0.0232 \cdot X_4 \cdot X_6$$

In the final part of this investigation there was a lack of correlation between regression results and experimental observations for sandwich panels with two-ply facesheets. This suggests that quadratic response surfaces have difficulty predicting the CAI strength for those test panels where facesheet penetration and/or bifurcation between failure modes are a concern. Similar to the previous results, response surface estimates of the CAI residual strength shows that increasing the number of facesheet plies results in a significant improvement in the damage tolerance properties. Regression results suggest that damage development and the CAI strength are somewhat sensitive to the velocity of the impactor; midrange values of impact velocity resulted in strength estimates that were a relative maximum. Hence, accurate characterization of expected impact scenarios should be an important part of the development of a damage tolerance plan for sandwich composites.

4. NONDISTRUCTIVE INSPECTION AND QUANTIFICATION OF IMPACT DAMAGE USING FIELD INSPECTION TECHNIQUES (FITs).

Because the implementation of an effective damage tolerance program dictates continual monitoring of airframe structures in service, it would be desirable to use NDI methods, which would enable in situ delineation of damage states in sandwich airframe structures. Some of the inspection techniques used in service are the manual tap test (coin tap test), automated (instrumented) tap hammer, mechanical impedance analysis (MIA), etc. In these investigations, the effectiveness of different FITs was appraised by comparing the damage size predicted by these techniques with that of the TTU C-scan (the damage size measured by TTU C-scan was found to correlate well with the underlying core damage for honeycomb cores [3]). For foam core sandwiches, the MIA was found to be more effective than TTU C-scan and, hence, was used as a baseline. The details of the TTU C-Scan equipment, calibration standards and damage quantification procedures can be found in reference 3. The damage delineation using FITs was conducted at Sandia National Laboratories. The FITs used are the manual impact tap hammer, the instrumented tap tester, and the MIA. The tapping methods are routinely used by airline repair depots, while the MIA is used by some airlines. All the FITs have been endorsed by the SAE's Commercial Aircraft Composite Repair Committee. The details of these techniques are summarized in the following sections.

4.1 TAP TESTING.

Tap testing can be classified into mechanical tap testing and acoustical tap testing. The mechanical tap testing involves the analysis of the mechanical response of the structure subjected to a localized excitation. The acoustical tap test relies on the analysis of the characteristic resonant sound emanating from the location of the tap. The localized excitation in both cases is typically provided by a light impact using a spherical-nosed impactor, with energy levels low enough to preclude any damage during the inspection itself. The tapping was accomplished manually or by using a sophisticated hand-held instrument where the impactor is driven by a solenoid mechanism.

In the mechanical tap testing, the impact (tap) force is measured using an accelerometer mounted behind the impactor. The magnitude of the force and impact duration will depend on the constitutive properties of the sandwich components, impact energy, and impactor properties. The duration of impact (period) has been reported to be rather insensitive to the magnitude of the peak impact force, for sandwich panels [10], which ensures repeatability. However, the impact duration will be significantly altered when the local stiffness of the sandwich structure is reduced due to the presence of damage. This change in impact duration is used to identify damage in sandwich structures. In the present investigation, Mitsui Woodpecker Automated tap tester [13], illustrated in figure 4-1, was used for identifying the impact damage in sandwich panel.

In the acoustical tap testing, the characteristic resonant sound emanating from the tap test is analyzed by the human ear. The audible resonant sound will depend on the sandwich local impedance and tap mass/hammer characteristics. The damaged region is characterized by a dull (dead) sound, which can be attributed to the decreased participation of the higher frequency modes. The manual tap test hammer (Airbus design) is shown in figure 4-2.

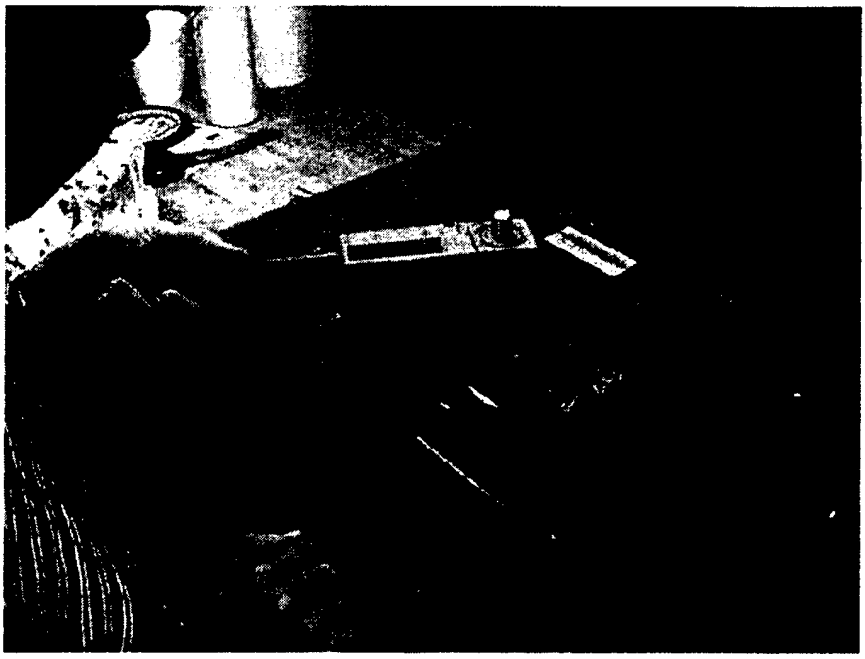

FIGURE 4-1. MITSUI WOODPECKER AUTOMATED TAP TESTER

FIGURE 4-2. MANUAL IMPACT HAMMER (AIRBUS DESIGN)

4.2 MECHANICAL IMPEDANCE ANALYSIS [14].

In this method, the stiffness of the structure in contact with a probe tip is measured. The mechanical impedance (stiffness) of the structure is a function of the constitutive properties of the sandwich components. This method has been popularly used for identifying flaws in adhesive bonds. The presence of facesheet or core damage will reduce the mechanical

impedance of the sandwich structure and can result in a phase or amplitude change to the displayed signal, depending on the frequency of the probe. The probe consists of two piezoelectric crystals with the driver positioned behind the receiver within the same holder. The driver converts electrical energy into sonic vibrations; the receiver, in direct contact with the test surface, converts the modified vibrations into electrical signals for processing by the instrument. The V95 low-frequency bond tester is illustrated in figure 4-3.

FIGURE 4-3. V-95 BOND TESTER USED FOR MECHANICAL IMPEDANCE ANALYSIS

4.3 EVALUATION OF FITs FOR IMPACT DAMAGE DETECTION.

The effectiveness of using the aforementioned FITs for detection and quantification of impact damage in honeycomb and foam core sandwich panels was investigated for different sandwich configurations. The various sandwich configurations were impacted with impactor diameters of 1.00″, 2.00″, and 3.00″ with different impact energy levels. The honeycomb sandwich panels were then subjected to nondestructive inspection using TTU C-scan to obtain the planar damage diameter $(2R_{damage})_{C\text{-}scan}$. The maximum residual indentation depth was also measured for all the sandwich configurations. The impact damage in foam core sandwich panels, however, could not be quantified using TTU C-scan due to practical limitations posed by the high attenuation property of the foam cores. The V-95 mechanical impedance analysis was used to generate baseline damage size for foam core sandwich panels.

The planar damage diameters obtained from the FITs were compared with that of the TTU C-scan data. The damage diameter obtained by TTU C-scan $[(2R_{damage})_{C\text{-}scan}]$ was used as the baseline for comparison for honeycomb core sandwich panels, while the damage diameter obtained by V-95 Bondcheck (MIA), $[(2R_{damage})_{V\text{-}95}]$, was used for foam core sandwich panels. In addition, the MAUS C-scan apparatus was used in the MIA mode for foam core sandwich

panels. This system adds the scanning capability to the MIA mode and eliminates the need to inspect the panels at discrete locations. Further, the damage diameters obtained by the FITs were normalized by their respective baseline damage diameters.

4.3.1 Honeycomb Core Sandwich Panels.

The effects of facesheet thickness on the detection capability of FITs were analyzed by comparing the average of all the normalized planar damage sizes for each facesheet type. The results are summarized and plotted as a function of the number of (90/45) ply groups in the facesheets in figure 4-4. The error bars in the figure correspond to one standard deviation about the respective mean value. From the figure, it can be observed that the FITs perform better with thinner facesheets. However, relatively higher scatter was observed for thinner facesheets. As the facesheets get thicker, the contribution of the core to the local stiffness (flexural) decreases, especially at the edge of the damage region. Thus, the facesheet tends to mask the core damage underneath, reducing the effectiveness of FITs, which rely on either the mechanical or the acoustical impedance of the sandwich panel. These trends are consistent with the observations of Georgeson, et al. [15] who used an electronic tap hammer for damage assessment.

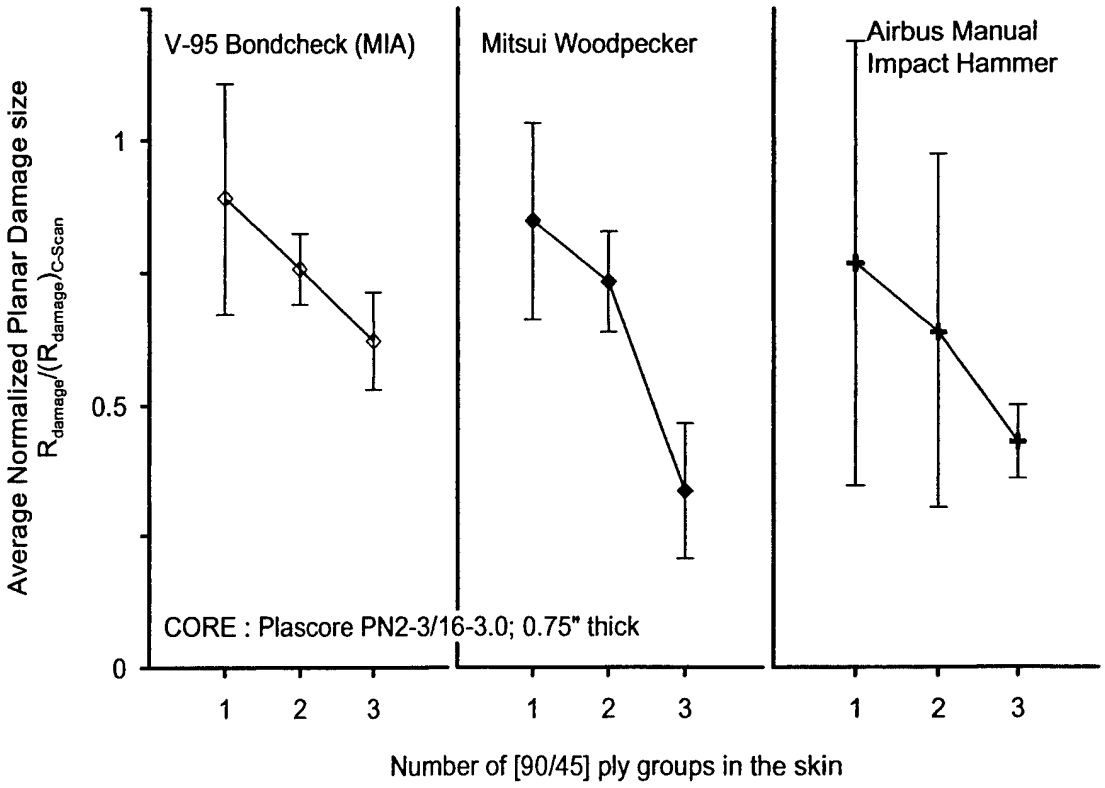

FIGURE 4-4. AVERAGE NORMALIZED DAMAGE SIZE FOR SANDWICH PANELS WITH DIFFERENT FACESHEET CONFIGURATIONS, WITH 0.75″ THICK, 3.0 lb/ft^3 CORES ONLY

4.3.2 Foam Core Sandwich Panels.

Similar to the honeycomb core sandwich panels, the foam core sandwich panels were impacted with different combinations of impact energies and impactor diameters. Unlike the honeycomb core sandwich panels, a baseline damage size could not be obtained using TTU C-scan due to the high acoustical impedance of the foam cores. Therefore, one of the FITs was used as the baseline damage detection method. In this study, the V-95 Bondcheck (MIA) method was used as the baseline method since it was the only method able to detect damage in all the specimens that were impacted. In addition to the FITs described for honeycomb core sandwich panels, MAUS C-scan was also used to detect damage in the foam core sandwich panels. This method was, however, used in the MIA mode rather than the through-transmission (TT) mode and was used as verification for the V-95 Bondcheck data.

The effects of facesheet thickness on the detection capability of FITs were analyzed by comparing the average of all the normalized planar damage sizes for each facesheet type. The results are summarized and plotted as a function of the number of (90/45) ply groups in the facesheets in figure 4-5. The error bars shown in the same figure correspond to one standard deviation about the respective mean value. Unlike in the case of honeycomb core sandwich panels, the Mitsui Woodpecker performs comparatively poorly with respect to the manual (acoustic) tap tests, especially as the facesheet gets thicker. This implies that the acoustic impedance of foam core sandwich panels is relatively more sensitive to impact damage.

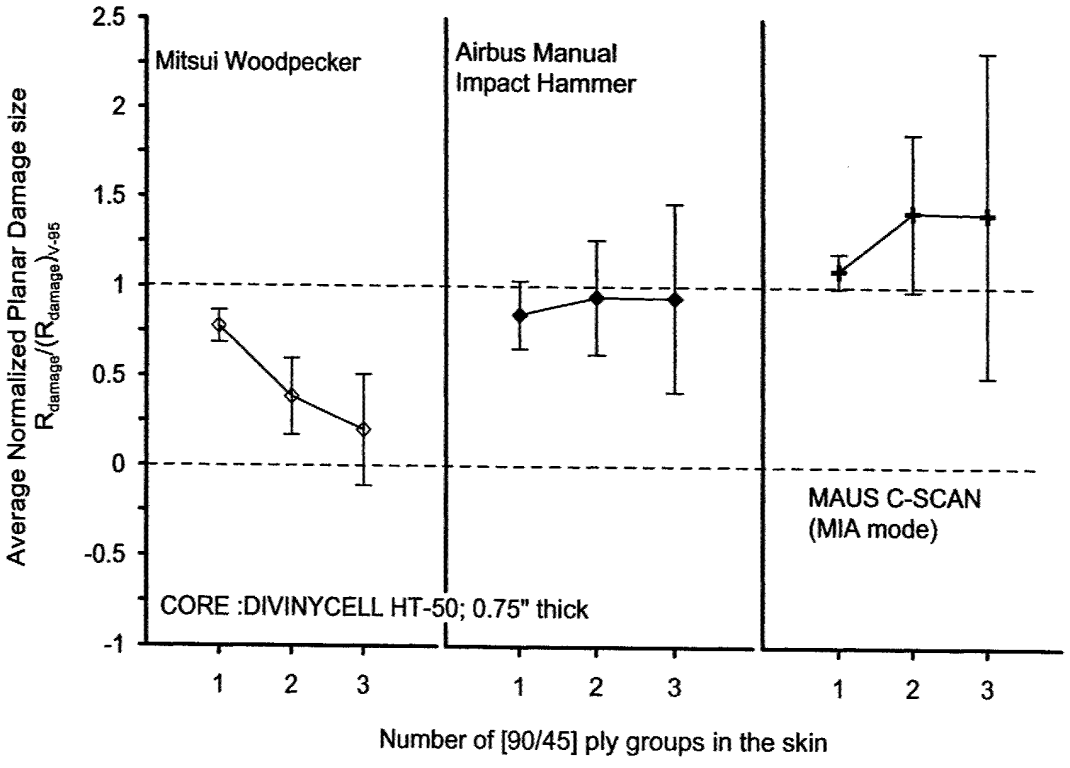

FIGURE 4-5. AVERAGE NORMALIZED DAMAGE SIZE FOR SANDWICH PANELS WITH DIFFERENT FACESHEET CONFIGURATIONS, WITH 0.75″ THICK, 2.6 lb/ft^3 CORES ONLY

5. ANALYSIS.

A low-velocity impact on a sandwich panel usually produces a small permanent indentation on the facesheet with local core crushing beneath the impacted site. For blunt objects, the damage may not be visible but internal crushing of the core may occur. In some cases, delaminations, fiber breakage, and matrix cracks can also occur, as shown in figure 5-1.

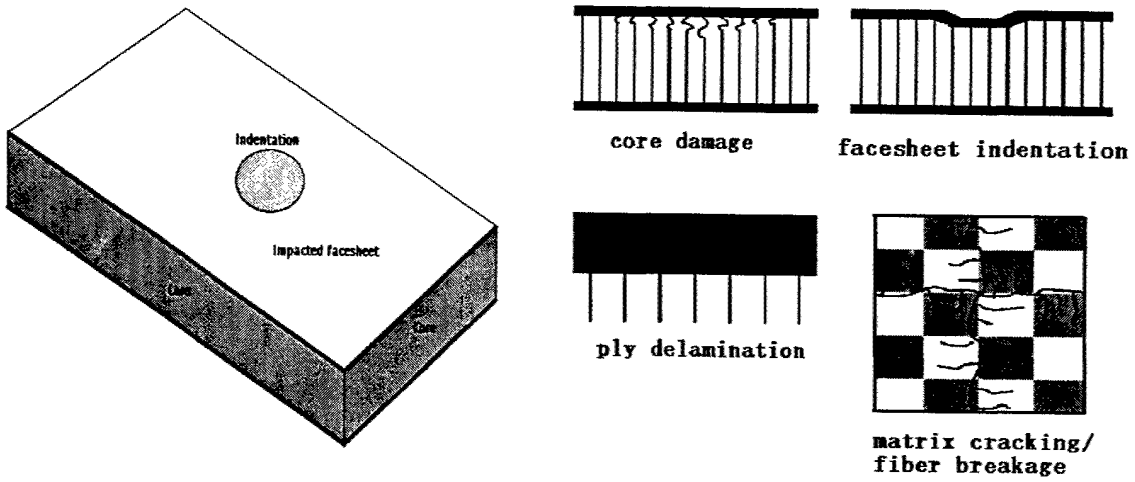

FIGURE 5-1. COMPOSITE SANDWICH PANEL WITH LOW-VELOCITY IMPACT DAMAGE

Based on the examination of impacted specimens and the observations in the unidirectional CAI tests, two analytical models were adopted to predict the damage propagation and failure of impacted sandwich panels under compression. The first model is an analytical model involving the solution of two sets of coupled partial differential equations. The second is a nonlinear finite element model. Two finite element models were constructed, one at University of Maryland using ANSYS [16] and one at Wichita State University using ABAQUS [17]. A test panel impacted with a blunt object, at a low energy level, was analyzed using both techniques. For a panel impacted with a sharp object, a conservative residual strength estimate is obtained by assuming a reduced facesheet stiffness or the existence of an open hole the size of the impactor diameter at the impacted site. The numerical results obtained by both models are compared to experimental data from reference 3 for panel response and residual strength.

5.1 FINITE ELEMENT ANALYSES.

5.1.1 ABAQUS Model.

Three-dimensional (3D) material and geometric nonlinear finite element models were developed that contain explicit representations of facesheet and core and account for the presence of damage. Large-scale, nonlinear numerical analyses investigating the effects of initial damage states, panel size, boundary conditions, and other relevant factors on the CAI damage tolerance characteristics of sandwich composites have been conducted using the nonlinear finite element code ABAQUS [17]. The finite element models were refined to account for material

nonlinearity associated with core crushing, large elastic facesheet deformations, as well as reduced facesheet moduli in the impact region. Figure 5-2 contains a plan view schematic of a typical idealized impact-damaged sandwich composite of rectangular dimensions, 2a x 2b. From symmetry, only one-fourth of a given sandwich panel need be considered in a numerical simulation. As indicated in figure 5-2, a Cartesian coordinate system was adopted so that the x-y plane corresponds to the mid-plane of the impacted facesheet with the z axis passing through the center of the impact site. The y axis corresponds to the direction of the CAI loading and also defines the core ribbon direction. It is assumed that for the given facesheet configurations, the planar regions containing damage of various types are circular in character. In figure 5-2, the radius, R_I, defines the region with a measurable residual facesheet indentation. The radius, R_f, defines the region where the effective elastic properties of the facesheet may be degraded due to the presence of impact damage (e.g., fiber breaks, matrix cracks, etc.); the degree of property degradation is highly dependent on the severity of the facesheet damage. The effective ply properties are generally expressed in terms of a fraction of the virgin ply properties. The radius, R_c, defines the region where the underlying core material was crushed due to impact. Consistent with reference 5, it is assumed that localized facesheet damage may extend beyond the region with a residual facesheet indentation and that facesheet damage will not occur beyond the undamaged core (i.e., $R_I \leq R_f \leq R_c$).

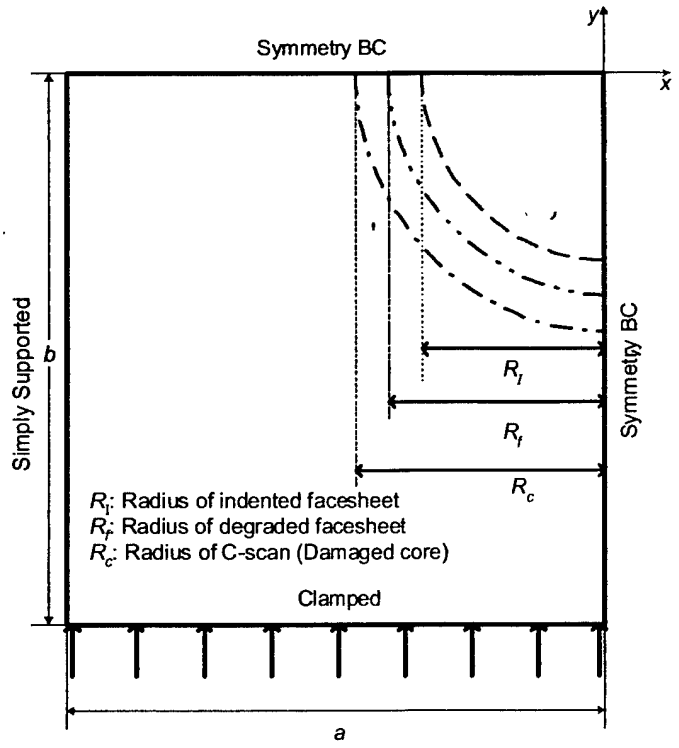

FIGURE 5-2. PLAN VIEW SCHEMATIC OF FINITE ELEMENT MODEL

Figure 5-3 contains a schematic of a section cut taken in the x-z plane through a representative impact-damaged sandwich specimen. From the figure, δ_I is the peak through-the-thickness depth of the residual facesheet indentation. δ_c is the peak depth associated with core cell wall buckling and/or fracture. In general, $\delta_I \neq \delta_c$ since the facesheet may rebound significantly after impact. Destructive sectioning performed by Tomblin, et al. [3] suggests that the ratio, δ_c/t_c, generally falls in the range 0.20-0.40, where t_c is the undamaged core thickness. Note that standard NDI techniques may be used to determine the residual facesheet indentation profile (e.g., δ_I, R_I) as well as the planar dimension of the crushed core, R_c, whereas destructive sectioning is required to determine the peak core crush depth, δ_c. Given the experimentally determined peak residual facesheet indentation, δ_I, and the radius, R_I, the residual facesheet indentation profile may be approximated as a function of radial distance from the center of the impact region using a cubic polynomial. A similar relation may be used to define the profile of the crushed core given δ_c and R_c, if δ_c is either known or estimated. For the sandwich panels considered in this study, there was no evidence of large-scale ply delaminations or disbonds between facing and core [3]; hence, a perfect interface was assumed to exist between constituent layers. Table 5-1 contains a summary of the geometric parameters necessary to define a typical finite element model.

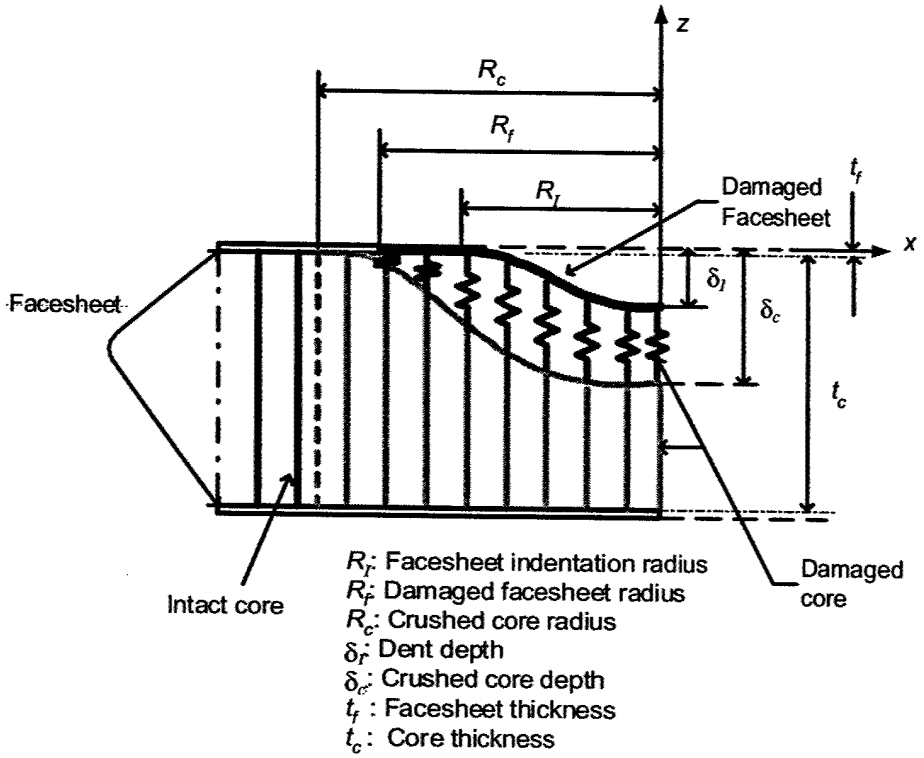

FIGURE 5-3. IMPACT-DAMAGED REGION

TABLE 5-1. REQUIRED GEOMETRIC PARAMETERS FOR FINITE ELEMENT MODEL

Facesheet:	$2a, 2b, t_f, R_I, R^*_f, \delta_I$
Core:	$2a, 2b, t_c, R_c, \delta^*_c$

*Must be estimated or determined from destructive sectioning.

The facesheets were considered as an elastic continuum with an equivalent inclusion idealization used to simulate the bulk effect of localized facesheet damage. The primary source of material nonlinearity is associated with inelastic deformation of the Nomex core. Figure 5-4 shows the idealized through-thickness (average) compressive stress-strain response for initially undamaged and impact-damaged cores, respectively. The initially undamaged through-the-thickness compressive stress-strain curve generally can be divided into three distinct regions (cf., figure 5-4(a): (1) a linearly elastic region until the stress reaches the ultimate stress, σ_{ult}, and ε_u is the strain at the ultimate stress; (2) a region corresponding to progressive crushing at nearly constant stress level, σ_{CRUSH}; and (3) a region of rapidly increasing stress with further deformation [18]. In figure 5-4(a), ε_{comp} is the strain at which core consolidation/compaction occurs. The undamaged core material properties used in this study were obtained from flat platen compressive testing performed by Tomblin, et al. [3].

Note that once the honeycomb core is crushed due to impact, the ensuing constitutive response may be distinct from that shown in figure 5-4(a). Figure 5-4(b) shows a schematic of the idealized through-the-thickness (average) compressive stress-strain response for Nomex honeycomb core with previous impact damage. Impact-damaged honeycomb cores subjected to uniaxial through-the-thickness compression may display nearly perfectly-plastic material behavior in bulk as suggested by region 3 in figure 5-4(b). To ensure numerical stability of the finite element solution, however, the initial slope of the stress-strain response may be given by σ_D/ε_D, where σ_D is some small fraction of the crush stress, σ_{CRUSH}. Once the average (through-the-thickness) strain reaches a certain value, ε_D, the apparent stiffness of the core may increase, $E' \approx \sigma_{CRUSH}/\varepsilon'_u$ (region 2 in figure 5-4(b)). The strain at which this transition occurs may be approximated as

$$\varepsilon_D \approx \frac{\delta_c - \delta_I}{t_c - \delta_I} \tag{5-1}$$

where $\delta_c=\delta_c(x, y)$ is the peak crush depth from the impact event, $\delta_I=\delta_I(x, y)$ is the residual facesheet indentation, and t_c is the undamaged core thickness. Note that the average strain level at which this transition occurs varies spatially from the center of the impact site (cf., figure 5-3). The onset of progressive core crushing at constant stress, σ_{CRUSH}, occurs when the average strain reaches a critical value

$$\varepsilon'_u = \frac{\sigma_{CRUSH} - \sigma_D}{E'} + \varepsilon_D \tag{5-2}$$

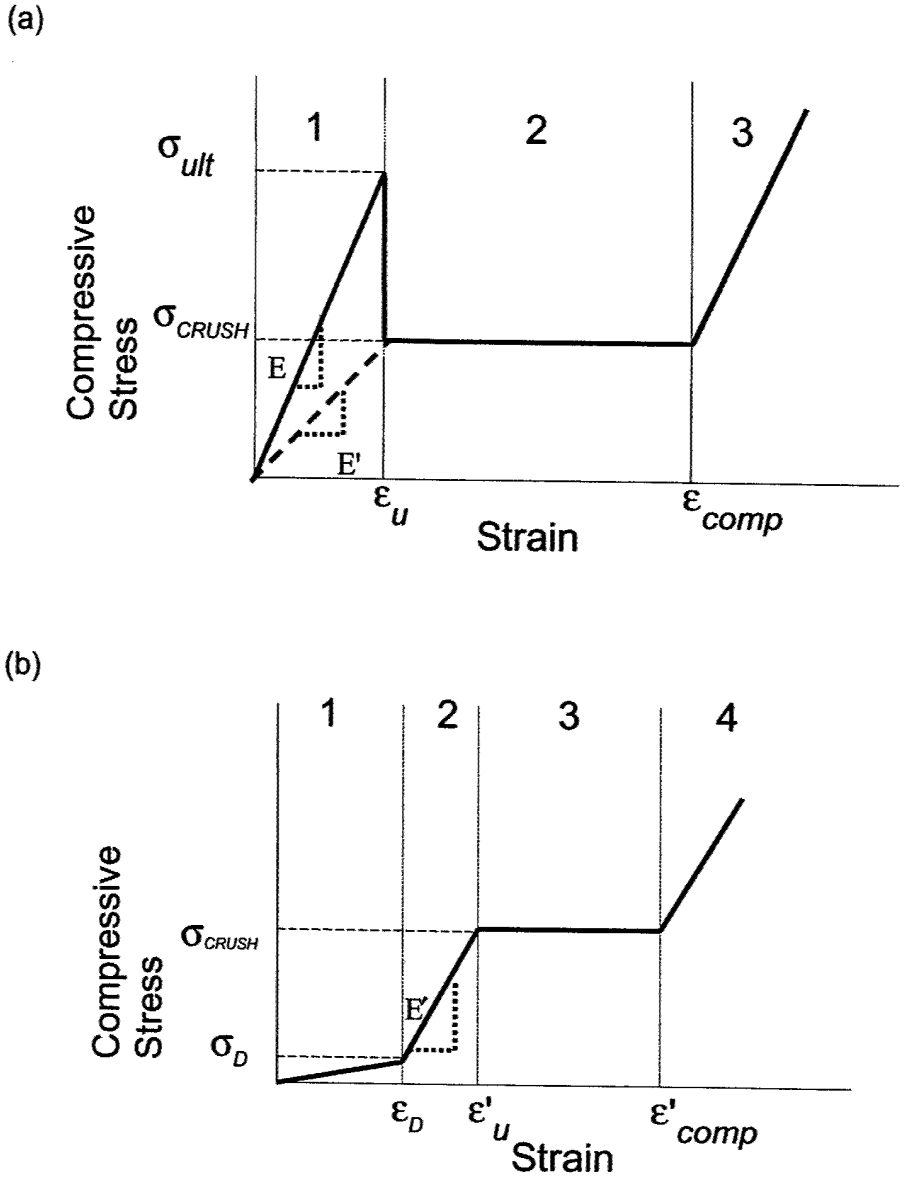

FIGURE 5-4. IDEALIZED COMPRESSIVE STRESS-STRAIN CURVE: (a) UNDAMAGED HONEYCOMB CORE AND (b) IMPACT-DAMAGED HONEYCOMB CORE

The remainder of the stress-strain response is similar to that shown in figure 5-4(a); $\varepsilon'_{comp} \approx \varepsilon_{comp}$ is the strain at which core consolidation occurs. Since the core material response obtained from flat platen testing [3] represents a spatial average of the point-wise varying stress-strain curve over the core thickness, t_c, the Nomex honeycomb core is considered a smooth varying and homogenous continuum in this study. Table 5-2 contains a summary of the material parameters necessary to define a typical finite element model.

TABLE 5-2. REQUIRED MATERIAL PROPERTIES FOR FINITE ELEMENT MODEL

Facesheet	$E_1, E_2, G_{12}, G_{23}, G_{31}, \nu_{12}$
Core	$E_1, E_2, E_3, G_{12}, G_{23}, G_{31}, \nu_{12}, \nu_{23}, \nu_{31}, \sigma_{ult}, \sigma_{CRUSH}$

Eight-node, large deformation elastic shell elements are employed to simulate the facesheet. Twenty-node orthotropic continuum solid elements that implement the appropriate idealized nonlinear constitutive behavior (cf., figure 5-4) are used to simulate the Nomex honeycomb core. Since the experimentally determined core response is averaged over the core thickness, t_c, a single finite element through-the-thickness was used in the numerical analysis. In the preceding discussion, it was assumed that impact damage was primarily limited to the core material and upper facing. In the presence of large-scale damage involving upper and lower facings and/or projectile penetration, the aforementioned techniques either cease to be valid or require substantial modification.

5.1.2 ANSYS Modeling.

The ANSYS [16] modeling was similar to that described for the ABAQUS modeling. Damage simulation included the incorporation of the residual facesheet indentation, the initially crushed core, and the delaminations in the facesheet (if there are any). A core crushing mechanism was also incorporated into the analysis.

The shape of the residual indentation was assumed to be a half of the surface of an ellipsoid represented by equation

$$\frac{x^2}{(r_x)^2}+\frac{y^2}{(r_y)^2}+\frac{z^2}{(r_z)^2}=1 \qquad (5\text{-}3)$$

where $r_{x;y;z}$ correspond to R_{Ix}, R_{Iy}, δ_I, respectively. This is in contrast to the quadratic representation used in ABAQUS modeling.

The part of the core that had been crushed in the impact was modeled as a gap between the facesheet and untouched core by assuming that it is incapable to sustain any load. The shape of the cutoff was also defined according to the above ellipsoidal equation by substituting $r_{x;y;z}$ with R_{cx}, R_{cy}, δ_c, respectively.

The determination of the location and geometric features characterizing delaminations is the most difficult part of the information about existing damage. The data can be obtained through the destruction of a specimen or specimens with the same damage level or through response surface formulations as described in section 3.1. According to the study by Kassapoglou [19], and as observed here, the delamination between the innermost ply and its neighboring layer is believed to be the biggest and plays the dominant role in the damage propagation for the sandwich panels with thin facesheets. To reduce the complexity of the model, only the delamination at this specific location was included in the finite element model. The

delamination was modeled as a gap between the two layers and in a shape of an ellipse defined by

$$\frac{x^2}{(r_{delamx})^2}+\frac{y^2}{(r_{delamy})^2}=1 \tag{5-4}$$

To prevent the interpenetration of core and facesheet elements, contact elements need to be defined along the two sides of the delamination. This is different than the ABAQUS model where no delamination between facesheet plies was assumed.

The core-crushing test reveals the existence of an ultimate strength corresponding to the core cell buckling. The nonlinear behavior of core material under compression along the thickness direction is shown in figure 5-5. The incorporation of this highly nonlinear core material property was accomplished by controlling the solving process in finite element analysis (FEA) with a macro program written in APDL. Two approaches have been taken to simulate the additional core crushing when the damage propagates. One uses the core material type change and the other one uses the technique of element birth and death.

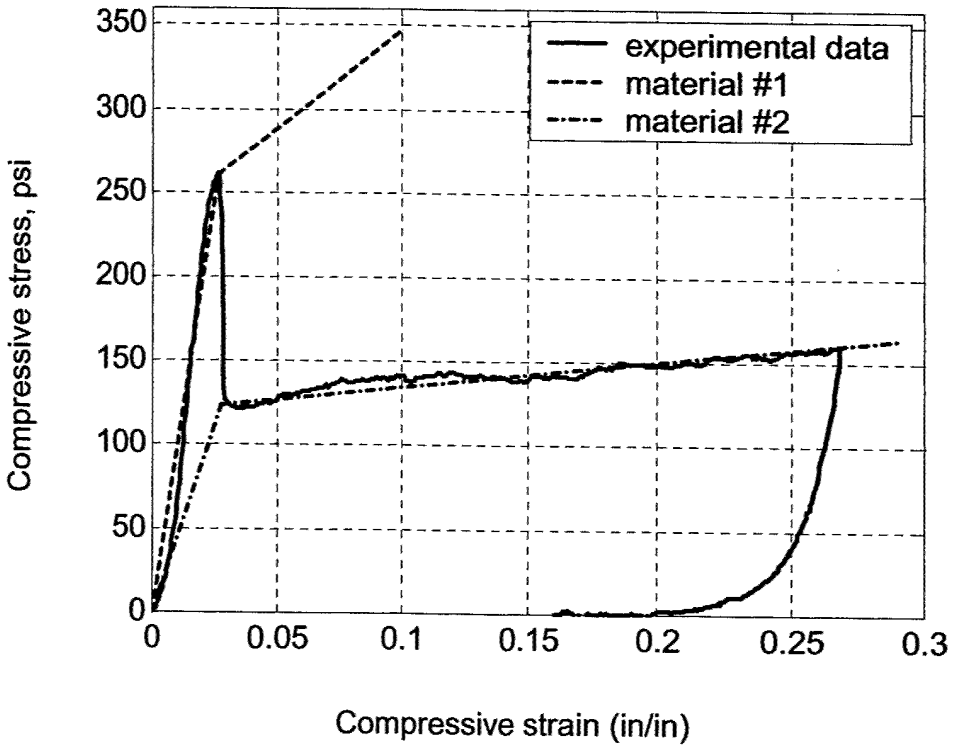

FIGURE 5-5. NONLINEAR CORE MATERIAL PROPERTIES

In the approach using the core material type change, two bilinear orthotropic materials are defined for the core elements, following the lines as shown in figure 5-5. Material no. 1 stands for the core property before the core crushing, while material no. 2 stands for the core properties

after core crushing. A monotonically increasing displacement is applied to one end of the model as a series of substeps. After each converged substep, the compression stress value in the thickness direction of all core elements is checked based upon the latest solution. If any core element has a compressive stress higher than the core-crushing strength, additional core crushing is assumed to occur at this specific location and the material type for this element is changed from no. 1 to no. 2. After sweeping over all the core elements in this way, the global stiffness matrix is updated and the solving process proceeds to the next displacement step. The above method circumvents the problem associated with the existence of two possible stress values at the same point of core-crushing initiation. The preceding process was repeated with increasing end displacement until a converged solution cannot be reached. The lack of numerical convergence may or may not indicate a structural failure.

The procedure in the second approach is the same as in the first approach except that, instead of changing the material type, the core elements with excessive compression stress are effectively removed by significantly reducing the appropriate values in the element stiffness matrix. The global stiffness is updated thereafter and the procedure continued until the solution fails to converge.

Although both approaches described above can successfully capture the point of the initiation of the consequential core crushing at the edge of the damage zone that directly leads to the damage propagation, the one using the element removal is superior in providing a post-core-crushing behavior similar to that in the CAI tests, as shown by the data comparison of a typical specimen in figure 5-6. Therefore, it was used in all of the case studies of ANSYS analysis.

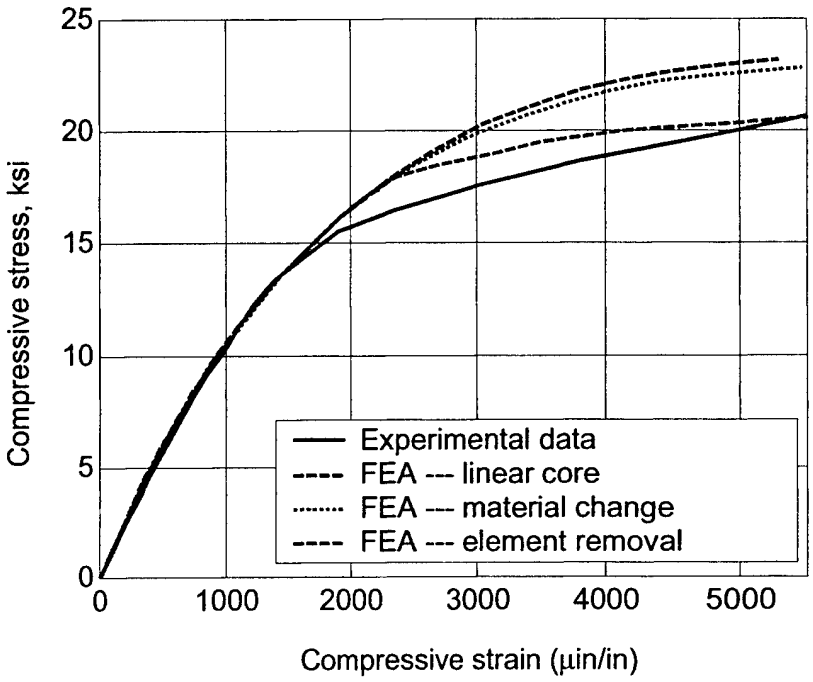

FIGURE 5-6. CORRELATION BETWEEN ANALYSIS WITH DIFFERENT CORE PROPERTIES AND EXPERIMENT

In the final ANSYS model, layered 8-node solid elements were used for the laminated facesheets; orthotropic 8-node solid elements were used for the honeycomb core. In addition, if there were any delaminations, point-to-surface contact elements would be defined along the two sides of the delamination to prevent the occurrence of penetration.

5.1.3 ABAQUS Results and Correlation With Tests.

To establish the capability of FEA modeling to predict structural response and residual strengths, finite element estimates for facesheet strains were compared to experimental results from Tomblin, et al. [3 and 6]. A semiempirical method was used to estimate residual strength in which the FEA strains were compared to the one test. The FEA results were then adjusted to match the experiment by decreasing the elastic properties in the damaged region and simple scaling. The adjusted FEA was then used to predict residual strengths of other similar panels impacted with the same impactor diameter but different energy level.

FEA modeled a symmetric flat sandwich composite panel ($[90/45]_2$/CORE/ $[45/90]_2$), comprised of plain-weave carbon fabric preimpregnated in epoxy resin (NEWPORT NB321/3K70P) facesheets and Plascore Nomex honeycomb (PN2-3/16-3.0) core, (Specimen ID: WXC29L; test section dimensions, ~8.0 in x 8.0 in). The core thickness and density were 3/4 in. and 3.0 lbf/ft^3, respectively. Prior to CAI testing, the panel was subjected to drop-weight normal impact with a 3.0-in. OD spherical steel impactor with an impact energy of 250 in-lbf. The test specimen displayed clear evidence of facesheet damage in the impact region (i.e., facesheet cracks oriented at ±45° from the x axis as well as evidence of distributed matrix cracking and fiber breaks in the indentation region). The extent of damage implies a loss of load carrying capability in the center of the impacted facesheet. NDI techniques (i.e., residual facesheet indentation and TTU C-scan measurements) were used prior to CAI testing to establish the facesheet indentation profile (e.g., δ_I, R_I) and spread of core damage, R_c. After CAI testing, destructive sectioning was performed to determine the peak core crush depth, δ_c.

Figure 5-7 shows a representative schematic of the test specimen used in the analysis. During CAI testing, the specimen was clamped along the loading edges ($y = \pm 4.0$ in.) and simply supported along the edges ($x = \pm 4.0$ in.). A total of 23 strain gages were positioned on the impacted and backside facesheets. Seven strain gages were located on the impacted facesheet at 0.5 in. intervals from the center of the impact site along the line $y = 0$, as shown. Analogous strain gages were located along the line, $y = 0$, on the backside facesheet. A series of strain gages were located on both facesheets just inside the grips along the line, $y = 4.0$ in. The dashed circle (radius, $R_c = 1.92$ in.) in the figure approximates the region with underlying crushed core based upon TTU C-scan measurements. Tables 5-3 and 5-4 contain a summary of the geometric parameters and relevant material properties, respectively, used in the FEA.

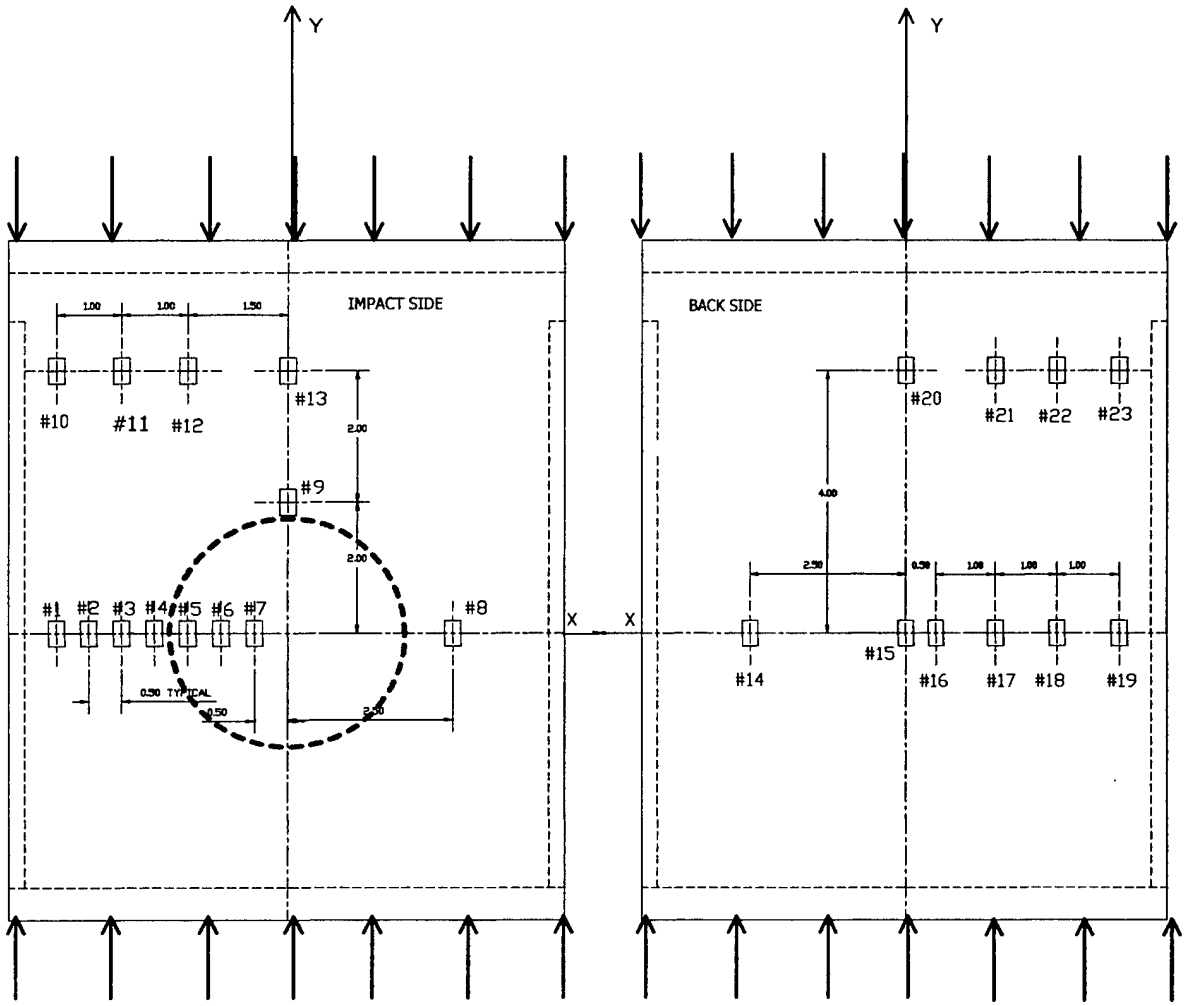

FIGURE 5-7. EXPERIMENTAL STRAIN GAGE LOCATIONS FROM REFERENCE 3
(Dimensions shown in inches)

TABLE 5-3. GEOMETRIC PROPERTIES FOR FINITE ELEMENT MODEL
(Dimensions shown in inches)

Facesheet	$2a$	$2b$	t_f	R_I	R_f*	δ_I
	8	8	0.032	1.356	1.625	0.165
Core	$2a$	$2b$	t_c	R_c	δ_c**	
	8	8	0.75	1.917	0.2605	

*Estimated by equation 5-5.
**Determined from destructive sectioning of similar specimens.

TABLE 5-4. MATERIAL PROPERTIES FOR FINITE ELEMENT MODEL

	Facesheet	Core
E_1 (psi)	10.06×10^6	3.5×10^3
E_2 (psi)	10.06×10^6	3.5×10^3
E_3 (psi)	–	20×10^3
G_{12} (psi)	0.62×10^6	50
G_{13} (psi)	0.6×10^6	5.8×10^3
G_{23} (psi)	0.6×10^6	20×10^3
ν_{12}	0.058	0.5
ν_{13}	–	1.0×10^{-9}
ν_{23}	–	1.0×10^{-9}
σ_{ult} (psi)	–	350
σ_{CRUSH} (psi)	–	150

The test specimen was subjected to monotonically increasing compressive loading up to the point of catastrophic failure. Consistent with figure 5-2, the radius of the region where the effective elastic properties of the facesheet were degraded due to the presence of impact damage in the finite element analysis was assumed to be roughly

$$R_f \approx \frac{R_I + R_c}{2} \tag{5}$$

Five separate sets of uniform facesheet ply properties were assumed for the equivalent inclusion located at the center of the impacted facesheet corresponding to 100%, 75%, 50%, 25%, and 0% of the virgin ply properties, respectively. For the case involving no degradation in ply material properties, the facesheet is fully effective in transferring load across the impact site. The case where no load carrying capability is assumed (i.e., 0% virgin ply properties) arguably simulates a facesheet with an open hole.

Strain gage data taken along the line, $y = 4.0$ in., suggests that use of displacement control boundary conditions in the finite element model was warranted. All four strain gages (nos. 20, 21, 22, and 23) in figure 5-7 showed uniform strains. Figures 5-8 to 5-10 show a comparison of the calculated and experimental nominal far-field stress resultant, N_{yy}, versus local facesheet surface strain, ε_{yy}, located at distances 3.5, 2.0, and 1.5 in., respectively, from the center of the impact site along the line, $y = 0$. These locations correspond to strain gages nos. 1, 4, and 5, respectively, in figure 5-7.

Figure 5-8 shows a comparison between the calculated and experimental nominal far-field stress resultant, N_{yy}, versus local facesheet surface strain, ε_{yy}, located at a distance of 3.5 in. from the center of the impact site along the line, $y = 0$ (strain gage no. 1 in figure 5-7). The experimental stress-strain response was fairly linear until the applied far-field load approached the peak failure load. Each of the predictions from finite element models with an equivalent inclusion having nonzero elastic properties correlated fairly well with the experimental data over the vast majority of the stress-strain range; the effect of variable inclusion properties was relatively insignificant at this strain gage location. This demonstrated the capability of the FEA to model the overall

response of the panel. The finite element solution corresponding to the open-hole case (i.e., 0% virgin ply properties for the equivalent inclusion) provided a linear estimate of the stress-strain response that appeared to slightly underpredict the actual strains at higher applied stress levels.

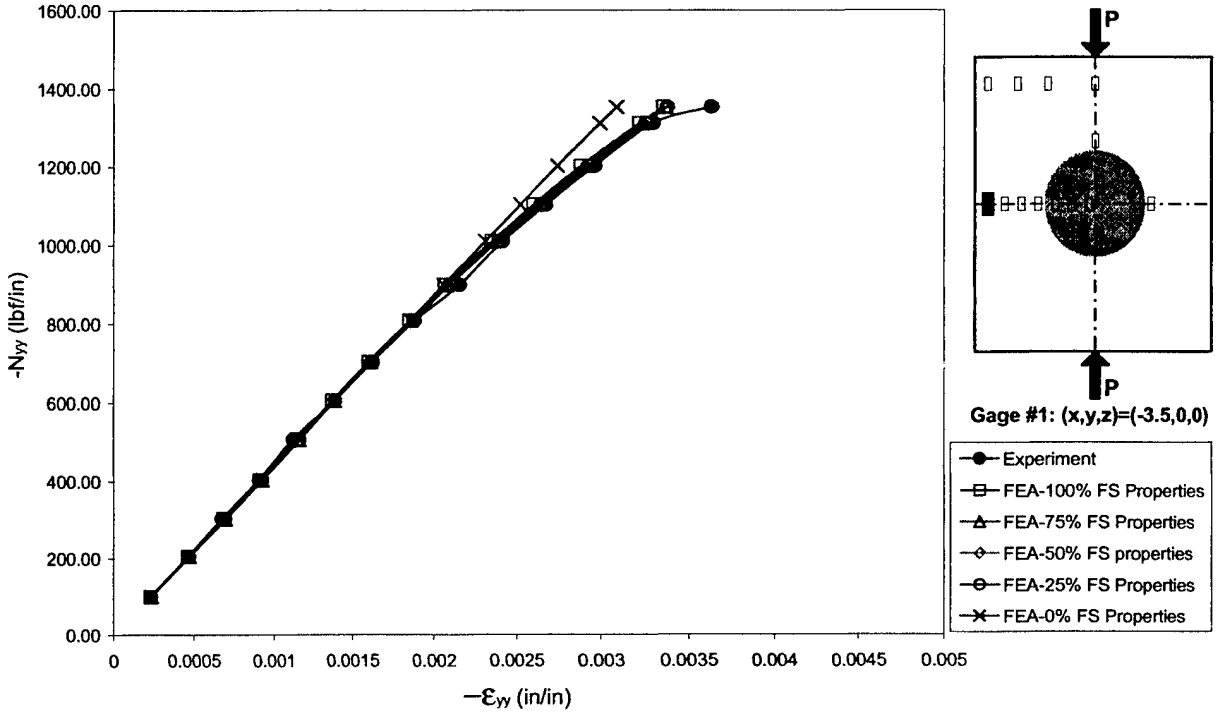

FIGURE 5-8. NOMINAL STRESS VERSUS LOCAL STRAIN (Gage no. 1)

Figure 5-9 shows a comparison between the calculated and experimental nominal far-field stress resultant, N_{yy}, versus local facesheet surface strain, ε_{yy}, located at a distance of 2.0 in. from the center of the impact site along the line, $y = 0$ (strain gage no. 4 in figure 5-7). Note that the strain gage location lies just outside the initial boundary of the crushed core based on TTU C-scan measurements ($R_c = 1.917$ in.). As indicated in the figure, the initial experimental response was somewhat nonlinear over the majority of the stress-strain range with a sharp decrease in the tangent modulus as the far-field stress approached the failure load. While the first four of the equivalent inclusion models also predicted a nonlinear response, the finite element simulation involving an equivalent inclusion with 50% of the virgin ply properties most closely matched the experimental results over the bulk of the stress-strain range. The finite element solution corresponding to the open-hole case (i.e., 0% virgin ply properties for the equivalent inclusion) provided a linear estimate of the stress-strain response that appeared to overpredict the strains at low to moderate applied stress levels. None of the finite element solutions, however, predicted the relatively large decrease in the local tangent modulus at the onset of incipient failure. Since the facesheet constitutive response and core/facing interface was assumed to be linear elastic throughout the entire CAI loading, the finite element models could not capture additional nonlinear material behavior associated with progressive fiber breaks, matrix cracks, and delamination prior to catastrophic failure. Audible acoustic emissions occurring at higher applied stress levels during experimental testing [3] suggest that such facesheet damage

nucleation and growth is a distinct possibility. This may explain the lack of correlation between the numerical results and experimental observations at the onset of incipient failure.

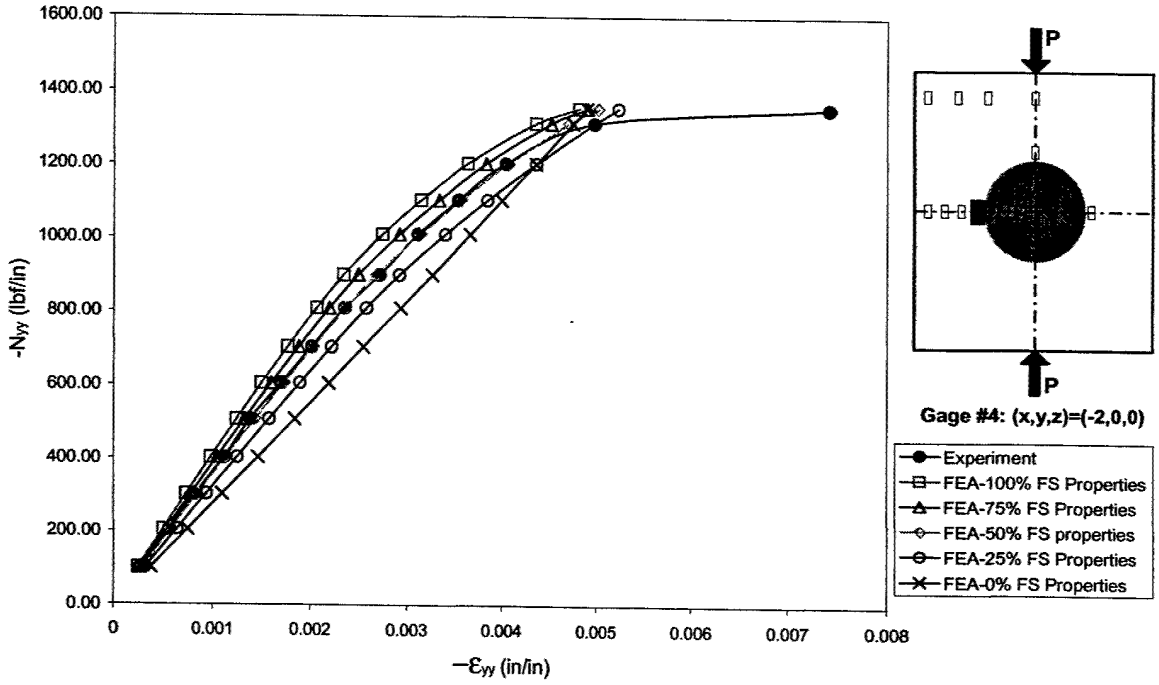

FIGURE 5-9. NOMINAL STRESS VERSUS LOCAL STRAIN (Gage no. 4)

Figure 5-10 shows a comparison between the calculated and experimental nominal far-field stress resultant, N_{yy}, versus local facesheet surface strain, ε_{yy}, located at the center of the impact site on the backside facesheet (strain gage no. 15 in figure 5-7). While there was no visible evidence of residual facesheet bulging or other damage to the backside facesheet after impact under CAI loading, the measured surface strain at this location transitioned from initial compression to tension. Each of the equivalent inclusion models with nonzero stiffness was able to predict the strain reversal in the unimpacted facesheet. These results suggest that the backside facesheet may play an important role in the failure process (i.e., local hemispherical crippling of the sandwich panel may be a real concern). Note that sandwich composite models that simulate the core material using an elastic or inelastic foundation idealization cannot capture this effect.

Figure 5-11 shows the predicted strain distribution, ε_{yy}, along the line, $y = 0$, on the impacted facesheet from numerical analyses involving elastic inclusions with 50% of the virgin ply properties. The 50% reduction in stiffness properties in the damaged area was found to best match the test data (see figure 5-9). The initial boundary of the crushed core, R_c, based upon TTU C-scan measurements is denoted in figure 5-11. The locus of points, $x < R_c$, defines the initial unsupported facesheet ligament where the facesheet receives relatively little in the way of local reinforcement from the core. As the remote compressive stress is monotonically increased, the size of the unsupported ligament generally increased somewhat due to facesheet dimple formation/progressive core crushing. The calculated strains correlated fairly well with experimentally observed values for that portion of the unsupported and supported ligament with no discrete facesheet damage (i.e., $x > R_f$).

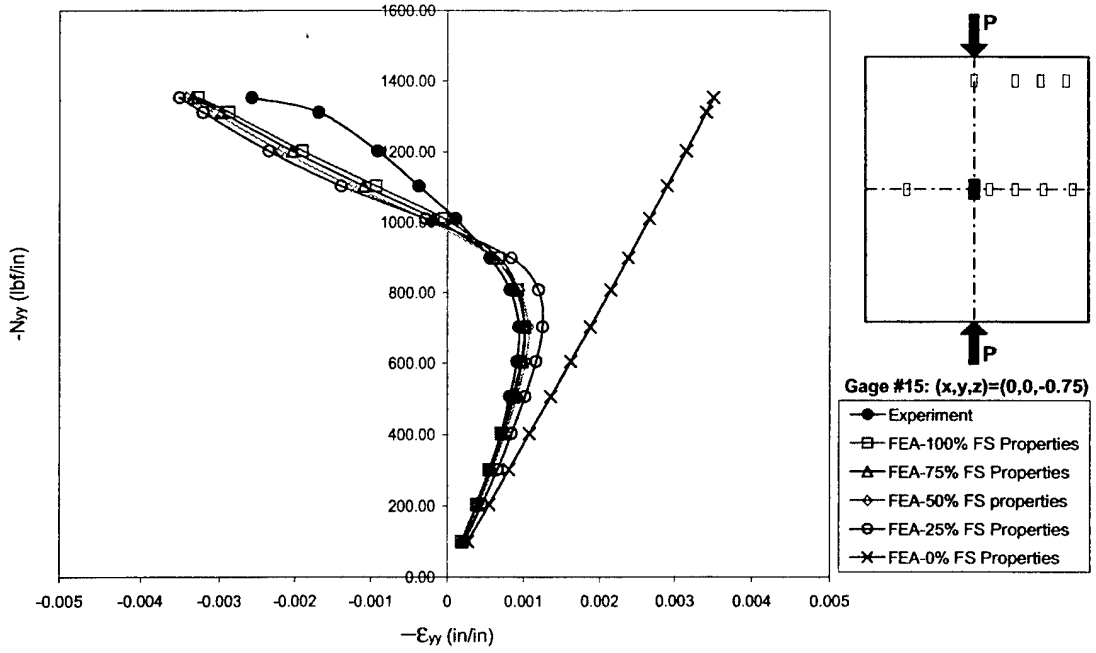

FIGURE 5-10. NOMINAL STRESS VERSUS LOCAL STRAIN (Gage no. 15)

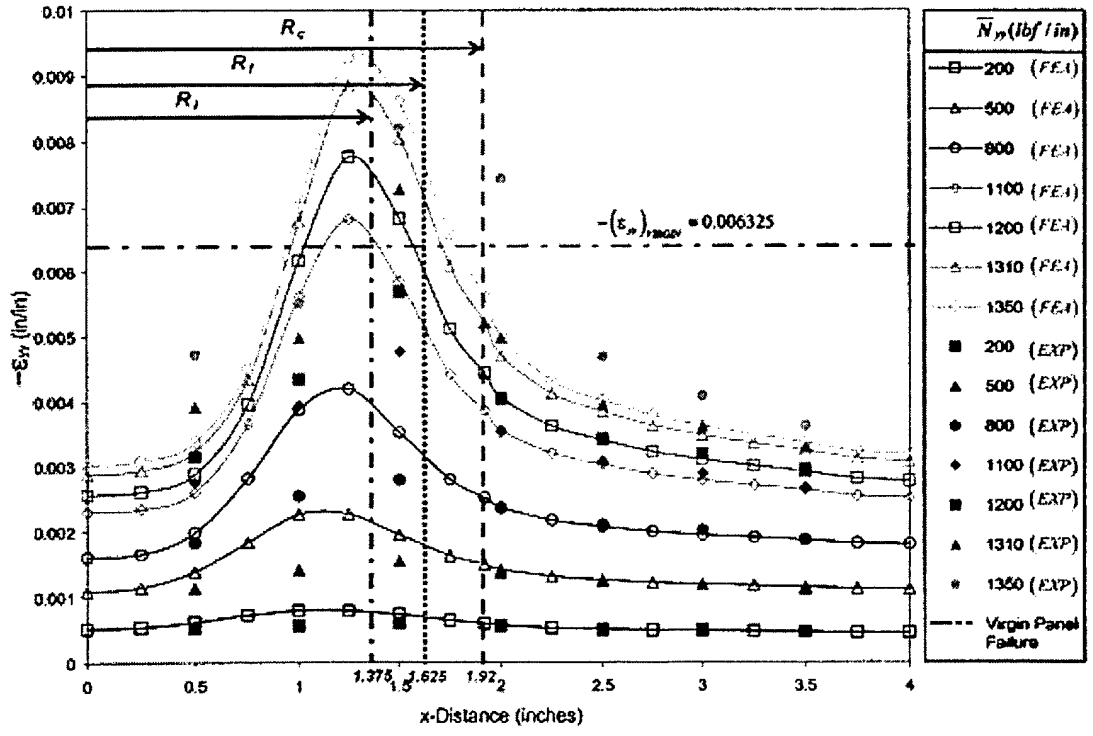

FIGURE 5-11. STRAIN DISTRIBUTION ALONG THE LINE, $y = 0$ (50% VIRGIN FACESHEET PROPERTIES)

Because the FEA was incapable of predicting the residual strengths of the virgin and impacted panels and because the panels failed by crippling or by a propagation of out-of-plane buckling, recourse was taken to use a semiempirical approach. In this approach, the FEA was calibrated to the panel WXC 29L test and then used to predict residual strength of other panels tested in reference 3. If successful, such an approach may reduce the amount of requisite testing and extend the database to other impact energies and facesheet thicknesses. The calibration was accomplished by comparing test and analysis strain at a distance of 2.5 in. from the center of the panel at y = 0 and at the failure load of the panel of 1350 lbf/in. The 2.5-in. location was chosen because it had the highest strain readings away from the damaged area with the additional advantage of having more than one reading. This resulted in increasing the residual strength prediction by a factor of 4500/3800 = 1.18. The test strain of 4500 μin/in is an average of the measured strains at gages 3, 8, 14, and 18. Thus, to predict residual strength for other test panels, this factor and the 50% reduction in stiffness properties in the damage area was used. Failure is assumed when the ligament strain at that location reaches 4800 μin/in.

Three additional symmetric flat sandwich composite panels were CAI tested in reference 3. The layup configuration for a given sandwich panel was given by $[90/45]_i$/CORE/$[45/90]_i$, where 2_i is the number of plies in a given facesheet. Table 5-3 describes sandwich panel configurations for each specimen as well as the impactor diameter and impact energy used in the impact tests. The impactor diameter (3.0 in.) was the same as for the originally modeled specimen. The variables that are different are facesheet thicknesses and impact energies. A combination of NDI and destructive sectioning was used to establish initial conditions for damage for use in finite element analyses of the given panels. Table 5-5 summarizes the measured damage sizes from reference 3. Note that several of the test specimens had very shallow residual facesheet indentations that approached the limits of mechanical measurements. To facilitate convergence of the numerical solutions for these cases, a peak residual facesheet indentation equal to 1/2 of the facesheet stackup thickness was assumed. Finite element estimates of the CAI residual strength were developed for the additional three sandwich panels in the two tables. Similar to the preceding analysis, a 50% reduction in ply properties was assumed for an equivalent inclusion located at the center of the impacted facesheet. Table 5-6 contains a summary of the predicted CAI residual strengths including the correlation factor of 1.18 for each specimen as well as the experimentally determined values from reference 3. Note that for each specimen, the numerical calculations generally provided very good estimates of the CAI residual strengths for thinner facesheet panels and an overestimate for thicker facesheet panel.

TABLE 5-5. SANDWICH PANEL CONFIGURATION AND IMPACT PARAMETERS

Test	Specimen ID	Facesheet Configuration	t_c (in.)	Impactor Diameter (in.)	Impact Energy (lbf-in)
1	WXC11D	[90/45]	3/4	3	63.6
2	WXC23G	$[90/45]_2$	3/4	3	63.6
3	WXC38P	$[90/45]_3$	3/4	3	98.4

TABLE 5-6. MEASURED AND PREDICTED RESIDUAL STRENGTHS

Test	R_I (in.)	R_f* (in.)	R_c (in.)	δ_f (in.)	δ_c (in.)	Inclusion Ply Properties (%)	Predicted Residual Strength (lbf/in)	Experimental Residual Strength (lbf/in)
1	0.625	0.625	1.0	0.0145	0.2445	50	980	945
2	0.375*	0.375	1.125	0.016*	0.178	50	2050	2024
3	0.5*	0.5	1.125	0.024*	0.188	50	3010	2453

*Assumed value.

This study suggests that finite element analyses have the potential to provide semiempirical estimates of residual strength for impact-damaged sandwich composites provided that the initial damage configuration can be determined via standard NDI techniques and the virgin panel failure behavior is well understood. Nonetheless, one should proceed with extreme caution when attempting to estimate sandwich composite residual strengths based solely on numerical analyses. Tomblin, et al. [3 and 6] demonstrated that there is a tremendous degree of scatter in the experimentally observed residual strengths for sandwich panels with similar levels of impact damage based upon nondestructive inspection, particularly for impacts involving sharper impactors. The onset of damage progression and failure may be highly sensitive to the details of the local damage distribution and residual stress field; such influences are difficult to address using the effective continuum approach adopted here.

5.1.4 ANSYS Results and Correlation With Tests.

The ANSYS FEA was performed for the same panel as the ABAQUS FEA described in section 5.3. The input data was slightly different and is shown in tables 5-7 and 5-8. Although in this analysis the damage zone can be modeled as an ellipse, a circle was assumed because it matched the test data.

TABLE 5-7. GEOMETRIC PROPERTIES FOR ANSYS FINITE ELEMENT MODEL
(Dimensions shown in inches)

Facesheet	$2a$	$2b$	t_f	R_I	R_f	δ_I
	8	10	0.032	1.5	-	0.135
Core	$2a$	$2b$	t_c	R_c	δ_c*	
	8	10	0.75	1.95	0.244	

*Determined from destructive sectioning.

TABLE 5-8. MATERIAL PROPERTIES FOR FINITE ELEMENT MODEL

	Facesheet	Core
E_1 (psi)	10.06×10^6	4.5
E_2 (psi)	10.06×10^6	4.5
E_3 (psi)	1.17×10^6	20×10^3
G_{12} (psi)	0.62×10^6	33.56
G_{13} (psi)	0.6×10^6	5.8×10^3
G_{23} (psi)	0.6×10^6	20×10^3
ν_{12}	0.058	0.6
ν_{13}	0.32	3.0×10^{-5}
ν_{23}	0.32	3.0×10^{-5}
σ_{ult} (psi)	–	350
σ_{CRUSH} (psi)	–	150

In the ANSYS model, instead of reducing the facesheet stiffness properties to obtain a better correlation with analysis, the core-crushing strength was varied from 350 to 150 psi. Also, the damaged portion of the core was permitted to grow once the assumed ultimate stress level was reached. Note that in figure 5-5, the 350 psi is equal to the crushing strength for a virgin core, while the 150 psi is the core strength after the core crushing initiates.

The far-field stress is plotted against local strains ε_{yy} at three strain gage locations, and the FEA results are compared with experimental data in figures 5-12 to 5-14. The locations are the same as indicated in figure 5-7. The comparison shows excellent correlation when 150 psi is used as the ultimate core-crushing strength. This suggests that the real core damage region is probably much bigger than the one shown in the C-scan picture for the damage level in this case because the damage was inflicted by a big tup (3″ in diameter) at a relatively high-impact energy level (250 in-lbf).

From figures 5-12 and 5-13, the knee point corresponds to the moment that the core damage propagation reaches the specific strain gage location. The apparent sudden softening at that point, shown on the curve is directly due to the local core crushing beneath that location. Both the experimental data and numerical analysis support this. This point could be treated as an indication of the initiation of damage propagation. The far-field stress corresponding to the knee point on the stress-strain curve of the location furthest from the initial damage could be used as the residual strength of the panel because the catastrophic failure would soon follow according to the observation in the strain response of gage no. 3, see figure 5-13. This is confirmed by strain gage no. 4, which is closer to the damage (see figure 5-13). Here, there is gradual nonlinear response starting at about 15 ksi and continuing until failure at 20 ksi. Note that the far-field strain response in figure 5-14 (gage no. 13) does not have the elastic-plastic behavior.

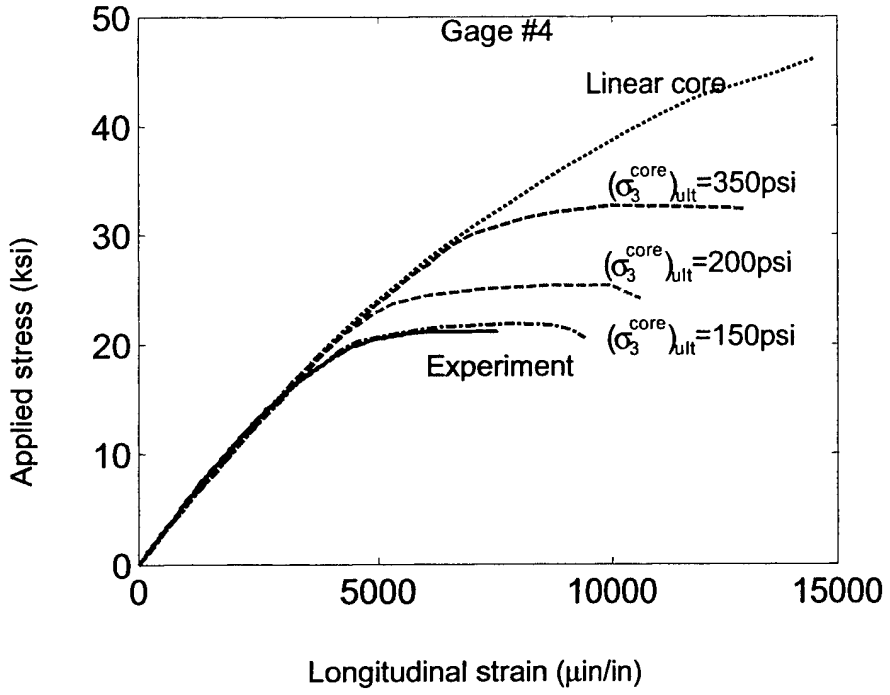

FIGURE 5-12. FAR-FIELD STRESS VERSUS STRAIN FOR GAGE NO. 4 LOCATION

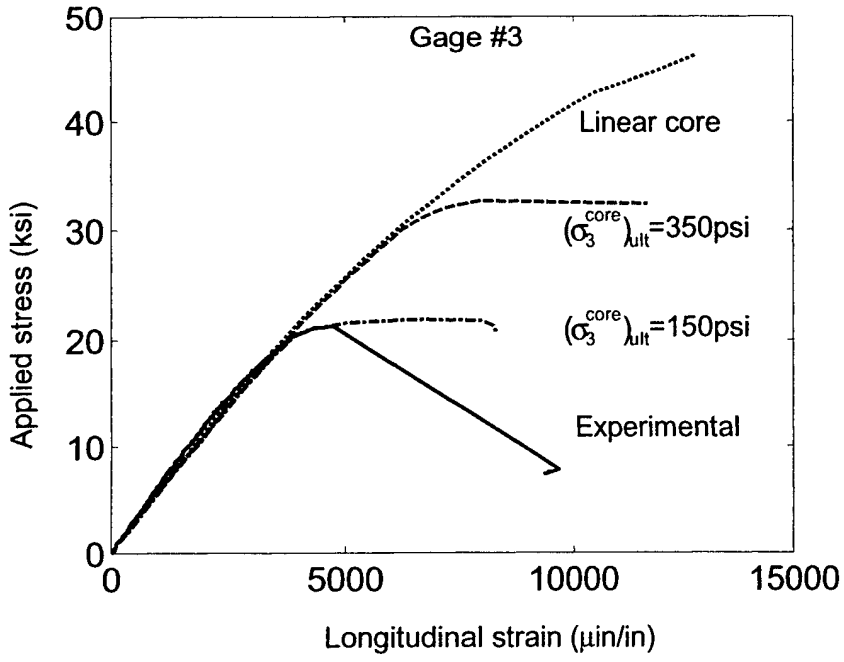

FIGURE 5-13. FAR-FIELD STRESS VERSUS STRAIN FOR GAGE NO. 3 LOCATION

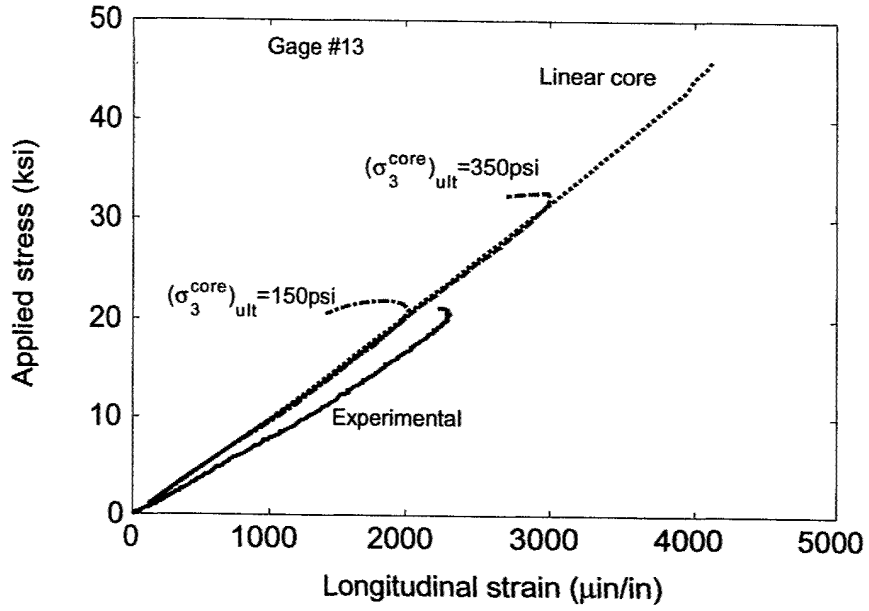

FIGURE 5-14. FAR-FIELD STRESS VERSUS LOCAL STRAINS FOR GAGE NO. 13 LOCATION

As introduced before, the element birth and death is used to simulate the additional core crushing. Figures 5-15 and 5-16 show the differences of results on structure deformation and stress contour, especially in the vicinity of the damage zone, with and without using this technology in analysis.

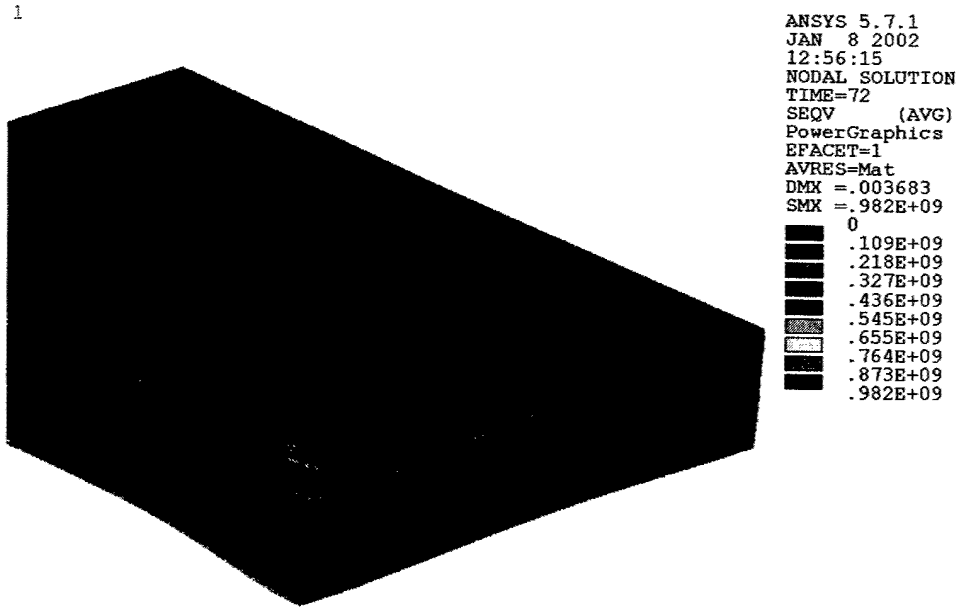

FIGURE 5-15. ANSYS MODEL INCLUDING PROPAGATION OF CORE CRUSHING

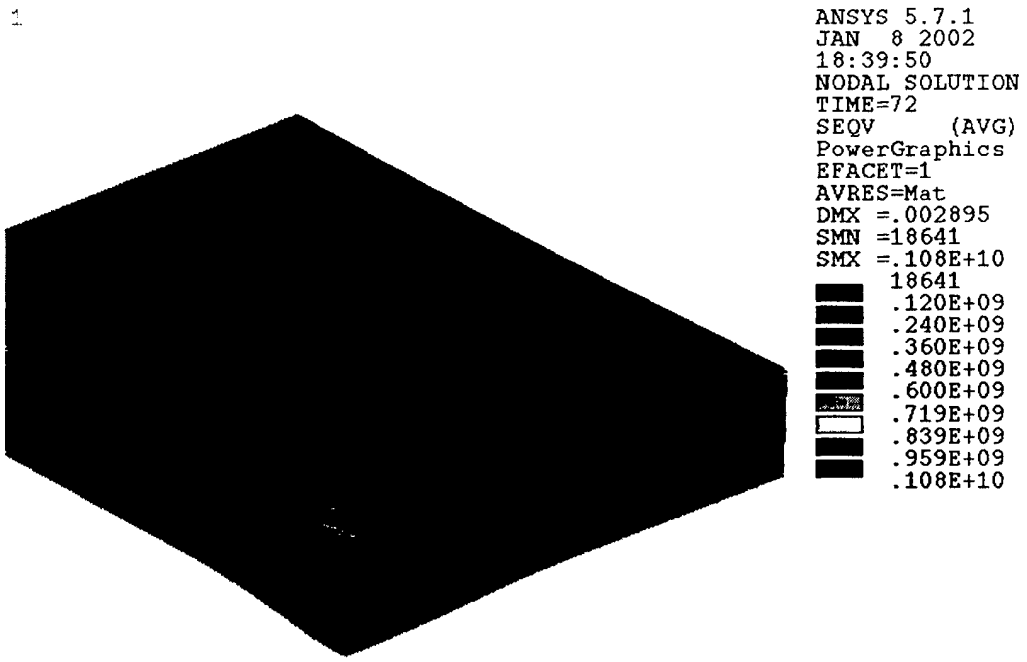

FIGURE 5-16. ANSYS MODEL WITHOUT PROPAGATION OF CORE CRUSHING

Due to the existence of a large damage, a small bulge in the middle of the backside facesheet of the panel could be observed in FEA. This phenomenon is in agreement with the observation in the experimentation and the ABAQUS analysis.

5.2 ANALYTICAL MODEL.

Based on experimental observations, an analytical model was proposed and applied to the damage propagation behavior of low-velocity impacted sandwich panels under compression. This model was first proposed by Minguet [8]. Thereafter, it was adopted and modified by Tsang [20] and by Moody [21] and [22]. One limitation of all their models was that it was restricted to symmetrical cross-ply facesheets. Further modifications have been made to expand the application of the model to the unsymmetrical angle-ply facesheets. The modified model also allows for propagation of the core-crushing region from the edge of the initial damage zone.

5.2.1 Basic Assumptions.

The facesheet of the impacted sandwich panel is modeled as a composite laminate with an initial deflection in shape and partially supported by an elastic foundation, residing in a compressive field. A nonlinear theory of asymmetrically laminated anisotropic elastic plates is then applied [23]. A standard x, y, z Lagrangian coordinate system, as shown in figure 5-17, is adopted in deriving the equations. The following basic assumptions are made:

- The backside facesheet has no influence on the damage propagation of the impacted facesheet. Only the damaged facesheet is necessary to be considered in the model.

- The facesheets of the sandwich structure are thin, i.e., the thickness is much smaller than the length and width.
- The facesheet has constant thickness.
- The in-plane displacements u and v are small compared to the plate thickness. This may not be the case with the out-of-plane deflection w.
- Tangential displacements u and v are linear with respect to the z coordinate.
- Transverse shear strains ε_{xz} and ε_{yz} are negligible, i.e., the Kirchhoff's theory still holds.
- The transverse normal strain ε_z is negligible.
- There are no body forces.
- Each ply is linearly elastic.
- The in-plane stiffness of honeycomb core is negligible compared with the out-of-plane stiffness and the shear stiffness between the z coordinate and the x, y coordinates.

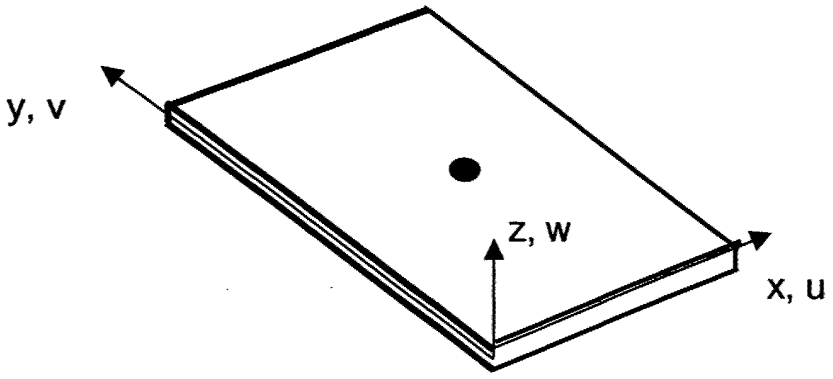

FIGURE 5-17. COORDINATE SYSTEM OF THE IMPACTED PANEL

5.2.2 Model Input and Output Parameters.

The solution of this problem depends on following 44 input parameters. They are divided into four categories.

1. Panel global geometric parameters (3):

   a ~ panel dimension in the x direction
   b ~ panel dimension in the y direction
   t ~ facesheet thickness

2. Damage geometric parameters (6):

Indentation:

z0 : center depth of the residual indentation
rdentx : radius of the residual indentation in the x direction
rdenty : radius of the residual indentation in the y direction

Initial crushed core region:

cd0 : maximum depth of the crushed core region
rcrushx : radius of the crushed core in the x direction
rcrushy : radius of the crushed core in the y direction

3. Material properties (25):

Facesheet:

a_{ij}^{i} : 6 unique components of matrix $A^{i} = A^{-1}$;

b_{ij}^{*} : 9 unique components of matrix $B^{*} = -A^{-1}B$;.

d_{ij}^{*} : 6 unique components of matrix $D^{*} = D - BA^{-1}B$.

Elastic foundation (Core):

kzz : out-of-plane stiffness of the intact core
kxz : shear stiffness in xz plane of the intact core
kyz : shear stiffness in yz plane of the intact core
cult: ultimate stress of the intact core

4. Implementation parameters in solving process (10):

modesx: number of modes in the x direction
modesy: number of modes in the y direction
maxdiv: maximum number of diverging iterations allowed for convergence
maxiter : maximum number of iterations allowed for convergence
maxer : maximum convergence error
syymax : maximum far-field stress in the y direction
delmin : minimum far-field stress increase allowed
syymin : initial far-field stress
delsyy : initial far-field stress increase
urf : under-relaxation-factor

The basic output values include (3 sets):

- z_{ij} ~ modal amplitudes for the initial panel indentation
- w_{ij} ~ modal amplitudes for the out-of-plane deflection at a specific far-field stress level
- f_{mn} ~ modal amplitudes for the airy stress function at a specific far-field stress level

where $i = 1,3,\ldots,$ (2*modesx-1) ; $j = 1,3,\ldots,$ (2*modesy-1);
and $m = 0,2,\ldots,$ 2*(modesx-1) ; $n = 0,2,\ldots,$ 2*(modesy-1).

The deflection, stress components, and strain components at any point on the facesheet can be derived from the above three sets of basic outputs.

5.2.3 Model Derivation.

The process adopted to derive the following equations is similar to what Moody used in his previous work [16]. Several modifications have been made.

1. The application of the model has been extended from the cases with cross-ply facesheet only to those with asymmetrical angle-ply facesheets.

2. Due to the difficulty in parameter characterization, the stiffness degradations used in Moody's model is not included here.

3. For the clarity in mathematics, the principle of virtual work is used here to derive the equilibrium equations instead of the minimization of the total potential energy.

4. The additional core crushing is considered in this model to simulate the damage propagation. The nonlinear equations for the amended model are in [24].

5.2.4 Correlation With Experimental Results.

The same CAI test that was used for FEA analysis was used to evaluate analytical model results, see section 5.1.3. The input data used in the analysis are displayed in table 5-9.

The comparison between analysis and test is shown by far-field stress versus local strain curves at four gage locations. Figures 5-18 and 5-19 are strain responses in the vicinity of the damage where the local strain values are elevated because of the effects from the large damage zone in this case. Initial response in both locations is excellent at low far-field stresses, but the final failure is predicted much lower, particularly in terms of strain. The predictions for far-field strains are much better, as shown in figures 5-20 and 5-21. The analysis indicates no additional core crushing in this case because of the numerical divergence of the program at a relatively low far-field stress value. This is due to the high damage level in this case. The failure stress that was predicted is 17 ksi, which is 15% lower than test.

TABLE 5-9. INPUT DATA

Variables	Value	Unit	Variables	Value	Unit
a	8	in.	b_{62}^{*}	0.0	in.
b	10	in.	b_{66}^{*}	3.0782e-3	in.
t	0.032	in.	d_{11}^{*}	21.1322	$\text{psi}-\text{in}^3$
z0	-0.135	in.	d_{12}^{*}	8.0714	$\text{psi}-\text{in}^3$
rdentx	1.5	in.	d_{16}^{*}	0.0	$\text{psi}-\text{in}^3$
rdenty	1.5	in.	d_{22}^{*}	21.1322	$\text{psi}-\text{in}^3$
cd0	0.244	in.	d_{26}^{*}	0.0	$\text{psi}-\text{in}^3$
rcrushx	1.95	in.	d_{66}^{*}	6.5309	$\text{psi}-\text{in}^3$
rcrushy	1.95	in.	kzz	85000	$\text{psi}-\text{in}$
a_{11}^{i}	4.3648e-6	$(\text{psi}-\text{in})^{-1}$	kxz	0	$\text{psi}-\text{in}$
a_{12}^{i}	-1.4427e-6	$(\text{psi}-\text{in})^{-1}$	kyz	0	$\text{psi}-\text{in}$
a_{16}^{i}	0.0	$(\text{psi}-\text{in})^{-1}$	cult	350	psi
a_{22}^{i}	4.3648e-6	$(\text{psi}-\text{in})^{-1}$	modesx	30	-
a_{26}^{i}	0.0	$(\text{psi}-\text{in})^{-1}$	modesy	30	-
a_{66}^{i}	1.1615e-5	$(\text{psi}-\text{in})^{-1}$	maxdiv	10	-
b_{11}^{*}	-1.5391e-3	in.	maxiter	200	-
b_{12}^{*}	1.5391e-3	in.	maxer	0.005	-
b_{16}^{*}	0.0	in.	syymax	-1e5	psi
b_{21}^{*}	1.5391e-3	in.	delmin	-1e3	psi
b_{22}^{*}	-1.5391e-3	in.	syymin	-10	psi
b_{26}^{*}	0.0	in.	delsyy	-1e-3	psi
b_{61}^{*}	0.0	in.	urf	1	-

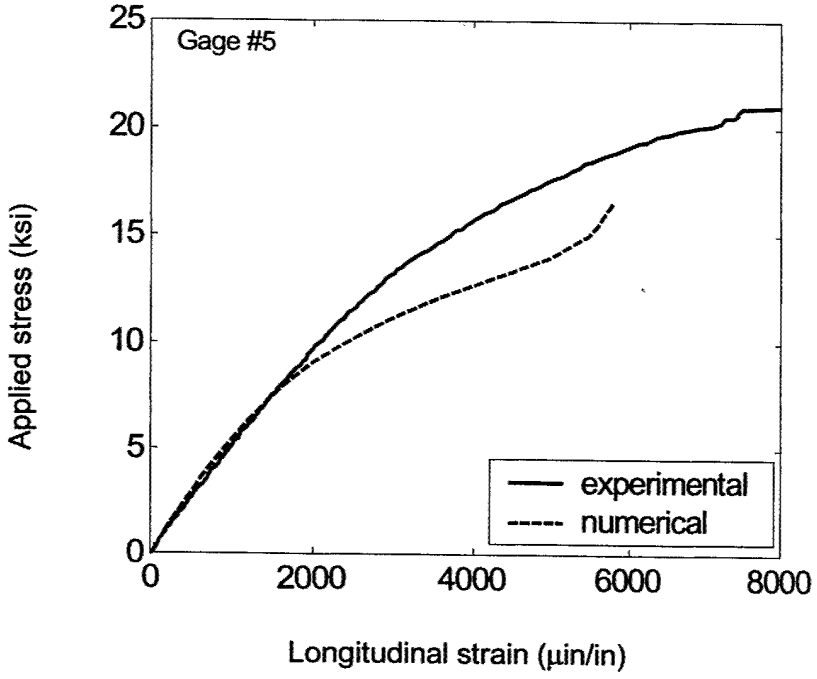

FIGURE 5-18. COMPARISON OF STRAINS AT GAGE NO. 5

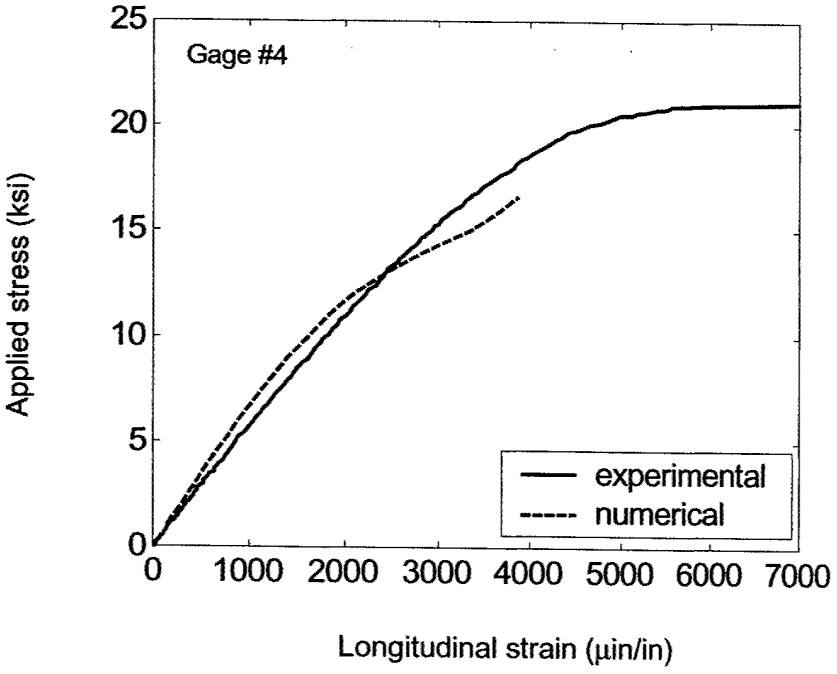

FIGURE 5-19. COMPARISON OF STRAINS AT GAGE NO. 4

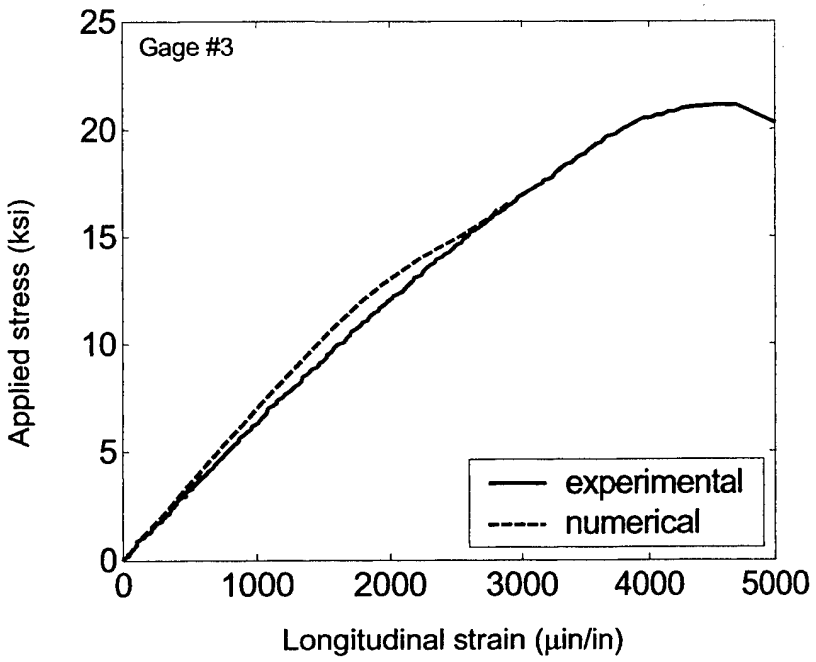

FIGURE 5-20. COMPARISON OF STRAINS AT GAGE NO. 3

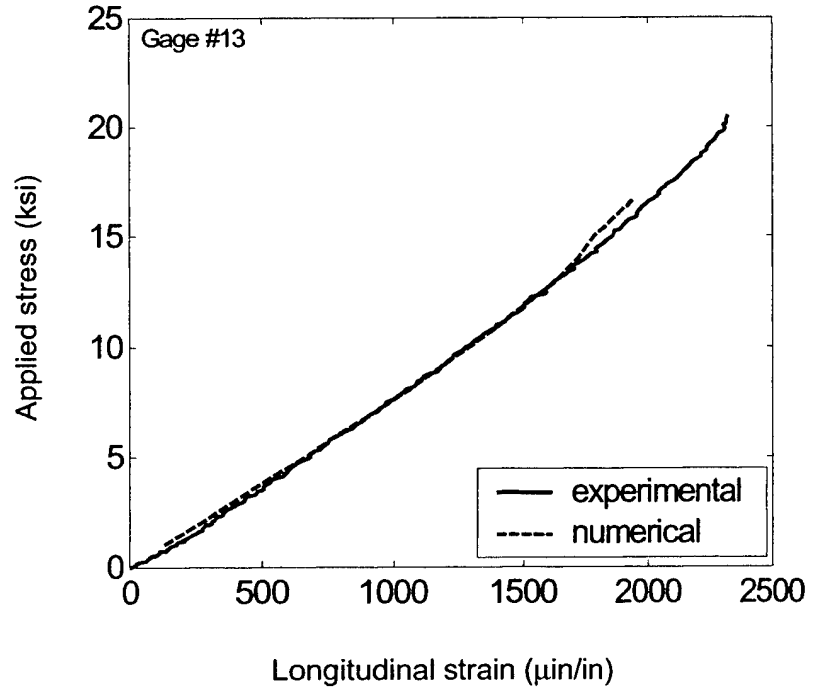

FIGURE 5-21. COMPARISON OF STRAINS AT GAGE NO. 13

5.3 COMPARISON OF ANALYTICAL AND FEA METHODS.

In this study, physically motivated numerical models have been developed for predicting the residual strength of impact-damaged sandwich composites comprised of woven fabric carbon/epoxy facesheets and Nomex honeycomb cores subjected to loading. Results from nondestructive inspection and destructive sectioning of damaged sandwich panels were used to establish initial conditions for damage (residual facesheet indentation, core crush dimensions, etc.) in the numerical analyses. Honeycomb core crush test results were used to establish the nonlinear constitutive behavior for the Nomex core. The influence of facesheet property and core degradation on the stress redistribution in damaged sandwich panels was examined. Positive attributes of the analysis effort were

- The ANSYS FEA and the analytical models can describe the damage growth behaviors similarly to what was observed in experiments by propagating core crushing. The ABAQUS approach can degrade core and facesheet properties but only as initial input.

- Estimates of far-field stress versus local strains from the FEA and analytical models showed relatively good correlation with the experimental data.

- The ABAQUS, ANSYS FEA, and the analytical models showed that the core stiffness and the core crushing strength play a big role in the behavior of impacted panels under unidirectional compression. The core-crushing strength directly relates to the initiation of damage propagation at the edge of the damage zone.

- The ABAQUS FEA model results show that improvement in strain correlation can also be obtained by reducing the stiffness of the facesheets in the damaged area.

- The ABAQUS FEA was used in a semiempirical approach to extend the test database to other sandwich configurations and energy impact levels.

Negative findings were

- Predictions of residual strength in both models were relatively poor and needed adjustments to correlate with experimental data.

- For FEA, it is not a trivial matter to construct a model that adequately simulates the mechanics of the problem.

- The analytical model has fewer requirements for the common user than the FEA, but there are other limitations. Lack of convergence is a concern when appropriate input parameters are not specified. In this case, the parameter adjustment needs to be conducted based on the specific problem studied combined with the user's experiences and knowledge.

In order to fully develop the concepts presented here, further investigations involving other classes of material systems, different types of damage, and other modes of loading may be warranted. In addition, consideration of progressive damage evolution in the facesheets and application of other more sophisticated failure criteria may be desirable. Such work may facilitate sandwich panel design by providing insights into relationships between structural configuration and damage progression that lead to better sandwich structures with improved damage tolerance characteristics.

6. DAMAGE TOLERANCE GUIDELINES.

6.1 GENERAL GUIDANCE.

Section 1.1 provided background on levels of composite damage and the associated design load requirements for composite structure. This provides a basis for the philosophy used in static strength, fatigue, and damage tolerance substantiation. Realistic composite damage that may never be discovered in manufacturing or service inspections has traditionally been required to sustain fatigue cycles without significant growth. A demonstration of such fatigue resistance usually culminates with a static strength test taken to ultimate loads. More severe composite damages, which are detectable using service inspection procedures are highly unlikely, are subjected to the more familiar damage tolerance practices of sustaining limit load for inspection intervals. Finally, damage that occurs with knowledge to the aircraft operator is expected to sustain continued safe flight loads.

Following the philosophy provided in section 1.1, some general guidance can be established for a damage threat assessment and the characterization of impact damage, which should be applied for static strength, fatigue, and damage tolerance substantiation. Recent efforts by an international Aviation Rulemaking Advisory Committee (ARAC) for damage tolerance and fatigue evaluation of composite rotorcraft structure provided the most definitive FAA guidance in this area [25 and 26]. Figure 6-1 illustrates the extent of the impact damage that needs to be considered in the damage tolerance and fatigue evaluation.

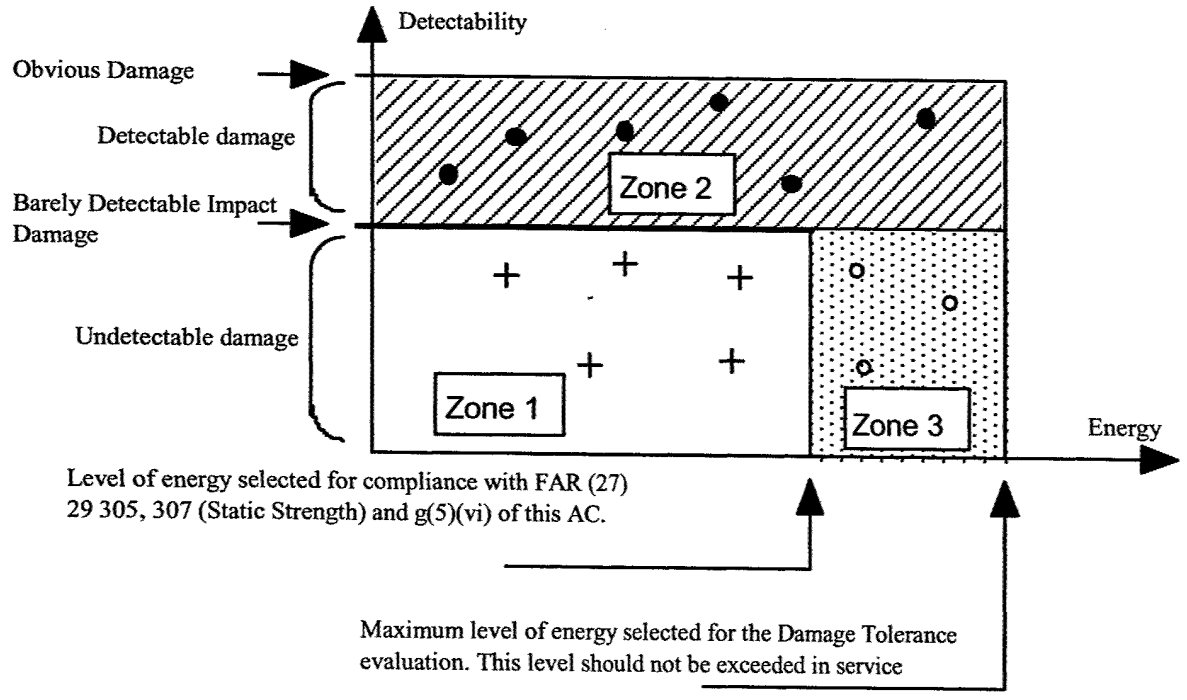

FIGURE 6-1. CHARACTERIZATION OF IMPACT DAMAGE

Both the energy level associated with static strength demonstration and the maximum energy level associated with the damage tolerance evaluation (defined in the figure above) are dependent on the part of the structure under evaluation and a threat assessment. Obvious impact damage is used here to define the threshold from which damage is readily detectable and appropriate actions taken before the next flight. Barely Detectable Impact Damage defines the state of damage at the threshold of detectability for the approved inspection procedure. BVID is that threshold associated with a detailed visual inspection procedure. Detectable damage defines the state of damage that can be reliably detected at scheduled inspection intervals. Visible Impact Damage (VID) is that state associated with a detailed visual inspection.

Three zones are defined by this figure:

- Zone 1: Because the damage is not detectable, ultimate load capability is required.

- Zone 2: Because the damage can be detected at scheduled inspection, limit load (considered as ultimate) capability is the minimum requirement for this damage.

- Zone 3: Because the damage is not detectable with the proposed in-service inspection procedures, ultimate load capability is required, unless an alternate procedure can show an equivalent level of safety. For example, residual strength lower than ultimate may be used in association with improved inspection procedures or with a probabilistic approach showing that the occurrence of energy levels is low enough so that an acceptable level of safety can be achieved.

Of the three zones, only zone 3 may have a residual strength requirement that can vary with alternate procedures and/or the probability of damage occurrence. In either case, any compromise for residual strength requirements less than the ultimate load requirement should only be considered when pursuing one of the options under a damage tolerance means of compliance (i.e., for composites, all safe life options for fatigue substantiation require a demonstration of ultimate load capability).

One example of the use of alternate procedures is for the rare damage threat from a high energy, blunt impact (e.g., service vehicle collision). Depending on the selected maintenance inspection scheme, such damage may fall under the category of zone 3. When considering such damage in the design of a part, it may be shown to be damage tolerant, even though the damage is not detectable, based on a very low probability of occurrence. As a result, the design would have sufficiently high residual strength (e.g., below ultimate, but well above limit to ensure safety without detection for long periods of time). If it is further determined that such impact events usually occur with the knowledge of maintenance or aircraft service personnel, then the alternate procedures may be added to the instructions for continued airworthiness. For example, advanced inspection methods, which can detect damage from high-energy blunt impacts, could be added to such instructions and used as alternate procedures to minimize the risk of catastrophic failure for such zone 3 damage.

The current effort described in this report has concentrated in the first two areas of figure 6-1 (i.e., static strength and damage tolerance considerations where repeated loads must be

sustained) using fairly small coupons, and thus, the results obtained may be subjected to structural scaling issues. Future efforts will address larger damages using larger elements and full-scale subcomponents and components.

6.2 GUIDELINES FOR TEST CHARACTERIZATION.

Impact damage in sandwich panels, which is caused by blunt impactors, has been found to lead to one of two contrasting final failure modes under in-plane compressive loads. The impact damage, which manifests in the form of a dimple, will be active well before the final failure occurs. The amount of this activity, which manifests itself in core failure as the dimple grows, will be dependent on the flexural properties of the facesheet, transverse compressive properties of the core, and the damage metrics. A thin facesheet with negligible flexural stiffness will promote a strain concentration adjacent to the impact damage and local compressive failure mechanism in the skin. This mechanism is dominant due to the instabilities of local skin damage and the inability of the thin skin to drive the dimple into progressive core failure. However, given enough flexural stiffness and local damage to the core, the facesheet will drive this dimple through a characteristic sequence of events leading to a stability-based failure mechanism. Both the strain concentration and stability-based failure mechanisms should be characterized in a damage tolerance test program whenever the threat assessment and sandwich design parameters indicate the potential exists. A complete assessment will provide safety assurance throughout the service life of the sandwich structure.

A threat assessment is needed to identify impact damage severity and detectability for design and maintenance [25 and 26]. A threat assessment usually includes damage data collected from service plus an impact survey. An impact survey consists of impact tests performed with configured structure, which is subjected to boundary conditions characteristic of the real structure. Many different impact scenarios and locations are typically considered in the survey, which as one goal, attempts to identify the most critical impacts shown in figure 6-1 (i.e., those causing the most serious damage but are least detectable). Until sufficient service experience exists to make good engineering judgements on energy and impactor variables, impact surveys should consider a wide range of conceivable impacts, including runway or ground debris, hail, tool drops, and vehicle collisions. Service data collected over time can better define impact surveys and design criteria for subsequent products as well as establish more rational inspection intervals and maintenance practice.

The current investigations based on test specimens impacted with a range of energies and impactor tip diameters (i.e., 1 inch and 3 inches) found that CAI residual strength degradation curves possibly approach an asymptote as damage areas become large (figure 6-2). Some evidence suggests that the stability-based failure mechanism, which includes dimple growth, has some dependence on sandwich specimen size. Analysis and test efforts should evaluate the potential for specimen size effects on the shape and asymptotic value of the CAI strength degradation curve.

After performing a threat assessment and impact survey, CAI strength degradation curves should be developed for a complete range of impact damage threats. In combination, this data provides the information on damage detectability and residual strength needed to establish rationale design criteria. As discussed previously, nondetectable damage should not lower the residual

strength below ultimate load levels unless a probabilistic argument can be made indicating that the impact scenario for such damage is very rare. In the current study, large diameter impactors and some combinations of sandwich design parameters led to nondetectable damage within the apparent asymptote of the residual strength curve. When configuration and impact variables for a specific design can result in this scenario, the asymptotic value can be used as the allowable design strain levels associated with ultimate static strength. This approach provides maximum airworthiness assurance of the sandwich structure under a variety of damage threats that result in undetected and detected damage. If a reliable NDI is available and used in service, this rule of thumb can be relaxed.

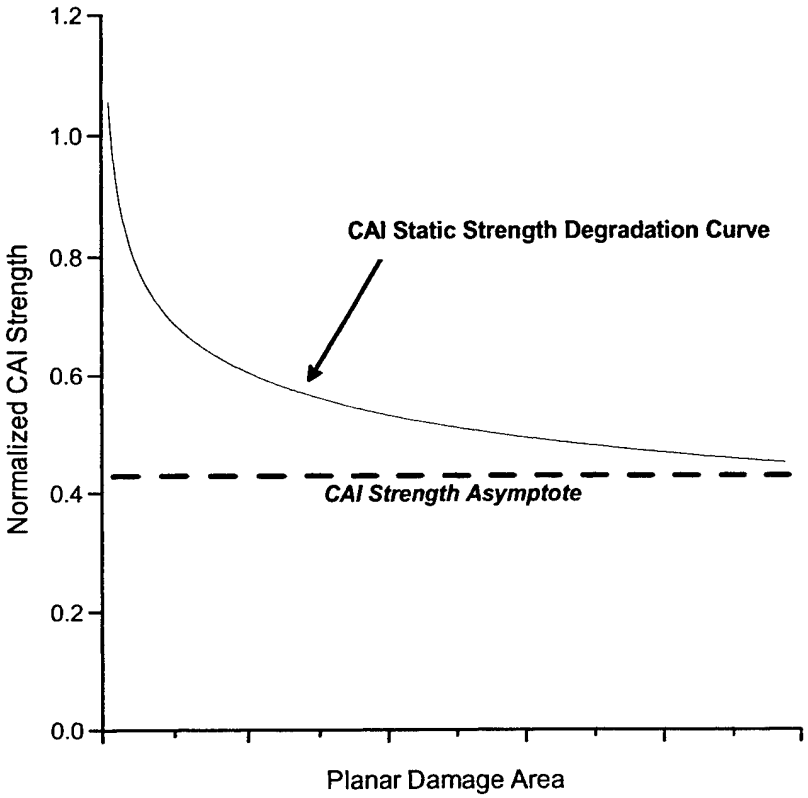

FIGURE 6-2. CAI STATIC STRENGTH DEGRADATION CURVE

Based on limited data, the fatigue threshold limit for 150,000 cycles was found to be approximately at 65% of CAI strength for carbon/epoxy facesheet honeycomb panels and 75% for fiberglass/epoxy facesheet foam panels. This data was derived for constant-amplitude testing. The guideline is that the maximum compressive load in a fatigue spectrum should not exceed the thresholds enumerated above. Repeated loads above the thresholds may lead to early fatigue failures, especially if such loads impinge on the static CAI strength distribution. For fatigue cycling below those limits, life will exceed 150,000 cycles of constant-amplitude fatigue, which is a very severe spectrum for most airplanes. Such cycling will also have very little effect on residual CAI strength.

6.3 GUIDELINES FOR NDI.

Impact results from the current investigations indicated that the larger-diameter impactor produced significantly different damage states when compared to the smaller impactor (at the same impact energy level) and that visual detection alone cannot be used to assess damage. The results indicated that the larger-diameter impactor produced a very benign-appearing damage state, wherein no surface fracture or cracks or visually perceptible levels of indentation existed, but NDI did indicate a large damage region, which likely related to the observed reduction in strength. This damage scenario proved to be the most elusive when the impacted specimens were inspected using a typical visual inspection protocol. The results of these investigations show that the visual inspection methods are misleading and the residual indentation cannot be used as a reliable damage metric for static ultimate strength and damage tolerance criteria for sandwich structures. The results indicate the use of field inspection instruments are much more reliable at detecting overall damage to the sandwich structure.

Under the assumptions that additional field inspection techniques must be used to quantify the extent of damage in the structure, various field techniques for NDI were investigated. Based on the experimental results, it can be concluded that the detection of impact damage in honeycomb and foam core sandwich panels cannot be accomplished to the same level of accuracy using a single field inspection technique when compared to laboratory techniques. The experimental data suggests that the impact damage in honeycomb core sandwich panels is better detected by a technique that measures the local stiffness of the sandwich, while the damage in foam core panels can be best assessed with a technique relying on the measurement of acoustic impedance. The trends observed for foam core panels may be biased by the normalization procedure due to the inability to corroborate the damage size using destructive sectioning.

Using the honeycomb core panels as a baseline, it can also be concluded that the reliability of detecting damage using field inspection techniques is generally reduced when compared to laboratory or manufacturing production C-scan methods. Figure 6-3 shows the extent of damage that was detected using various field inspection instruments as a function of facesheet thickness. The error bars shown in figure 6-3 indicate the range of reported measurements. As the facesheet thickness increases, the ability of each field inspection technique to locate and characterize the extent of damage reduces, as shown in figure 6-3. It should also be noted that the maximum number of plies in this study was six fabric plies. For thicker facesheets, the measurement reliability will decrease. Thus, the measured damage in the laboratory may actually be two times greater than that measured in the field, which will likely influence the damage tolerance and inspection plan developed based on a ADL and/or CDT size.

In the beginning of a damage tolerance test program, it is advisable for the user to define a similar detectability ratio plot, as shown in figure 6-3, to account for the sensitivity of the field inspection technique used for the specific design detail of a given aircraft product. All efforts in establishing reliable NDI for field inspection should be coupled with work on the threat assessment, impact survey, residual strength, and fatigue testing. The relationships developed should then be incorporated into an appropriate inspection plan for damage throughout the service life of the structure.

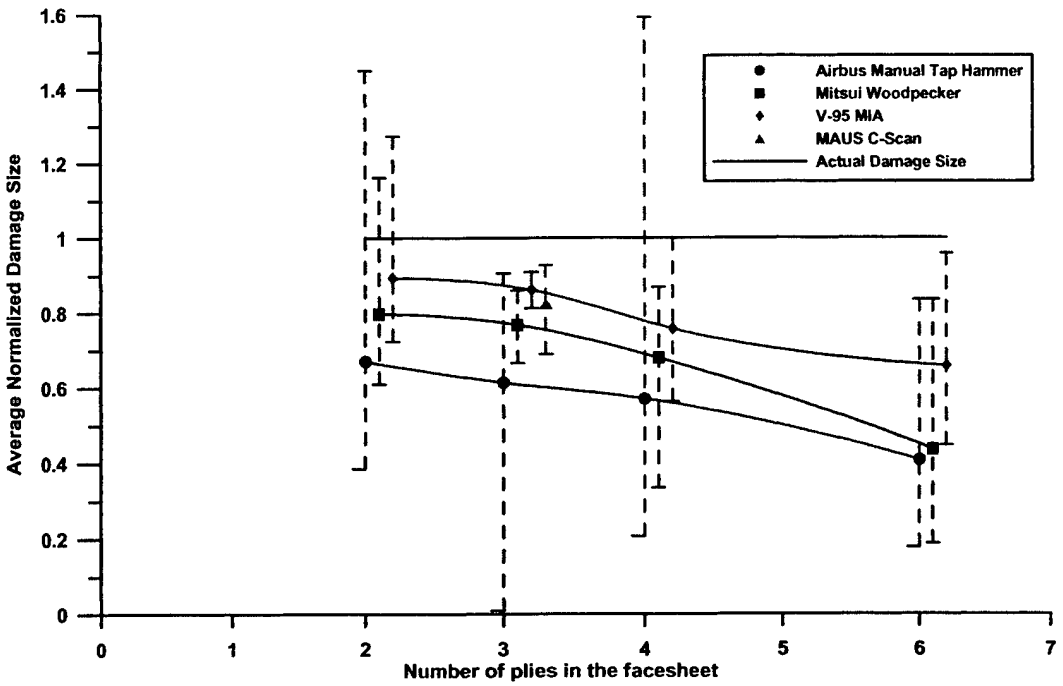

FIGURE 6-3. DETECTED DAMAGE SIZE BASED ON DAMAGE DIAMETER USING DIFFERENT FIELD DETECTION INSTRUMENTS AS A FUNCTION OF FACESHEET THICKNESS

6.4 GUIDELINES FOR ANALYSIS.

Analysis, whether performed by closed form solutions or finite element models, can be useful in design and certification of impact-damaged composite sandwich structures. The current state of the art is such that analysis cannot be reliably applied without supporting tests. However, it can be useful in directing and analyzing test results and expanding test data to untested configurations by semiempirical methods. The analytical work completed and documented in this report showed that careful modeling can describe the structural response of the impacted panel under compressive load, but some adjustments were needed to predict failure. The analysis performed also showed that damage progression capability is vital to the fidelity of the analysis.

Statistical response surfaces that were generated by this research program can be used as guidance to determine what size damage is expected in terms of the pertinent variables. This will reduce hunt and peck testing to find the energy levels for barely visible damage or planar damage when interpolating within the variables studied. Furthermore, response surface damage metrics can be used as input in consequent structural analysis methods. However, the user should be careful in directly applying results from this study to a somewhat different set of design details and impact threats. Instead, a similar approach should be applied to additional experiments using design and impact variables more closely associated with the particular application.

In concert with testing the structure, FEA can be of help to develop the residual strength curves (figure 6-2) as a function of damage size or impact energy for different impactors and structural locations. This will reduce the cost of generating such data.

7. FUTURE WORK.

There is a current effort to extend the present studies to larger structures and relate the results obtained in the present work at the coupon level to specimens more representative of actual sandwich structures. Testing and analysis is being performed on carefully scaled specimens in both geometry and impact severity. This will allow the translation of small coupon data to more realistic structure that includes curvature. Further plans are to test full-scale structure whether they are subcomponents or components. The full-scale tests will be able to interrogate the effects of rogue damage on nonpressurized and pressurized fuselage structures, which includes curvature.

Results generated to date indicate that the size scaling efforts may be most important to the failure mechanism where a buckled skin dimple drives progressive core failure. The residual strength for this failure mechanism tended to be nearly constant and independent of the starting damage size, which suggests some possible dependence on structural geometry (i.e., CAI specimen width was held constant in the study). Size scaling issues are also expected when considering the impact event and resulting damage, which is likely to depend on structural boundary conditions.

There is a need to develop higher fidelity analytical methods that have the capability to address damage progression. The analysis that has been performed to date clearly shows the benefit of damage progression to more accurately predict final failure. Supporting analyses are also needed in the size-scaling studies to separate material size effects from those related to structural boundary conditions. Without analyses, the numbers of tests that are economically feasible at larger scales will not suffice in establishing a complete understanding of the sandwich impact and related damage tolerance phenomena.

Future NDI efforts need to continue to link with structural analysis and test efforts, including those discussed above for scaling issues. The recommended focus is on defining reliable damage metrics, which can be related to residual strength and damage tolerance to repeated loads. More reliable NDI procedures for maintenance and a better understanding of the results can help to move towards an advanced approach to damage tolerance for composite sandwich structure while relieving conservatism in the associated design criteria.

Additional fatigue testing on CAI specimens is needed to more accurately define the fatigue threshold. The testing that was performed, although it permitted the establishment of a rough estimate of such a threshold, was not sufficient to establish it with high confidence. Large scatter in such testing will require a large increase in specimen replicates. These future efforts are best pursued after scaling issues are understood.

Finally, service databases for impact damage to sandwich structure are needed to help develop additional guidance for a threat assessment and provide the basis for future efforts in testing, analysis, NDI, and design criteria. Since the critical threats will likely have some differences related to the design detail and associated application, service databases are needed for rotorcraft, transport aircraft, and small airplanes.

8. REFERENCES.

1. Tomblin, J., T. Lacy, B. Smith, S. Hooper, A. Vizzini, and S. Lee, "Review of Damage Tolerance for Composite Sandwich Airframe Structures," DOT/FAA/AR-99/49, August 1999.

2. Moody, R.C. and Vizzini, A.J., "Damage Tolerance of Composite Sandwich Panels Structures," DOT/FAA/AR-99/91, January 2002.

3. Tomblin, J., K.S. Raju, J. Liew, and B.L. Smith, "Impact Damage Characterization and Damage Tolerance of Composite Sandwich Airframe Structures," DOT/FAA/AR-00/44, January 2001.

4. Lacy, T.E., Smarah, I.K., and Tomblin, J.S., "Damage Resistance Characterization of Sandwich Composites Using Response Surfaces," DOT/FAA/AR-01/71, March 2002.

5. Moody, R.C. and Vizzini, A.J., "Test and Analysis of Composite Sandwich Panels With Damage," DOT/FAA/AR-01/124, March 2002.

6. Tomblin, J., K.S. Raju, J. Acosta, B. Smith, and N. Romine, "Impact Damage Characterization and Damage Tolerance of Composite Sandwich Airframe Structures – Phase II," DOT/FAA/AR-02/80, October 2002.

7. Lacy, T.E., Smarah, I.K., and Tomblin, J.S., "Damage Tolerance Characterization of Sandwich Composites Using Response Surfaces," DOT/FAA/AR-01/101, November 2002.

8. Minguet, Pierre J., "A Model for Predicting the Behavior of Impact-Damaged Minimum Gage Sandwich Panels Under Compression," AIAA91-1075-CP, 1991.

9. Raju, K.S., "The Static Indentation Behavior of Composite Sandwich Panels With Thin Quasi-Isotropic Skins," Ph.D. Dissertation, Department of Aerospace Engineering, Wichita State University, December 2001.

10. Hsu, D.K., J.J. Peters, D. Fei, D.J. Barnard, and V. Dayal, "Imaging Flaws in Composite Honeycomb Aircraft Structures Using Instrumented Tap Test," SPIE *Proceedings on Nondestructive Evaluation of Aging Materials and Composites*, Vol. 3585, edited by G.Y. Baaklini, C.A. Libowitz, and E.S. Boltz, 1999, pp. 236-245.

11. Sendeckyj, G.P., "Fitting Models to Composite Materials Fatigue Data," *Test Methods and Design Allowables for Fibrous Composites, ASTM STP 734,* C.C. Chamis, ed., American Society for Testing and Materials, 1981, pp. 245-260.

12. Box, G.E.P. and Behnken, D.W., "Some New Three Level Designs for the Study of Quantitative Variables," *Technometrics*, 2(4), pp. 455-475, 1960.

13. Mitsui Woodpecker, Mitsui & Co. (U.S.A.), Inc., 1001 Fourth Avenue, Suite 4000, Seattle, WA 98154-1196.

14. SAE ARP5089, Aerospace Recommended Practice.

15. Gary Georgeson, Scott Lea, and Jeff Hansen, "Electronic Tap Hammer for Composite Damage Assessment," SPIE *Proceedings, Nondestructive Evaluation of Aging Aircraft, Airports and Aerospace Hardware*, Vol. 2945, edited by R.D. Rempt and A.L. Broz, 1996.

16. "ANSYS Advanced Analysis Techniques," ANSYS Inc., February 2000.

17. ABAQUS 6.2 Hibbitt, Karlsson & Sorensen, Inc. 2001.

18. Abrate, S., "Localized Impact on Sandwich Structures With Laminated Facings," *Appl. Mech. Rev.*, 50(2), pp. 69-82,1997.

19. Kassapoglou, C., 1998, "Compressive Strength of Composite Sandwich Panels After Impact Damage: An Experimental and Analytical Study," *Journal of Composite Technology & Research*, Vol. 10, pp. 65-73.

20. Tsang, P.H., "Impact Resistance and Damage Tolerance of Composite Sandwich Panels," Ph.D. Thesis, Massachusetts Institute of Technology, Wilson, June 1994.

21. Moody, R. Clifton, "Damage Tolerance of Impacted Composite Sandwich Panels," M.S. Thesis, University of Maryland at College Park, November 2000.

22. Moody, R. Clifton and Vizzini, A.J., "Incorporation of a Compliance Change Due to Impact in the Prediction of Damage Growth in Sandwich Panels," to be published.

23. Chia, C.Y., "Nonlinear Analysis of Plates," McGraw-Hill Inc., 1980.

24. Xie, Z.H. and Vizzini, A.J., "A Modified Analytical Model for Damage Propagation of a Low Velocity Impacted Sandwich Panel," *Proceedings of the American Society for Composites*, 7th Technical Conference, Purdue University, October 2002.

25. AC 29-2C, Advisory Circular, Certification of Transport Category Rotorcraft, ARAC draft updates to MG 8 (Substantiation of Composite Rotorcraft Structure), Paragraphs 5 and 6, February 11, 2002.

26. AC 27-1B, Advisory Circular, Certification of Normal Category Rotorcraft, ARAC draft updates to MG 8 (Substantiation of Composite Rotorcraft Structure), Paragraphs 5 and 6, February 11, 2002.

•U.S. GOVERNMENT PRINTING OFFICE: 2003/504-042/60074